Deliverable D3.4: WP3 overall public deliverable

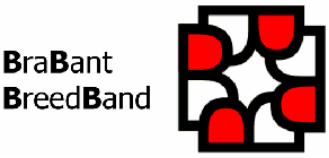

Information Report Number: Philips_WP3_PUB_01_v01_wp3overview

Date of Delivery:	2005-07-04
Report Title:	Deliverable D3.4: WP3 overall public deliverable
Editor:	Guido Dolmans (Philips Research)
Authors:	M. Collados (Philips Research) G. Dolmans (Philips Research) I. Modonesi (former: Agere Systems) T. Schenk (TU/e) A. van Zelst (former: TU/e & Agere Systems)
Reviewers:	

Abstract:

Agere Systems, KPN Research, Philips Research, TNO Telecom and the Eindhoven University of Technology (TU/e) were co-operating in a strategic alliance called the Broadband Radio@hand (BR@H) project from April 1st, 2001 to July 1st, 2005. Workpackage 3 (WP3) of this project focussed on a pre-competitive study of the physical layer of future wireless local-area-networks (LAN) to fulfil bandwidth and quality needs in the office and at home. This should facilitate the design of new generation multimedia services in the Netherlands.

Broadband Radio@hand project is part of the B4-initiative (BraBant BreedBand, "B4"); a co-operation between Lucent Technologies, KPN Research and TU/e. More information on B4 and Broadband Radio@hand can be found at www.brabantbreedband.nl.

WP3 focused on the use of smart antennas as a candidate for next generation broadband cellular or wireless communications systems. The use of smart antennas is a potential breakthrough in the improvement of data rates and quality-of-service (QoS) in cellular and wireless systems.
A particular method to establish wireless broadband communications is the use of multiple-input multiple-output (MIMO) technology.

Several scenarios are described which are typical for the Broadband Radio@hand requirements. MIMO link-level, system-level simulations and measurements are carried out to predict the performance in these scenarios. The two MIMO prototypes (test-beds) developed in this project are described in this report. These test-beds are used to demonstrate the Broadband Radio@hand concept.

It can be concluded that the preferred MIMO scheme for the Broadband Radio@hand project requirements is MMSE with receive diversity (more receive antennas than transmit antennas). For symmetric transmit/receive MIMO systems, V-BLAST is preferred when latency is not an issue.

Key word list: MIMO, smart antennas, space-time coding, test-beds, capacity, indoor radio channels

Confidentiality: Public

Document History

Date	Version	Comment	Editor
04/07/05	1	Draft version	GD (Philips)
17/07/05	2	Revised version	TSc (TU/e)
14/08/05	3	Final version	GD (Philips)

Table of Contents

List of Notation

ADC	Analogue-to-Digital Converter
AGC	Automatic Gain Control
AWGN	Additive White Gaussion Noise
BER	Bit Error Rate
BLAST	Bell Labs Layered Space Time
BPSK	Binary Phase Shift Keying
CC	Convolutional Coding
CCI	Co Channel Interference
CDF	Cumulative Distribution Function
DAC	Digital-to-Analogue Converter
D-BLAST	Diagonal-BLAST
DC	Direct Current
DFB	Decision Feedback decoding
FER	Frame Error rate
FFT	Fast Fourier Transform
FPGAs	Field Programmable Gate Arrays
I	In-Phase
IFFT	Inverse Fast Fourier Transform
IC	Ideal Channel
ICSI	Ideal Channel State Information
IF	Intermediate Frequency
ISA	Industry Standard Architecture
ISI	Inter Symbol Interference
ISM	Industry, Scientific and Medical
LOS	Line-of-Sight
MAC	Medium Access Control
MAC c	MAC connector
MAP	Maximum a Posteriori
MAPU	Multi Antenna Processing Unit
MIMO	Multiple-Input Multiple-Output
MLD	Maximum Likelihood Detection
MLSE	Maximum Likelihood Sequence Estimator
MMSE	Minimum Mean Square Error
MRC	Maximum Ratio Combining
NLOS	Non-Line-of-Sight
OD	Optimal Detection
OFDM	Orthogonal Frequency Division Multiplexing
PAC	Per Antenna Coding
PDF	Probability Distribution Function
PDP	Power Delay Profile
PER	Packet Error Rate
PS	Portable Station
Q	Quadrature
QAM	Quadrature Amplitude Modulation
QPSK	Quadrature Phase Shift Keying

QoS	Quality of Service
RDS	Rms Delay Spread
RF	Received Frequency
rms	root mean square
Rx	Receive
SDM	Space Division Multiplexing
SIC	Successive Interference Cancellation
SIMO	Single-Input Multiple-Output
SINR	Signal to Interference Noise Ratio
SIR	Signal to Interference Ratio
SISO	Single-Input Single-Output
SNR	Signal to Noise Ratio
SO	Soft Output
S/P	Serial/Parallel
STBC	Space Time Block Coding
STC	Space Time Code
STTC	Space-Time Trellis Coding
TC	Turbo Coding
T_g	Guard Time
Tx	Transmit
V-BLAST	Vertical-BLAST
WER	Word Error Rate
WLAN	Wireless Local Area Network
ZF	Zero Forcing

1 Purpose and Scope of Deliverable 3.4

The BraBant BreedBand consortium (B4) focuses on joint research on broadband telecommunications technology. The consortium partners are Lucent, KPN and the Eindhoven University of Technology (TU/e). The research is organised in three taskforces: the Broadband Radio@hand project (broadband wireless connectivity), the RETINA project (optical fibre for residential gateway) and a Campus pilot project. The partners of Broadband Radio@hand are Agere Systems, KPN Research, Philips Research, TNO-telecom and TU/e. Several work packages are defined in the Broadband Radio@hand project: Scenarios, Channel Models, Diversity Techniques and Smart Antennas, Radio Network Planning, WLAN system simulation, Hybrid Wireless Networks and Proof of Concept. This report describes the results of Workpackage 3 (WP3) over the full project period disclosed for the public.

WP3 focuses on the use of smart antennas as a candidate for next generation broadband cellular or wireless communications systems. The use of smart antennas is a potential breakthrough in the improvement of data rates and quality-of-service (QoS) in cellular and wireless systems. High data rate communication in wireless and cellular networks is emerging. In the IEEE standardisation body, a High Throughput Study Group is formed. Promising antenna technology is considered to be the main driver. Among the possible options to meet the demanding requirements is to design a novel physical (PHY) layer by making use of multiple-input multiple-output (MIMO) technology.

Space-time communication and broadcast systems, also known as multiple-input multiple-output (MIMO) systems, make use of temporal and spatial antenna processing techniques to increase capacity and to improve Quality-of-Services (QoS). A high spectral efficiency can be achieved by creating multiple radio channels (sharing the same time-frequency slot) between transmitters and receivers. Theoretical analysis has shown that the transmission with a K-element antenna array and reception with a U-element antenna array is capable of achieving rates that increase linearly with min(U,K). This means that the increase in capacity is proportional to the number of antenna elements without any penalty in power and bandwidth. Therefore, the employment of multiple antennas at user terminals is potentially beneficial when providing high bit-rate multimedia services. However, from the scientific literature it is not clear how a realistic and cost-effective radio can be build around this concept.

Two prototypes (test-beds) of MIMO systems are presented. These test-beds are used to measure the MIMO channel, from which MIMO channel models were extracted. An extensive list of MIMO algorithms and models are described in this deliverable.

Chapter 2 gives insight into the derivation of theoretical capacity curves for MIMO systems. Sophisticated channel models, including Rayleigh fading, spatial

correlation and multi-tapped delay lines, are used to give a first impression of the bit-error-rate (BER) curves of these systems.

Chapter 3 presents the two 5 GHz MIMO test-beds developed in WP3. These test-beds are used to verify the theoretical capacity and BER studies. The test-beds also serve as a platform for MIMO algorithm development.

Chapter 4 presents a general description of link level algorithms suitable for both wireless local-area-network (WLAN) and UMTS systems. Several linear, non-linear space-division multiplexing (SDM) and space-time block codes based algorithms are described in detail.

Chapter 5 presents specific WLAN topics related to MIMO. The most important OFDM parameters of current WLANs are summarized. Finally, simulations in noise-limited and interference-limited scenarios are shown.

Chapter 6 describes an extensive evaluation of MIMO algorithms for various scenarios. As an outcome, PHY tables with the packet-error-rate (PER) vs. SNIR (signal-to-noise plus interference ratio) are documented. These tables are used in the system level simulations carried out within another workpackage of this project, i.e., WP5.

Chapter 7 describes the workflow for to combine the link-level simulations presented in this deliverable with the system-level simulations.

Chapter 8 uses the derived BER performance tables to predict the achievable throughput in the uplink and downlink channel for an access point and mobile terminals in a single radio channel. The throughput is calculated using a simple propagation model with a single breakpoint and a simple link-adaptation and transmit power control mechanism.

2 MIMO Fundamentals

2.1 Introduction

The objective of this chapter is to describe and compare the multiple-input multiple-output (MIMO) techniques which have been proposed in literature in the past years. Unfortunately most of the available papers focus on narrowband (single carrier) wireless communication. Few papers consider broadband applications and usually they use assumptions tailored for mobile communication. The following describes for a number of narrowband MIMO algorithms and, when available, the broadband adaptation or application.

Workpackage 3 focussed on the use of smart antennas as a candidate for next generation broadband cellular or wireless systems. The use of smart antennas is a potential breakthrough in the improvement of quality, transmission capacity and data rates in wireless and cellular systems. Basically, the idea is to make use of a strong multi-path propagation environment instead of being limited by it. In the receiver, the multi-path streams are transformed into independent channels by using a combination of adaptive antennas, appropriate transmission coding and receiver detection algorithms.

The 'hidden' capacity of a wireless medium could be exploited by the introducing spatial (de-)multiplexing of several communications channels within the same bandwidth and the same time-slot. This is shown in Figure 2-1.

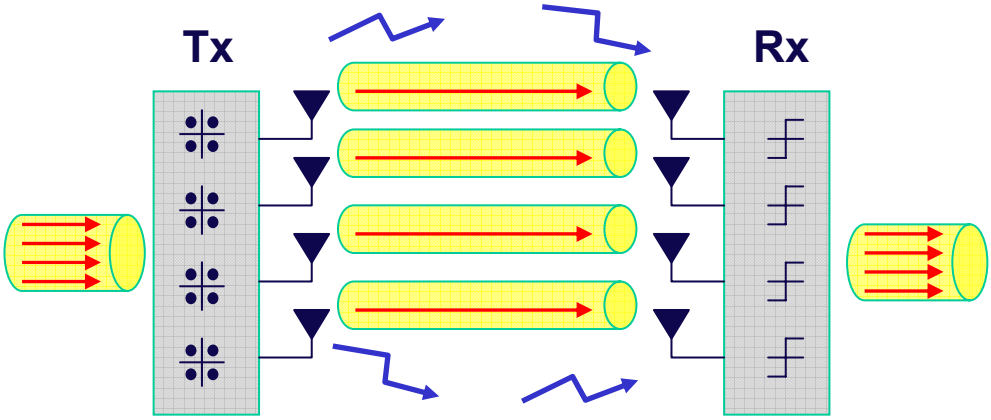

Figure 2-1: Principle of launching multiple communications channels at the same time instant and frequency band by making use of the unbounded spatial air interface.

The use of multiple antennas at both transmit and receive side is also referred to as multiple-input multiple-output (MIMO) systems. MIMO systems could serve multiple objectives. This is shown in Table 2-1.

	Coverage	Link Quality	Capacity	Data Rate
Array Gain	X	X		
Int. Reduction		X	X	
Diversity		X	X	
Multiplexing			X	X

Table 2-1: Several ways to exploit the unbounded air-interface to improve either coverage, link quality, capacity or data rates.

Multiple receive antennas will lead to array gain (3 dB signal-to-noise improvement when doubling the number of receive antennas) even in a non multi-path environment. This could be used to increase the coverage of a base-station or access point. Another possibility is use interference reduction schemes at the receive array to suppress interference from unwanted sources and/or users. Basically, this will improve the link quality but also more users can be used in a cell, which will lead to more capacity. In a multi-path fading environment, a large improvement (more than 10 dB) can be obtained by using multiple receive antennas by mitigating the weak signal fades (see [Dol97]). The focus of this workpackage will be on high data rates; therefore the spatial multiplexing is chosen as the suitable candidate. Spatial multiplexing has the potential to increase the transmission rate with a factor n, where n is the minimum of the number of transmit and receive antennas.

2.2 MIMO Theoretical Capacity

Before analysing different MIMO techniques, it is important to show the capacity that can be achieved by using multiple transmitters and multiple receivers. These theoretical bounds will be used later to compare how close the algorithm capacity is to the theoretical one. Here, a summary is given of the capacity for different channels as reported in [Fos98].

The following assumptions have been considered to formulate the results given below:

- Number of transmit and receive antennas is, respectively, N_t and N_r
- The total transmit signal vector is composed of N_t statistically independent equal power components. The total irradiated power is independent of the number of transmit antennas.
- The communication channel **H** is assumed to be flat over frequency
- Average SNR at each receiver branch: $\rho = P/N_0$ where P is the received power independent of N_t
- Noise at the receiver is modelled as AWGN vector of dimension N_r, with independent components of identical power N_0 for each of the N_r branches.

The capacity for a MIMO system, for the assumptions given above is:

$$C = \log_2 \det\left(1 + \frac{\rho}{N_t}\mathbf{H}\mathbf{H}^H\right) \text{ bps/Hz}, \quad (1)$$

where $(.)^H$ denotes the conjugate transpose of a vector or matrix. Since usually in indoor environments, we come across channels that can be modelled by a Rayleigh distribution, it is useful to report the capacity achievable in such channels for different antennas configurations.

We now assume:

- Quasi-static channel **H** (N_t columns, N_r rows): i.e. the randomly selected channel is not changing during a single packet transmission.
- Channel follows the Rayleigh distribution. The element of the channel **H** (N_r x N_t matrix) are i.i.d., complex, zero-mean, unit variance entries:

$$h_{ij} = \text{Normal}\left(0,1/\sqrt{2}\right) + \sqrt{-1}\cdot\text{Normal}\left(0,1/\sqrt{2}\right), \quad (2)$$

  consequently, $|h_{ij}|^2$ is a χ_2^2 variate but normalized so $E(|h_{ij}|^2) = 1$.
- H is known at the receiver.

The capacity for different antennas configurations becomes [Uys01]:

A) No diversity: $N_r = N_t = 1$

$$C = \log_2\left(1 + \rho\cdot\chi_2^2\right) \text{ bit/s/Hz}. \quad (3)$$

B) Receive Diversity: $N_t = 1$, $N_r = N$

$$C = \log_2\left(1 + \rho\cdot\chi_{2N}^2\right) \text{ bit/s/Hz}. \quad (4)$$

C) Transmit Diversity: $N_t = N$, $N_r = 1$

$$C = \log_2\left(1 + \frac{\rho}{N_t}\cdot\chi_{2N}^2\right) \text{ bit/s/Hz}. \quad (5)$$

D) Combined Transmit-Receive Diversity: $N_t = N_r$

$$C > \sum_{k=N_t-(N_r-1)}^{N_t} \log_2\left(1 + \frac{\rho}{N_t}\cdot\chi_{2k}^2\right) \text{ bit/s/Hz}. \quad (6)$$

The best theoretical capacity is achieved in case D. This theoretical result confirms that the combination of transmit and receive diversity improves the data rate and the performance of wireless links.

2.3 MIMO and SIMO Feasibility Study under Rayleigh Conditions

2.3.1 Introduction

The feasibility study is confined to the prediction of capacities in indoor non line-of-sight wireless channels. The propagation environment typically consists of many scatterers, so that the signal travels multiple paths before arriving at the receiver. Such a propagation environment is shown in Figure 2-2.

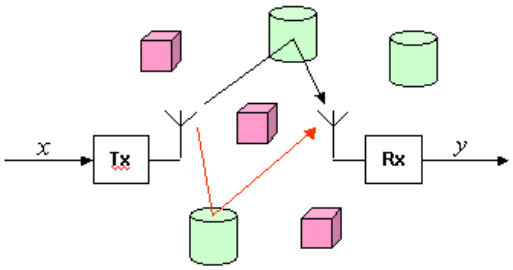

Figure 2-2: Indoor wireless fading environment.

In the limit of many scatterers, it can be shown that the Rayleigh distribution is appropriate to describe the spatial fluctuations of the amplitude of a narrowband signal. Shannon's equation explains the dependency of the capacity C on the bandwidth B and signal-to-noise ratio SNR.

$$C = B\log_2(1+\mathrm{SNR}) \text{ [Bits/s]} \quad (7)$$

Let's take the bandwidth fixed (because of spectral regulations or system requirements). A Rayleigh number generator is taken for the signal-to-noise ratio and we study the probability density function (PDF) of the normalised capacity (given by $\log_2(1+SNR)$).

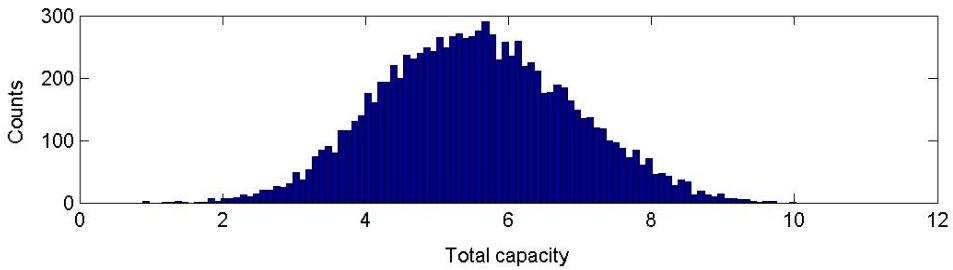

Figure 2-3: Probability density function of the capacity [bit/s-Hz] under Rayleigh fading conditions.

The capacity is treated as a stochastic variable. It is characterized by its mean value (around 5 bits/s-Hz in the figure above) and the variation around the mean. The variation around the mean has a relation to the reliability of the wireless communications link. The aim of this workpackage is to propose systems with high data rates and a good reliability. The reliability can be evaluated by having a look at the tail of the PDF. Therefore, the concept 'outage' is now introduced. Outage is the chance that the user will experience a capacity below x bits/s-Hz.

In the remainder of this report, outage levels of 10 % and 1 % will be taken. Drawing a cross-section of the CDF with those outage levels will give us the capacity. This capacity is guaranteed within 90 % or 99 % of the indoor space, respectively.

2.3.2 Average capacity of SIMO and MIMO systems

Consider a system with n_T transmit antennas and n_R receive antennas. The generalised Shannon capacity for this MIMO system can be written as shown in Eq. (1). A Rayleigh number generator is used to describe the spatial variations of the signal-to-noise ratio ρ. The Rayleigh fading model is the most popular model which describes fading as a complex Gaussian process. The elements of the channel matrix are taken as unit variance circular symmetric Gaussian stochastic variables.

The average capacity for various MIMO systems as a function of the average signal-to-noise ratio Γ is shown in Figure 2-4. In addition, the capacity for a single-input multiple-output system (SIMO) is also shown. The SIMO case denotes the classical diversity system with only multiple antennas on one side of the communication link.

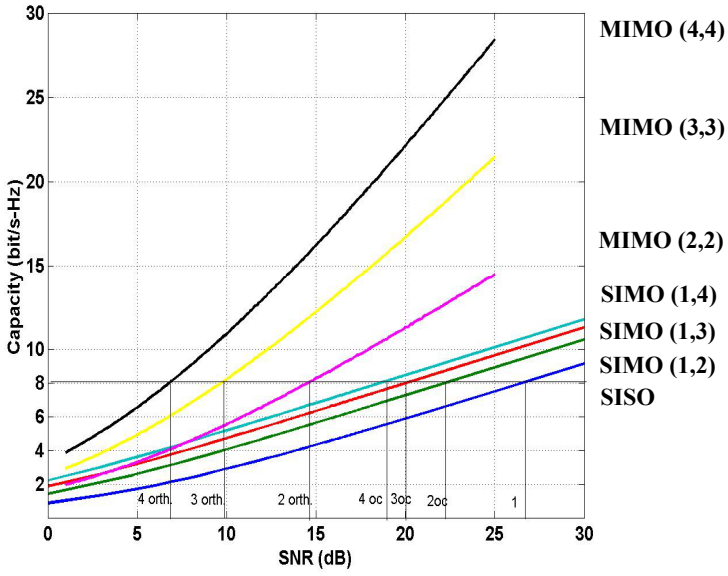

Figure 2-4: Average capacity of a n = 1...4 SIMO system ('oc') compared to (n,n) MIMO system ('orth') for uncorrelated Rayleigh fading channels.

As a reference, the conventional single antenna systems (SISO) is included as a reference. Consider that conventional systems (GSM, UMTS etc..) have rather low spectral efficiencies around 1 – 2 bits/s-Hz. Take an arbitrary target of 8 bits/s-Hz for our broadband MIMO research, the following table shows the signal-to-noise ratio to reach this capacity target.

System	SNR [dB]
SISO	26.5
SIMO (1,2)	22.2
SIMO (1,3)	20.0
SIMO (1,4)	18.6
MIMO (2,2)	14.5
MIMO (3,3)	9.7
MIMO (4,4)	6.8

Table 2-2: Signal-to-noise ratio [dB] to get a average spectral efficiency of 8 bits/s-Hz.

2.3.3 Outage capacity of SIMO and MIMO systems

A mean capacity of 8 bit/s-Hz is an interesting figure, but it does not tell us what the capacity will be 90 % or 99 % of the time or space. Therefore, another interesting performance measure for the reliability of the service is the outage capacity. Outage capacity means that the capacity equal or higher than a certain fixed value is guaranteed for 90 % or 99 % of all spatial locations. The SNR threshold for an outage capacity of 8 bit/s-Hz is shown in Table 2-3.

System	Outage = 10 %	Outage = 1 %
SISO	33.8 dB	44.0 dB
MIMO (2,2)	18.7 dB	25.7 dB
MIMO (3,3)	12.1 dB	14.2 dB
MIMO (4,4)	9.0 dB	10.0 dB

Table 2-3: Signal to noise ratio to get an outage spectral efficiency of 8 bit/s-Hz for outage of 10 % and 1 %, respectively.

Note that a conventional single antenna system requires an unrealistic 44 dB signal-to-noise ratio to achieve a reliable capacity of 8 bits/s-Hz, while a (4,4) MIMO system only needs a signal-to-noise ratio of 10 dB.

2.3.4 Conclusions of feasibility study

The conclusions about the feasibility of spectral efficiency of 8 bit/s-Hz are:

- For Rayleigh channels, an improvement in the SNR of 4.3, 6.5, and 7.9 dB is feasible when implementing a (1,*n*) diversity system instead of a single antenna pair to get a mean capacity of 8 bit/s-Hz for $n = 2, 3, 4$, respectively.
- For Rayleigh channels, an improvement in the SNR of 12, 16.8, and 19.7 dB is feasible when implementing a (*n*,*n*) MIMO system instead of a single antenna pair to get a mean capacity of 8 bit/s-Hz for $n = 2, 3, 4$, respectively
- For Rayleigh channels, an improvement in the SNR of 15.1, 21.7, and 24.8 dB is feasible when implementing a (*n*,*n*) MIMO system instead of a single antenna pair to get a capacity of 8 bit/s-Hz at an outage of 10 % for $n = 2, 3, 4$, respectively
- For Rayleigh channels, an improvement in the SNR of 18.3, 29.8, and 34 dB is feasible when implementing a (*n*,*n*) MIMO system instead of a single antenna pair to get a capacity of 8 bit/s-Hz at an outage of 1 % for $n = 2, 3, 4$, respectively

3 MIMO Test Systems

Two MIMO test systems were developed within WP3 of the Broadband Radio@hand project. The first one was developed at Agere Systems, in cooperation with the TU/e and the second one at Philips Research. This chapter presents the build up of these systems and shows some basic results from these systems.

3.1 TRIO – The 3x3 MIMO Test System at Agere Systems

3.1.1 Introduction

In Agere Systems, a MIMO test system, named Triple Input Output (TRIO) was built with two goals: 1) to verify the theoretical MIMO propagation studies and 2) to serve as a platform for MIMO algorithm development. With the testbed (broadband) MIMO channel measurements were performed to provide an answer to the first goal. Furthermore, these measurements were used as a basis for algorithm selection and development. As a platform for algorithm development, different approaches for MIMO processing can be explored quickly by keeping the processing off-line to avoid implementation problems.

To have enough flexibility in achieving above goals, Agere Systems has chosen to build-up the testbed with in-house developed components. To access this dedicated hardware, two PCs, the transmitter (TX) and receiver (RX) platform, respectively, are used. Each PC has three boards, where every single board represents a TX or RX branch, resulting in a 3×3 MIMO system as shown in Figure 3-1. Every board consists of a baseband part, an IF part and a RF front-end based on a 5.x GHz GaAs radio chip. The test system operates in the 5.x GHz ISM band, and is capable of transmitting broadband signals with a bandwidth up to 20 MHz. A picture of the transmitter equipment is given in Figure 3-2. The TX and RX platforms are synchronised with a cable, for the ease of verification of the testbed.

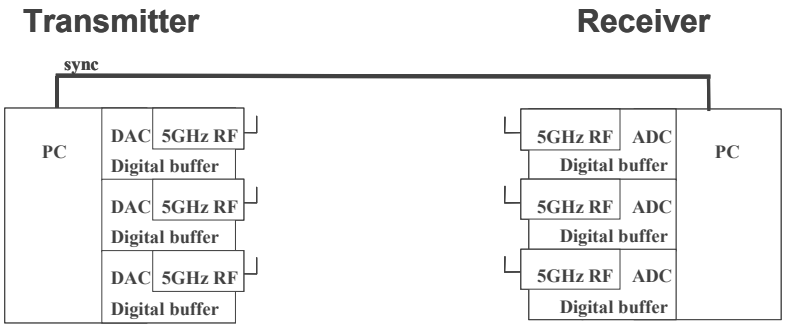

Figure 3-1: Schematic of the TRIO system.

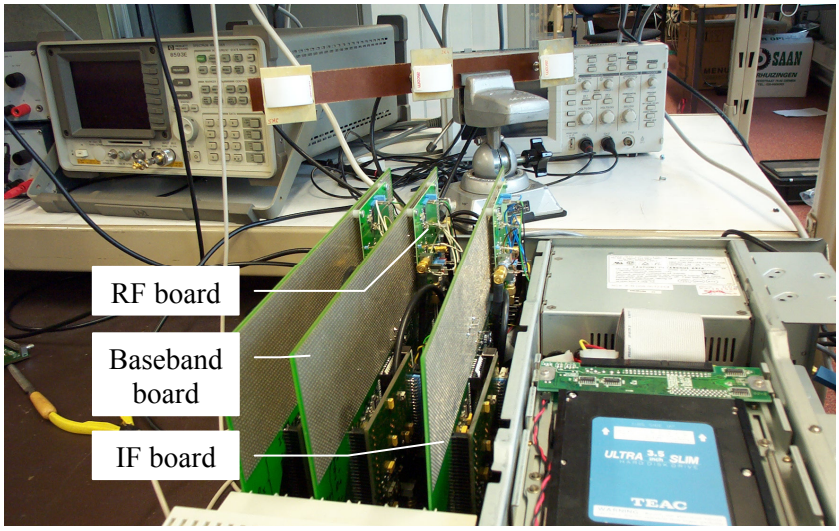

Figure 3-2: Transmitter equipment: a PC with three boards representing the three transmitter branches.

3.1.2 Baseband hardware

The baseband processing is build around two (with a possible extension to three) Field Programmable Gate Arrays (FPGAs) per board (see Figure 3-3 for a schematic representation of a baseband board). The FPGAs that are used are Xilinx Virtex 800's. The FPGAs can be reprogrammed and/or accessed via the ISA bus very easily, thus, provide a flexible baseband solution. The baseband boards are capable of transmission and reception, while the IF and RF part are only set up to transmit or receive, respectively, for the TX and RX platform, so that only the respective parts of the baseband boards are used.

The transmitter is set up to send signals at zero-IF, meaning that it can send baseband signals centred around 0 Hz. To send such a signal, an in-phase (I) and quadrature (Q) part must be available, i.e., the baseband signal is complex and its real and complex part are needed for further processing. The I and Q-signals are converted to the analogue domain by the Analogue-to-Digital Converters (ADCs) and after filtering sent to the IF and RF stage, where they are up-converted to the carrier frequency and sent by the TX antennas.

At the receiver, the received signals are down-converted to low-IF signals, meaning that baseband board gets a signal that is centred around a low Intermediate Frequency (for the TRIO system it is chosen to be 15 MHz). The down-conversion to baseband is done in the digital domain. The advantage of this so-called sampled-IF principle is that the DC-component can be easily filtered out and that I-Q imbalance is (hardly) not introduced.

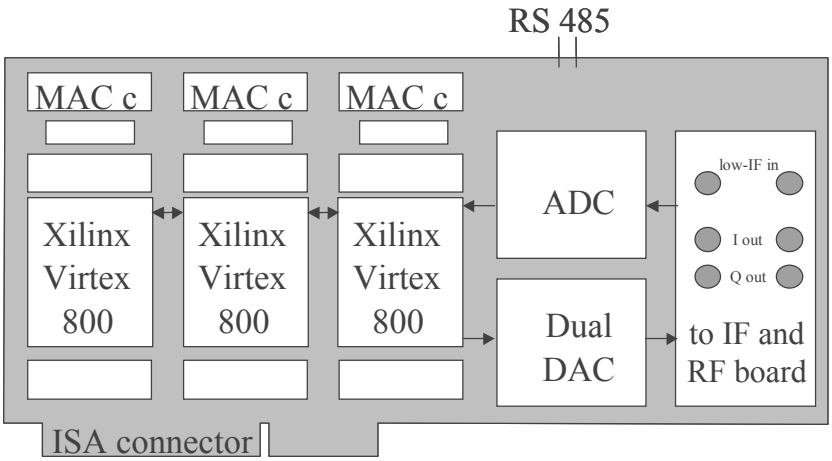

Figure 3-3: Schematic representation of a TRIO baseband board.

As mentioned before, the FPGAs provide a flexible baseband solution. It is, for instance, possible to load the FPGAs with a real-time implementation of the baseband processing. In that way, the boards can run stand-alone and real-time. Moreover, if they are connected to a Medium Access Control (MAC) board using the MAC connectors (denoted by "MAC c" in Figure 3-3), a complete point-to-point link can be tested.

It is also possible to program the FPGAs as memory banks and perform the necessary processing off-line. At the transmitter, waveforms can be loaded into and sent from the memory banks and they can be recorded at the receiver. These recorded data can then be processed off-line in software (so not in real-time), to calibrate the system, do channel measurements, perform capacity analysis, compare different MIMO algorithms, etc.

The RS 485 connector that is shown in Figure 3-3, is used as an interface between the TX and RX to do the synchronisation that is, for the moment, being done per cable, as explained before.

3.1.3 Software

To exploit the flexibility provided by the design of the TRIO test system, the baseband processing of both TX and RX was implemented in MATLAB. In the TX part of the software complex data was generated, where different packet formats, modulations and coding rate could be selected. This digital data was subsequently loaded in the memory banks of the TX boards.

When transmitted through the wireless the RX data was captured from the RX board and loaded into the MATLAB interface again. There synchronization, channel estimation, detection and decoding were applied. The different detection algorithms presented in Chapter 4 were implemented here. Bit-error-rate (BER) measurements were possible by comparing the transmitted and received data. Figure 3-4 shows the graphical user interface developed with the MATLAB

software. It shows a successful 108 Mbit/s transmission, with 3 TX antennas and 16-QAM modulation.

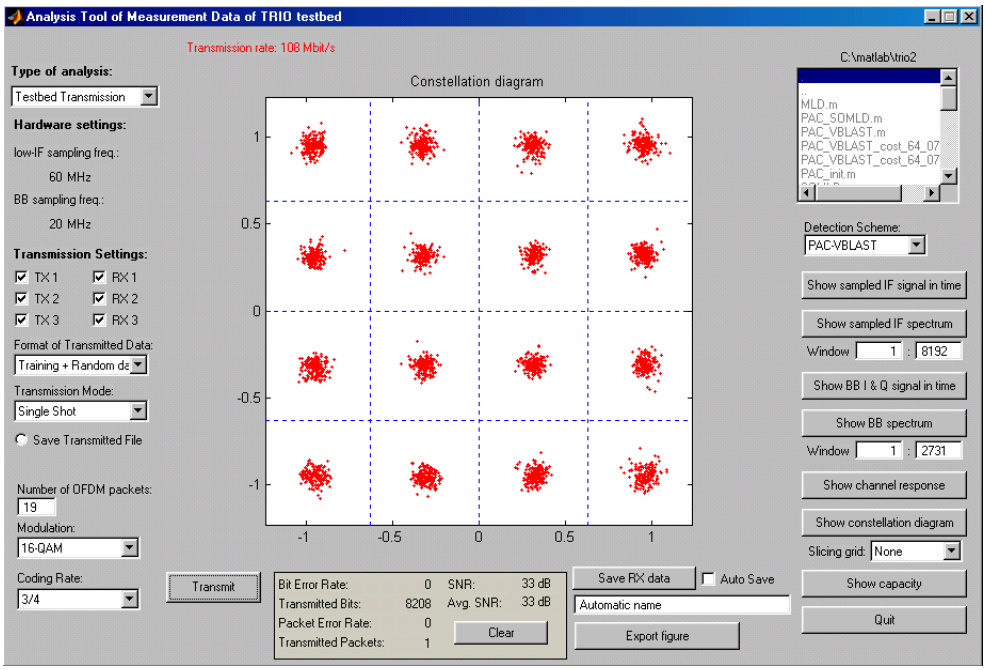

Figure 3-4: Graphical User Interface of the MATLAB software developed for the TRIO test system.

3.1.4 Measurement Results

Some of the measurement results achieved with the TRIO test system have been presented in [ZelSc04]. This paper shows measurement results of measurements carried out in a wing of the former Agere Systems building in Nieuwegein. The results indicate that transmissions of 162 Mbit/s are possible with a 3×3 MIMO system.

3.2 The 4x4 Space-time Testbed at Philips Research

The aim for the development an experimental testbed for wireless broadband MIMO systems within Philips Research was twofold. Firstly, knowledge, insight and modelling of the MIMO radio channels can be gained. Secondly, different RF transceiver architectures can be tested and important system parameters can be derived.

3.2.1 Requirements

This resulted in the following requirements:

- **Modularity**: The system should be reconfigurable to accommodate new measurement scenarios and new wireless transceiver systems. The latter means that different RF architectures can be tested and new processing algorithms can be implemented.
- **Frequency range**: The system must be able to sound broadband signals up to 20 MHz signal bandwidth in a 5.x GHz ISM band. Different carrier

frequencies can easily be adopted by changing the LO frequency and the up and down mixers.

- **Raw data storage**: Raw data is stored and processing is done off-line where MIMO algorithms can be verified and debugged on the same raw data.
- **Multiple channels**: The system should have the ability to sound simultaneously 4 transmit and 4 receive channel.
- **Autonomously**: The transmit and receive systems should be completely separate, and do not require a dedicated synchronisation cable.
- **Range**: Transmit power and receiver sensitivity should be sufficient to measure all typical indoor scenarios with at least 20 dB SNR at 20 meters Tx-Rx separation.

3.2.2 Hardware

The following subsections describe the hardware that meets these goals. Referring to the application, the number N_t of transmitters and the number N_r of receivers are both limited to 4 which is called a (4,4) system.

The RF Tx and Rx parts were initially built around commercial off-the-shelf 50 Ohm components and were later on in the project partly replaced by home-made RF components.

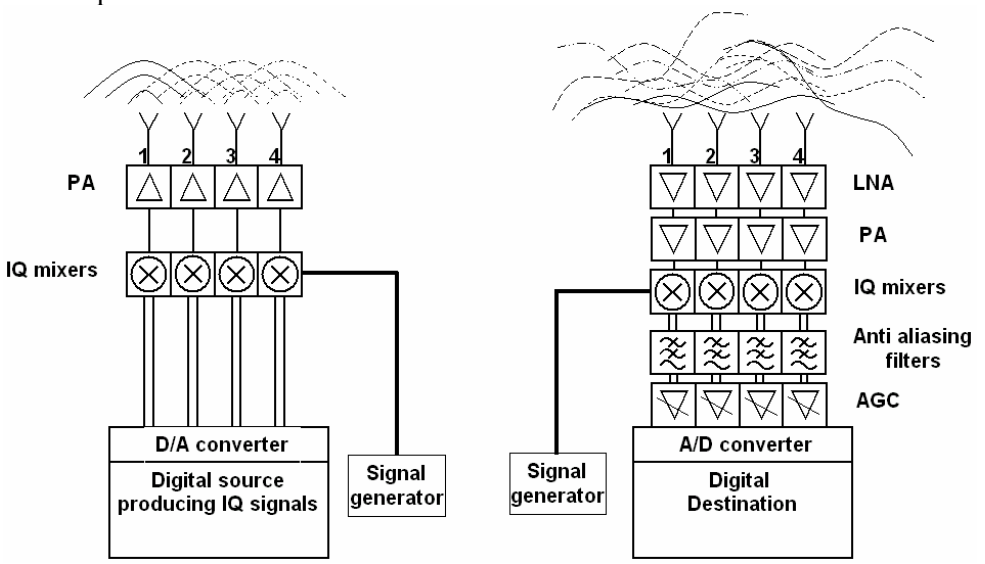

Figure 3-5: Block diagram of the (4,4) test-bed.

Transmitter

Figure 3-5 depicts the transmit subsystem on the left and can be described as:

- Independent digital I and Q signals are generated at a near-zero intermediate frequency (IF) (which can also be zero Hertz) from MATLAB script files and are fed to two 4 channel D/A cards maintaining full synchronisation between those waveform generators. Those PCI cards have a 14 bits resolution at 64 MHz sample frequency.

- Successively low pass filtering is applied.
- The baseband data is up-converted to the specified RF carrier frequency of 5.8 GHz, with I/Q mixers.
- The RF signal is amplified with power amplifiers and transmitted using four patch antennas with directivity properties only in a half plane. The maximum transmit power of each transmit antenna equals 10 dBm.

A picture of the transmitter subsystem is shown in Figure 3-6.

Figure 3-6: 4 transmit array (left) and 4 receive array (right).

Receiver

At the receiver, shown in the right part of Figure 3-5 and Figure 3-6, down conversion is applied as follows:

- The four patch antennas receive the superposition of all transmitted signals.
- These signals are amplified with low noise amplifiers (LNA) optionally followed by amplifiers.
- IQ mixers are used to down-convert the signals.
- Baseband filtering and amplification with automatic gain control amplifiers (AGC) is done before sampling with 4 dual channel A/D converters on PCI cards.

XY-scanner

In order to obtain channel statistics in the spatial domain (like outage results) the transmit antennas are mounted on an 1 m^2 *xy*-scanner which is controlled by an *xy*-controller and a PC (see Figure 3-7). This square plane is sub-divided into *K* points (read grid size). The distance between successive points is a fraction of the wavelength of observation.

The developed LabVIEW automation software allows to control and configure the *xy*-table and is also used to control third parties software like Microsoft C++ and MATLAB. With those features, the testbed is fully automated and the measurements can be performed overnight (free from people moving around).

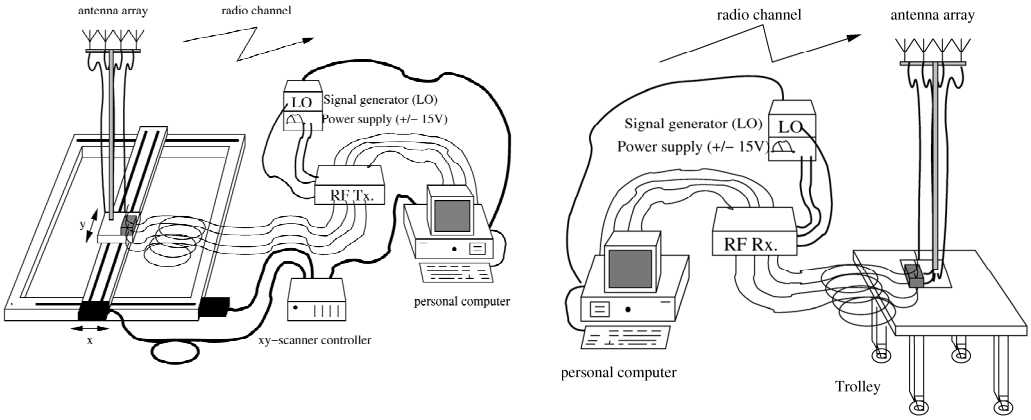

Figure 3-7: Transmitter (left) on xy-scanner and receiver (right) on trolley.

3.2.3 Baseband signal processing

In the digital domain we also want to maintain maximum flexibility. Thus all the baseband blocks are MATLAB functions which can easily be changed and upgraded. The main blocks are:

Transmitter

- Four independent data sequences having zero mean are created and mapped onto symbols (M-ary QAM).
- A training part is inserted at the beginning of the data sequence to form a frame. The signals can be orthogonal frequency modulated by the use of an IFFT at this stage.
- The symbols in the frame are up-sampled for pulse shaping in the digital domain.
- A digital frequency shift can be applied to the pulse shaped symbols.(E.g. to avoid DC offset problems).
- Finally the symbols are fed to the memory of the waveform generator boards.

Receiver

- At the receiver, the incoming information is downloaded from the boards in the MATLAB environment and a matched filtering is performed.
- The synchronisation estimator calculates the best sampling moment with the use of training sequences known at the receiver site.
- The information is then down sampled to symbols and the beginning of frame is detected.
- Hereafter the channel estimation is carried out; this block is important when considering wideband MIMO channel measurements and characterisations. To do so, a MIMO-FIR channel **H** is calculated with a total number of taps $L+1$ (longer than the maximum delay spread).
- After the channel estimation, a MIMO filter (MMSE filter) is implemented to correct for the 20 MHz channel behaviour and extract our transmitted symbols.

Various MIMO filters / combiners can be implemented to test several interference-cancelling algorithms (e.g. BLAST) or space time coding algorithms.

3.2.4 Measurement Results

An example of a QPSK (2,2) transmission is shown in Figure 3-8. This figure shows the received constellation diagram of the received QPSK symbols at two receive antennas without applying the MIMO algorithm.

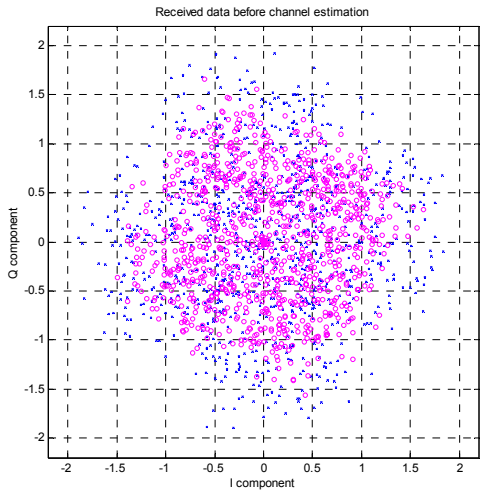

Figure 3-8: Received constellation diagram without MIMO processing.

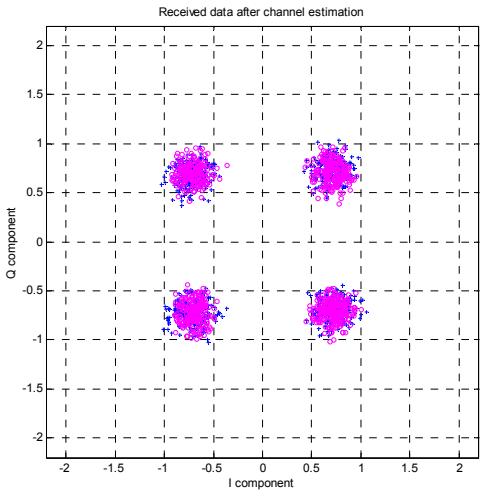

Figure 3-9: Received constellation diagram with MIMO processing.

The blue QPSK symbols are received by one antenna and the pink QPSK symbols by the other antenna. As expected, a recovery of the QPSK symbols is not possible because of all the interference. When applying the MIMO algorithm, the constellation diagram is as given by Figure 3-9. The original QPSK can now be recovered without errors. The actual bit-rate was 16 Msymbols/s x 2 antennas x 2 bits/symbol = 64 Mbps.

More measurement results of this testbed are reported in [Dol02], [Van02] and [B4-D2.2].

4 MIMO algorithms and architectures

Different MIMO architectures have been proposed in literature of the last few years. This chapter reviews the different MIMO techniques. Section 4.1-4.4 focuses on space division multiplexing systems (SDM) and space time block codes (STBC) are treated in Section 4.5.

4.1 Space Division Multiplexing and Layered Architectures

SDM techniques exploit the spatial dimension using multiple antennas at both transmitter and receiver. These techniques transmit different signals on different transmit antennas simultaneously. The goal is to increase the capacity and the SNR performance. At the receiver, the different signals are recovered using the Space Division Multiplexing techniques described in Sections 4.3-4.4. Multiple antennas are required at the receiver to recover the transmit signals more accurately.

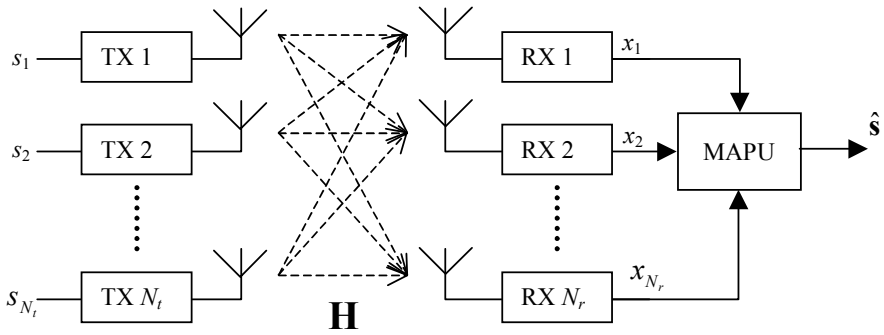

Figure 4-1: The physical model of a system with SDM.

4.2 Signal model

A communication system comprising N_t transmit (TX) and N_r receive (RX) antennas is considered. This system, assumed to operate in a Rayleigh flat-fading environment, exploits the spatial dimension by using Space Division Multiplexing (SDM) (see Figure 1, where MAPU stands for Multi Antenna Processing Unit).
Suppose we model the channel impulse response H as a zero-mean complex Gaussian variable, like:

$$H = A + jB \tag{1}$$

where A and B are zero-mean statistically independent real Gaussian variables, each having a variance $\sigma^2/2$. The variance of the complex Gaussian variable H can be shown to be:

$$\begin{aligned}\mathrm{var}(H) &= E\left[H^2\right] - E\left[H\right]^2 = E\left[(A+jB)(A+jB)\right] \\ &= E\left[A^2 + 2jAB + B^2\right] = E\left[A^2\right] + E\left[B^2\right] = \sigma^2\end{aligned} \tag{2}$$

Suppose that at discrete times, the transmitter sends an N_t-dimensional (complex) signal vector **s** (i.e., it transmits N_t parallel streams of data), and the receivr records an N_r-dimensional complex vector **x**. Then the following signal model describes the relation between **s** and **x**:

$$\mathbf{x} = \mathbf{H}\mathbf{s} + \mathbf{n} \tag{3}$$

-

where **H** is an $N_r \times N_t$ complex propagation matrix that is constant with respect to the symbol time and assumed known at the receiver (e.g. via transmitting training sequences) and the vector $\mathbf{n}$ (N_r -dimensional) represents additive receiver noise. The vector **s** is assumed to have zero-mean, uncorrelated random variables with variance equal to σ_s^2. The total power of **s** (i.e., $E[\mathbf{s}^H\mathbf{s}]$) is assumed to be P_s. Thus, the covariance matrix of **s** equals:

$$E\left[\mathbf{s}\mathbf{s}^*\right] = \sigma_s^2 \mathbf{I}_{N_t} = \frac{P_s}{N_t}\mathbf{I}_{N_t} \tag{4}$$

where ^{H} denotes the conjugate transpose of a vector or matrix and the matrix **I** with subscript N_t represents the identity matrix with dimension N_t. Note that the total transmitted power does not depend on the number of transmit antennas but is assumed fixed at P_s.

The vector $\mathbf{n}$ is N_r -dimensional and represents additive receiver noise. The vector $\mathbf{n}$ is assumed to have zero-mean, uncorrelated random variables with variance σ_n^2 and a covariance matrix equal to:

$$E\left[\mathbf{n}\mathbf{n}^*\right] = \sigma_n^2 \mathbf{I}_{N_r} \tag{5}$$

Furthermore, it is assumed that the vectors **s** and $\mathbf{n}$ are independent and thus the following holds: $E[\mathbf{s}\mathbf{n}^H] = 0$. To explain the different Space Division Multiplexing techniques, the following notations will be used:

$$\mathbf{x} = \begin{bmatrix} x_1 \\ \vdots \\ x_{N_r} \end{bmatrix},\ \mathbf{s} = \begin{bmatrix} s_1 \\ \vdots \\ s_{N_t} \end{bmatrix} \text{ and } \mathbf{H} = \begin{bmatrix} \mathbf{H}_1 \\ \vdots \\ \mathbf{H}_{N_r} \end{bmatrix} = \begin{bmatrix} \mathbf{h}_1 & \dots & \mathbf{h}_{N_t} \end{bmatrix} \tag{6}$$

where x_i and s_i represent the i-th element of **x** and **s** respectively. The $\mathbf{H}_i$ and $\mathbf{h}_i$ vectors denote the i-th row and i-th column of **H**, respectively.

4.3 Transmission schemes

Depending on the coding architecture used in the multiple antenna transmitter, two main types of SDM scheme are possible: per antenna coding and joint coding scheme [Li00].

Joint coding: In this transmission scheme a single code is used to encode all the signals going to different antennas. After coding, interleaving and mapping, the Serial input bit stream is converted to N_t Parallel sub-streams (S/P). See figure 5.2. Notice that it is also possible to set the interleaver and QAM on the right side of the serial/parallel converter.

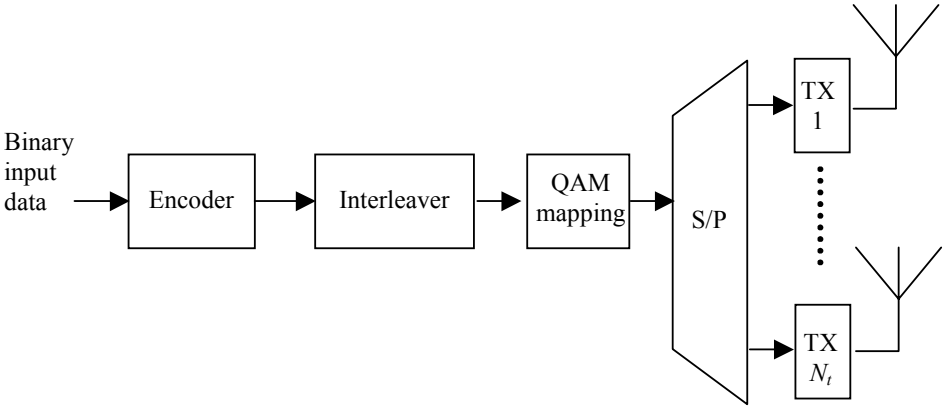

Figure 4-2: MIMO transmission scheme deploying a joint coding architecture**.**

Per antenna coding: In this transmission scheme the serial input bit stream is first converted in N_t parallel sub-streams, then each sub-stream is separately coded. See figure 5.3.

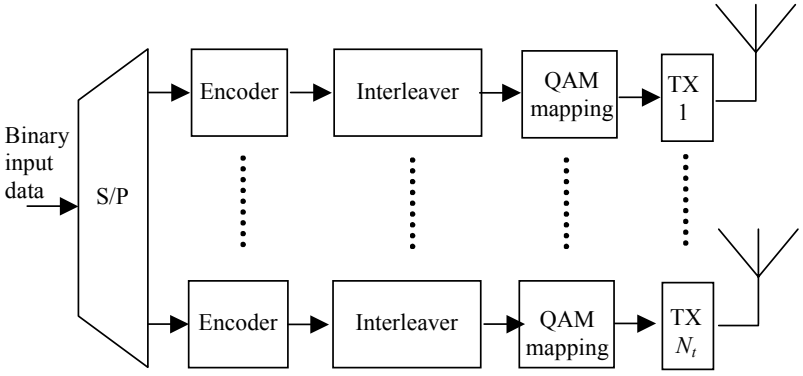

Figure 4-3: MIMO transmission scheme deploying a per antenna coding architecture.

4.4 Linear receiver scheme

4.4.1 The Zero Forcing Algorithm

The ZF algorithm is based on a conventional adaptive antenna array (AAA) technique, namely, linear combinatorial nulling [Wol98]. In this technique, each substream in turn is considered to be the desired signal, and the remaining data

streams are considered as "interferers". Nulling of the interferers is performed by linearly weighting the received signals so that all interfering terms are cancelled. For Zero Forcing, nulling of the "interferers" can be performed by choosing weight vectors $\mathbf{d}_i$ (with $i = 1, 2, \ldots, N_t$) such that

$$\mathbf{d}_i^T \mathbf{h}_j = \begin{cases} 0, & j \neq i \\ 1, & j = i \end{cases} \tag{7}$$

where ^{T} stands for the transpose of a vector or matrix and $\mathbf{h}_j$ denotes the j-th column of the channel matrix $\mathbf{H}$. However, when we take a closer look to this criterion, solving the weight vectors is equal to finding a matrix $\mathbf{D}$ such that:

$$\mathbf{D} \cdot \mathbf{H} = \mathbf{I} \tag{8}$$

where $\mathbf{D}$ is a matrix that represents the linear processing in the receiver. The i-th row of $\mathbf{D}$ is equal to the transpose of the i-th weight vector $\mathbf{d}_i$ and $\mathbf{I}$ is the identity matrix. So, by forcing the "interferers" to zero, each desired element of $\mathbf{s}$ can be estimated. If $\mathbf{H}$ is not square, $\mathbf{D}$ equals the *pseudo-inverse* of $\mathbf{H}$:

$$\mathbf{D} = \mathbf{H}^+ = \left(\mathbf{H}^H \mathbf{H}\right)^{-1} \mathbf{H}^H \tag{9}$$

where $^+$ represents the *pseudo-inverse*. In order for the pseudo-inverse to exist, N_t must be less than or equal to N_r, because for N_t larger than N_r, $\mathbf{H}^H\mathbf{H}$ is singular and its inverse does not exist [Str88]. Furthermore, note that in order for the inverse to exist, the columns of $\mathbf{H}$ must be independent. Regarding the independent and identically distributed (i.i.d.) assumption of the elements of $\mathbf{H}$, independence is usually an approximation, which is justifiable if 1) the antenna spacing is chosen equal to or larger than $\lambda/2$ [Fos98] (where λ represents the wavelength of the transmission frequency) and 2) the system operates in a rich-scattered environment, which can be modelled by Rayleigh flat-fading. Thus, for $Nr \geq N_t$ and if the inverse of $\mathbf{H}^H\mathbf{H}$ exists, the estimates of $\mathbf{s}$ (given by $\mathbf{s}_{\text{est}}$) can be found by:

$$\begin{aligned} \mathbf{s}_{\text{est}} &= \mathbf{D}\mathbf{x} \\ &= \left(\mathbf{H}^H \mathbf{H}\right)^{-1} \mathbf{H}^H \mathbf{x} \end{aligned} \tag{10}$$

or, equivalently:

$$\mathbf{s}_{\text{est}} = \mathbf{H}^+ \mathbf{x} \tag{11}$$

Using Formula (11), $(s_{\text{est}})_i$, i.e. the i-th component of $\mathbf{s}_{\text{est}}$, can be written as:

$$\left(s_{\text{est}}\right)_i = \mathbf{H}_i^+ \mathbf{x} \tag{12}$$

where $\mathbf{H}_i^+$ represents the *i*-th row of $\mathbf{H}^+$, which, according to Formula (7), is equal to the transpose of the *i*-th weight vector $\mathbf{d}_i$. Note that $\mathbf{d}_i$ is a so-called *nulling vector* [Wol98]. As a final step, $(s_{\text{est}})_i$ can be sliced to the nearest Quadrature Amplitude Modulation (QAM) constellation point, these sliced signals are denoted by $\hat{\mathbf{s}}$. In this way, all N_t elements of **s** can be decoded at the receiver. The diversity order of an (N_t,N_r) system based on ZF is equal to N_r-N_t+1, as shown in [Win94]. Note that a diversity order of one means that the BER improves by a factor of 10^1 if the SNR is increased by 10 dB. In case of a diversity order of two, if the SNR is increased by 10 dB, the BER improves 10^2 times, etc.

4.4.2 The Minimum Mean Square Error solution

Another approach in estimation theory to the problem of estimating a random vector **s** on the basis of observations **x** is to choose a function **g**(**x**) that minimises the Mean Square Error (MSE) [Rap96]

$$\varepsilon^2 = E[(\mathbf{s}-\mathbf{s}_{\text{est}})^H(\mathbf{s}-\mathbf{s}_{\text{est}})] = [(\mathbf{s}-\mathbf{g}(\mathbf{x}))^H(\mathbf{s}-\mathbf{g}(\mathbf{x}))] \tag{13}$$

An exact function ***g(x)*** is usually hard to obtain, however, is we restrict this function to be a linear function of the observations, an exact solution can be achieved. Using linear processing, the estimates of **s** can be found by:

$$\mathbf{s}_{\text{est}} = \mathbf{D}\mathbf{x} \tag{14}$$

Now, to obtain the linear Minimum Mean Square Error (MMSE), **D** must be chosen such that the Mean Square Error ε^2 is minimised:

$$\varepsilon^2 = E[(\mathbf{s}-\mathbf{s}_{\text{est}})^H(\mathbf{s}-\mathbf{s}_{\text{est}})] = E[(\mathbf{s}-\mathbf{D}\mathbf{x})^H(\mathbf{s}-\mathbf{D}\mathbf{x})] \tag{15}$$

To minimise the Mean Square Error (over **D**), the processing at the receiver must be equal to:

$$\mathbf{D} = (\alpha\mathbf{I}+\mathbf{H}^H\mathbf{H})^{-1}\mathbf{H}^H,\ \alpha > 0 \tag{16}$$

where α is equal to $\sigma_n^2/\sigma_s^2 = N_t/\rho$.
From Formula (10) it becomes clear that the ZF solution correspond to an MMSE solution with $\alpha = 0$.

4.5 Non Linear receiver scheme

4.5.1 ZF with Decision Feedback Decoding

The linear nulling approach as described in the previous section is viable, but as will become clear from the results in Section 4, superior performance is obtained if non-linear techniques are used. One can imagine that if somehow first the most

reliable element of the transmitted vector **s** could be decoded and used to improve the decoding of the other elements of **s**, superior performance can be achieved. This is called *symbol cancellation* [Wol98] and it exploits the timing synchronism inherent in the system model (the assumption of co-located transmitters makes this completely reasonable). Furthermore, linear nulling (i.e., ZF) is used to perform detection. In other words, symbol cancellation is based on the subtraction of interference from already detected components of **s** from the receiver signal vector **x**. This results in a modified receiver vector in which, effectively, fewer interferers are present. Because this principle is somewhat analogous to decision feedback equalisation, it is also called Decision Feedback Decoding (DFB).

When symbol cancellation is used, the order in which the components of **s** are detected becomes important to the overall performance of the system. To determine a good ordering of detection, the covariance matrix of the estimation error $\mathbf{s} - \mathbf{s}_{\text{est}}$ will be used. For ZF, this covariance matrix can be shown to be:

$$\begin{aligned} E\left[\left(\mathbf{s}-\mathbf{s}_{\text{est}}\right)\left(\mathbf{s}-\mathbf{s}_{\text{est}}\right)^{H}\right] &= E\left[\left(\mathbf{s}-\left(\mathbf{H}^{H}\mathbf{H}\right)^{-1}\mathbf{H}^{H}\mathbf{x}\right)\left(\mathbf{s}-\left(\mathbf{H}^{H}\mathbf{H}\right)^{-1}\mathbf{H}^{H}\mathbf{x}\right)^{H}\right] \\ &= E\left[\left(\mathbf{s}-\mathbf{s}-\left(\mathbf{H}^{H}\mathbf{H}\right)^{-1}\mathbf{H}^{H}\mathbf{n}\right)\left(\mathbf{s}-\mathbf{s}-\left(\mathbf{H}^{H}\mathbf{H}\right)^{-1}\mathbf{H}^{H}\mathbf{n}\right)^{H}\right] \\ &= E\left[\left(\mathbf{H}^{H}\mathbf{H}\right)^{-1}\mathbf{H}^{H}\mathbf{n}\mathbf{n}^{H}\mathbf{H}\left(\mathbf{H}^{H}\mathbf{H}\right)^{-1}\right] \\ &= \sigma_n^2\left(\mathbf{H}^{H}\mathbf{H}\right)^{-1} \triangleq \sigma_n^2\mathbf{P}_H \end{aligned}$$

(17)

or, using the pseudo-inverse:

$$\mathbf{P} = \mathbf{H}^{+}\left(\mathbf{H}^{+}\right)^{H} \tag{18}$$

Let $(s_{\text{est}})_i$ be the i-th entry of $\mathbf{s}_{\text{est}}$, then, the "best" estimate, $(s_{\text{est}})_i$, is the one for which $\mathbf{P}_{ii}$ (i.e., the i-th diagonal element of $\mathbf{P}_{\text{H}}$) is the smallest, because this is the estimate with the smallest error covariance. From Formula (18) it becomes clear that $\mathbf{P}_{ii}$ is equal to the squared length of the i-th row of the pseudo-inverse. So find the minimum squared length row of $\mathbf{H}^{+}$ is equivalent. Suppose that the order in the pseudo-inverse of **H** is arranged so that the row with the least squared length becomes the last row (the i-th row of $\mathbf{H}^{+}$ is permuted with the N_t-th row), then the N_t-th element of $\mathbf{s}_{\text{est}}$ can be independently decoded. Let $\hat{s}_N$ denote the decoded value, then this value can be used to improve the estimate of the remaining N_t–1 signals (i.e., symbol cancellation). If this procedure to find the “best” estimate is performed in a recursive way, the so-called Optimal Detection (OD) method as described in [Wol98] is obtained. Here it is called the Decision Feedback Decoding algorithm with optimal detection. The recursive algorithm can be described as follows:

1. Compute $\mathbf{H}^{+}$;

2. Find the minimum squared length row of $\mathbf{H}^{+}$ and permute it to be the last row, permute the columns of **H** accordingly;

3. Form the estimate of the last component of **s**. In case of ZF: $\left(\mathbf{s}_{\mathbf{est}}\right)_{N_t} = \mathbf{H}_{N_t}^{+}\mathbf{x}$, where the transpose of $\mathbf{H}_{N_t}^{+}$ is said to be the N_t-th nulling vector [Wol98];

4. Obtain $\hat{\mathbf{s}}_{N_t}$ (via slicing) from $\left(\mathbf{s}_{\mathbf{est}}\right)_{N_t}$;

5. (While $N_t - 1 > 0$) go back to step 1, but now with:
$\mathbf{H} \to \mathbf{H}^{(N_t-1)} = [\mathbf{h}_1 \quad \cdots \quad \mathbf{h}_{N_t-1}]$, $\mathbf{x} \to \mathbf{x} - \mathbf{h}_{N_t}\mathbf{s}_{N_t}$ and $N_t \to N_t - 1$.

Note that in case step 2 is skipped, the DFB algorithm is performed without optimal detection and the overall performance will be less, however, processing time is saved.

4.5.2 Minimum Mean Square Error with Decision Feedback Decoding (V-BLAST)

In order to perform Decision Feedback Decoding with Minimum Mean Square Error decoding, the DFB algorithm of Section 2.6.1 has to be adapted somewhat. Again, the covariance matrix of the estimation error **s** – $\mathbf{s}_{\text{est}}$ will be used to determine a good ordering of detection. For MMSE, this covariance matrix can be shown to be:

$$
\begin{aligned}
E[(\mathbf{s}-\mathbf{s}_{\mathbf{est}})(\mathbf{s}-\mathbf{s}_{\mathbf{est}})^H] &= E[\big(\mathbf{s}-\mathbf{D}(\mathbf{Hs}+\mathbf{v})\big)\big(\mathbf{s}-\mathbf{D}(\mathbf{Hs}+\mathbf{v})\big)^H] \\
&= E[\big((\mathbf{I}-\mathbf{DH})\mathbf{s}-\mathbf{Dv}\big)\big((\mathbf{I}-\mathbf{DH})\mathbf{s}-\mathbf{Dv}\big)^H] \\
&= \sigma_s^2\left(\mathbf{I}-\mathbf{DH}-\mathbf{H}^H\mathbf{D}^H+\mathbf{DHH}^H\mathbf{D}\right)+\sigma_v^2\mathbf{DD}^H \\
&= (\sigma_s^2\{\alpha\mathbf{I}+\mathbf{H}^H\mathbf{H}-\mathbf{H}^H\mathbf{H}-\left(\alpha\mathbf{I}+\mathbf{H}^H\mathbf{H}\right)^{-1}\mathbf{H}^H\mathbf{H}\left(\alpha\mathbf{I}+\mathbf{H}^H\mathbf{H}\right) \\
&\quad +\left(\alpha\mathbf{I}+\mathbf{H}^H\mathbf{H}\right)^{-1}\mathbf{H}^H\mathbf{HH}^H\mathbf{H}\}+\sigma_v^2\left(\alpha\mathbf{I}+\mathbf{H}^H\mathbf{H}\right)^{-1}\mathbf{H}^H\mathbf{H})\left(\alpha\mathbf{I}+\mathbf{H}^H\mathbf{H}\right)^{-1} \\
&= \sigma_v^2\left(\alpha\mathbf{I}+\mathbf{H}^H\mathbf{H}\right)^{-1} \hat{=} \sigma_v^2\mathbf{P}
\end{aligned}
\tag{19}
$$

Note that **P** is somewhat different from the case where ZF is used as detection. In order the do DFB based on the MMSE algorithm, the DFB algorithm is adapted and becomes:

1. Compute **D** (**P** is obtained while computing **D**);

2. Find the smallest diagonal entry of **P** and suppose this is the *i*-th entry. Permute the *i*-th column of **H** to be the last column and permute the rows of **D** accordingly;

3. Form the estimate of the "best" component of **s**: $(s_{\text{est}})_{N_t} = \mathbf{D}_{N_t}\mathbf{x}$, where $\mathbf{D}_{N_t}$ represents the last row of **D** and its transpose is the N_t-th nulling vector [Wol98];

4. Obtain $\hat{\mathbf{s}}_{N_t}$ (via slicing) from $(\mathbf{s}_{\text{est}})_{N_t}$;

5. (While $N_t - 1 > 0$) go back to step 1, but now with:

$\mathbf{H} \to \mathbf{H}^{(N_t-1)} = [\mathbf{h}_1 \quad \cdots \quad \mathbf{h}_{N_t-1}]$, $\mathbf{x} \to \mathbf{x} - \mathbf{h}_{N_t}\hat{\mathbf{s}}_{N_t}$ and $N_t \to N_t - 1$.

In the following chapters, we will refer to this algorithm as V-BLAST (Vertical Bell Laboratory Space Time Architecture) which is the widely spread name used in literature to identify this technique.

4.5.3 Maximum likelihood Decoding

MLD is a method that compares the received signal with all possible transmitted signals and estimates **s** according to the Maximum Likelihood principle. Suppose a matrix **C** gives all possibilities in **s** that could occur (the dimensions of **C** are $N_t \times K$, where $K = Q^{N_t}$ and Q represents the number of constellation points). Then, the receiver should store a matrix **Y** such that:

$$\mathbf{Y} = \mathbf{H} \cdot \mathbf{C} = [\mathbf{y}_1 \quad \cdots \quad \mathbf{y}_K] \tag{20}$$

At the receiver, the most likely transmitted signal is determined, as the one for which

$$\left\|\mathbf{x} - \mathbf{y}_j\right\|^2 \tag{21}$$

is minimal (with $1 \le j \le K$), i.e., the signal $\mathbf{s}_j$ that corresponds with the vector $\mathbf{y}_j$ which lays closest to the received vector is said to be the most likely signal to be transmitted. Thus, $\hat{\mathbf{s}}$ is chosen to be the j-th column of **C**. This can be rewritten to the following formula where $\mathbf{s}_{\text{ml}}$ represents the maximum likelihood detection of the transmitted signal **s**:

$$\hat{\mathbf{s}} = \mathbf{s}_{\text{ml}} = \arg \min_{\mathbf{s}_j \in \{\mathbf{s}_1, \ldots, \mathbf{s}_K\}} \left\|\mathbf{x} - \mathbf{H}\mathbf{s}_j\right\|^2 \tag{22}$$

MLD is optimal in terms of BER performance. However, a major disadvantage is that the complexity of MLD is proportional to Q^{N_t}, due to the fact that the size of **Y** grows exponentially with N_t.

Another way to show the superiority in BER performance of MLD over the other SDM techniques is by checking its diversity order. It is shown in [Nee00-1] that the diversity order of a MLD system with N_r receive antennas is equal to N_r.

Note that in the case of MLD, it is not required that $N_t \le N_r$.

Soft Output MLD

The MLD technique can be modified to deliver not only the most likely transmitted symbol, but also reliable values, which are known as soft-decision outputs. Hagenauer presents in [Hag89] a method to derive soft-decision values. There, the log likelihood ratio is used as an indication for the reliability of a bit. If **x** denotes the received vector, b_l is the l-th bit to estimate, **H** is the estimated channel matrix and $\mathbf{s}_j$ is one of the possible transmitted vectors (with $1 \le j \le K$, where $K = Q^{N_t}$ and Q represents the number of constellation points), then the L-value of the estimated bit is:

$$L(b_l) = \ln \frac{P(b_l = 1|x)}{P(b_l = 0|x)} = \ln \frac{\sum_{s_j|b_l=1} P(s_j|x)}{\sum_{s_j|b_l=0} P(s_j|x)} = \ln \frac{\sum_{s_j|b_l=1} p(x|s_j)P(s_j)}{\sum_{s_j|b_l=0} p(x|s_j)P(s_j)} \tag{23}$$

Because the vectors $\mathbf{s}_j$ are equally likely to be transmitted, $P(\mathbf{s}_j)$ is equal for all vectors $\mathbf{s}_j$. Using the probability density function of a multivariate normal distribution give a certain channel, we find the soft-output decisions:

$$L(b_l) = \ln \frac{\sum_{s_j|b_l=1} \exp\left(-\frac{\|x - Hs_j\|^2}{\sigma_n^2}\right)}{\sum_{s_j|b_l=0} \exp\left(-\frac{\|x - Hs_j\|^2}{\sigma_n^2}\right)} \approx \ln \frac{\exp\left(\max_{s_j|b_l=1} -\frac{\|x - Hs_j\|^2}{\sigma_n^2}\right)}{\exp\left(\max_{s_j|b_l=0} -\frac{\|x - Hs_j\|^2}{\sigma_n^2}\right)} \tag{24}$$

$$= \frac{1}{\sigma_n^2}\left(\min_{s_j|b_l=0} \|x - Hs_j\|^2 - \min_{s_j|b_l=1} \|x - Hs_j\|^2\right)$$

Soft Output technique will be used together with MLD for simulation. We will refer to it as SOMLD.

4.6 Space time block codes

In STBC the input to the encoder is a stream of modulated symbols from a real or complex constellation. The encoder operates on a block of K symbols which are distributed on different antennas (space) and on T symbol times. The result are matrix codewords whose rows correspond to antennas and columns correspond to symbol times. The ratio K/T gives the coding rate.

Alamouti scheme

At the transmitter side Alamouti scheme exploits two transmitting antennas that in two transmission time slots (*T1, T2*), emit two symbols according to the following scheme [Ala98]:

	Antenna 1	Antenna 2
T1	S_1	S_2
T2	$-S_2^*$	S_1^*

Table 4-1: Alamouti scheme.

Where the sign '*' means conjugation.
The first stage receiver combines the signals coming from two different transmit branches in the two consecutive times while the second stage performs Maximum Likelihood Detection (MLD).

The received signal will be:

$$\begin{bmatrix} x_1 \\ x_2 \end{bmatrix} = \begin{bmatrix} s_1 & s_2 \\ -s_2^* & s_1^* \end{bmatrix} \begin{bmatrix} h_1 \\ h_2 \end{bmatrix} + \begin{bmatrix} n_1 \\ n_2 \end{bmatrix} \quad (25)$$

The above equations can be written using the equivalent orthogonal channel matrix as:

$$\begin{bmatrix} x_1 \\ x_2^* \end{bmatrix} = \begin{bmatrix} h_1 & h_2 \\ h_2^* & -h_1^* \end{bmatrix} \begin{bmatrix} s_1 \\ s_2 \end{bmatrix} + \begin{bmatrix} n_1 \\ n_2^* \end{bmatrix} \quad (26)$$

If the channel is known, the estimated transmit signal can be easily found through the channel match-filter. This algorithm reaches the optimum capacity [Ala98].

$$\begin{bmatrix} \hat{s}_1 \\ \hat{s}_2 \end{bmatrix} = \begin{bmatrix} h_1^* & h_2 \\ h_2^* & -h_1 \end{bmatrix} \begin{bmatrix} x_1 \\ x_2^* \end{bmatrix} = \left(|h_1|^2 + |h_2|^2 \right) \begin{bmatrix} s_1 \\ s_2 \end{bmatrix} + \begin{bmatrix} h_1^* n_1 + h_2 n_2^* \\ h_2^* n_1 - h_1 n_2^* \end{bmatrix} \quad (27)$$

Generalization of Alamouti Scheme
The generalization of orthogonal matrix codewords for more than 2 transmit antennas does not reach unitary transmission rate. Different Space Time Blocks schemes for 3 and 4 antennas were proposed in [Tar99], see Table 5.2.

Antenna Configuration	*Coding Rate*
2x2	1
3x1-3x2	½
3x1-3x2	¾
4x1-4x2	½
4x1-4x2	¾

Table 4-2: Proposed STBC schemes from [Tar99].

4.7 Conclusions

Different MIMO algorithms are presented in this chapter.
Space Division Multiplexing techniques:

- ZF: is linear and does not use any other knowledge that the channel estimation. Its diversity is equal to N_r-N_t+1
- MMSE: is also linear but requires the noise variance estimation and channel estimation.
- ZF and MMSE with DFB: Direct feedback is used together with respectively ZF and MMSE to improve their performance. VBLAST is another name for theses techniques.
- MLD: non linear, but provides the maximum likelihood solution. Its diversity is equal to N_r.

Space Time Block Codes algorithms:

- Alamouti: it is a simple algorithm at both transmitter and receiver. It reaches the optimum capacity but only for a 2x1 system.

5 Applying MIMO techniques in WLAN systems

This chapter regards the application of MIMO techniques to wireless LANs. It assesses of the performance of WLAN systems applying the MIMO techniques proposed in the previous chapter. These results enable us to rank the performance and robustness of the MIMO techniques in noise and interference limited scenarios. Simulations are the first mean of evaluation.

Section 5.1 specifies the most important OFDM parameters, as in the WLAN IEEE 802.11a/g standard. Section 5.2 presents the transmitter and receiver blocks. In Section 5.3 some simulation results are shown and analysed. In Section 5.4 co-channel interference and its impact on MIMO-OFDM systems are discussed. Finally, in Section 5.5 conclusions are drawn.

5.1 MIMO with OFDM

The previously described SDM algorithms are narrowband single carrier algorithms. WLAN system are generally broadband and based on orthogonal frequency division multiplexing (OFDM). OFDM is a multi carrier technique and, within the standards, the signal time per subcarrier is defined to be T_S = 3.2 μs. Based on the observations that indoor rms delay spreads are most likely smaller then 250 ns [Nee00], we can assume that every subcarrier undergoes flat-fading, since T_S is (much) larger than the rms delay spread [Rap89]. So, in order to combine SDM with OFDM, a SDM algorithm can be performed per subcarrier. Thus, suppose the transmitter consists of N_t transmit antennas, then every subcarrier carries N_t data streams. At the N_r-th receive antennas the subcarrier information is separated by using FFTs. After that the N_r information symbols belonging to subcarrier i are routed to the i-th MIMO decoder where one of the algorithms of Chapter 4 is implemented to recover the transmitted data signals ($d_{1,i}$,…, $d_{N,i}$), where the first subscript indicates the transmit antenna and the second one indicates the subcarrier number. This is shown in Figure 5-1 and Figure 5-2. The SDM techniques of Section 4.3-4.4 combined with OFDM have been programmed in MATLAB. Simulations have been performed to obtain Bit Error Rate (BER) and Packet Error Rate (PER) characteristics in order to compare the performance of the different SDM techniques.

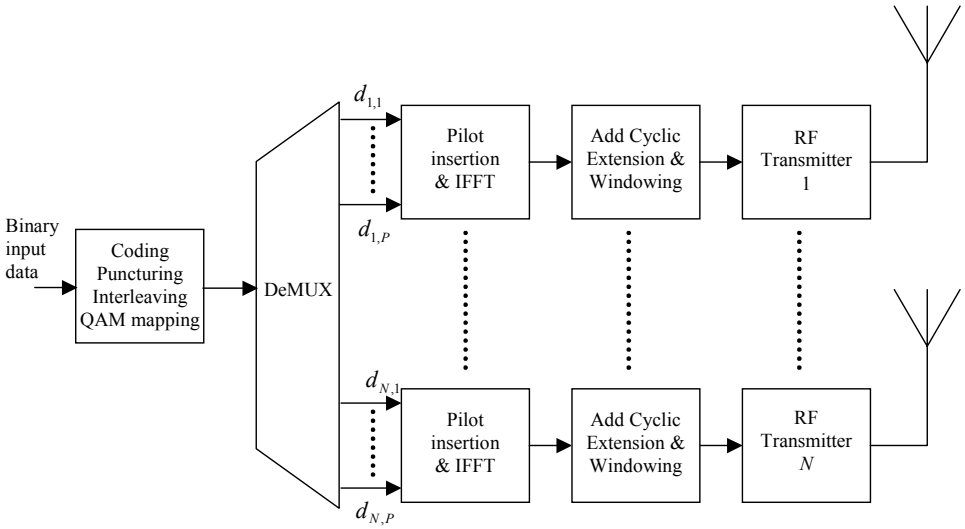

Figure 5-1: Multi-antenna joint coding architecture transmitter using OFDM.

5.2 Transmitter and receiver design

The transmitting part consists of a multi-antenna transmitter, which is represented schematically in Figure 5-1. The binary input data is fed to the encoder. A convolutional code with the IEEE 802.11a standard rate 1/2, constraint length 7 and generator polynomials (133,171) is chosen as a forward error correction code. Higher coding rates of 2/3 and 3/4 are obtained by puncturing the rate 1/2 code. In order for the forward error correction to correct for subcarriers and/or antennas that are in deep fades, the coded data is interleaved over frequency and space to reduce the number of bit errors in one burst. The interleaver size is chosen based on the assumption that the channel is quasi-static. The bits are then mapped on QAM symbols according to the IEEE 802.11a standard. The output of the decoder is then demultiplexed into N_t blocks of N_c streams, where N_c is the number of subcarriers. After pilot insertion, the Inverse Fast Fourier Transform (IFFT) is performed on each block, resulting in N_t signals in the time domain. Cyclic extension and windowing are based on the IEEE 802.11a standard.

At the receiver, as depicted in Figure 5-2, perfect synchronisation (time and frequency wise) and channel knowledge is assumed. After the payload is received, the cyclic extension is removed, the FFT is executed and the pilots are removed. Once the subcarrier information is retrieved, the desired MIMO processing (i.e. ZF, VBLAST or MLD…) can be performed. The output of the MIMO processing is sliced (i.e., demodulated), deinterleaved and depunctured. Finally, the depunctured bits are decoded using a Viterbi decoder.

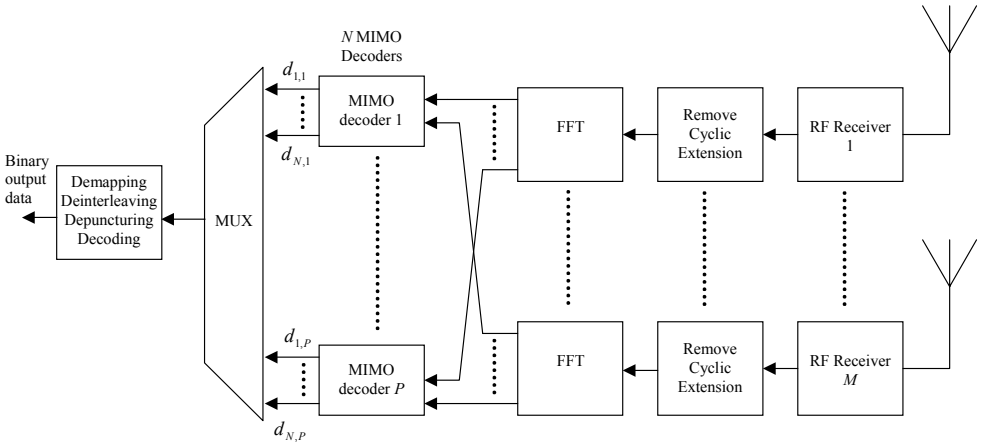

Figure 5-2: Multi-antenna receiver using SDM with OFDM.

Per-Antenna-Coding (PAC) architecture, as illustrated in Figure 5-3, is also assessed through link level simulations. V-BLAST (Section 4.5.2) is used at the receiver. Per Antenna Coding V-BLAST is a variant of V-BLAST based on per antenna coding architecture (see Section 4.3). The difference with joint coding architecture is that the coding and the interleaving at the transmitter are now done per antenna branch. At the receiver, the idea is first to go through the decoding stage before the Successive Interference Cancellation (SIC) is executed. In this way Forward Error Correcting coding is performed on the SIC information. In Figure 5-3 and Figure 5-4 a schematic representation of the transmitter and the receiver of a system deploying PAC V-BLAST is represented [Zel03]. The MIMO OFDM transmitter consists of N_t OFDM transmitters among which the incoming bits are spread, then each branch in parallel performs encoding, interleaving (Π), QAM mapping, N_c-point Inverse Fast Fourier Transformation (IFFT), and adds the cyclic extension before the final TX signal is upconverted to RF and sent.

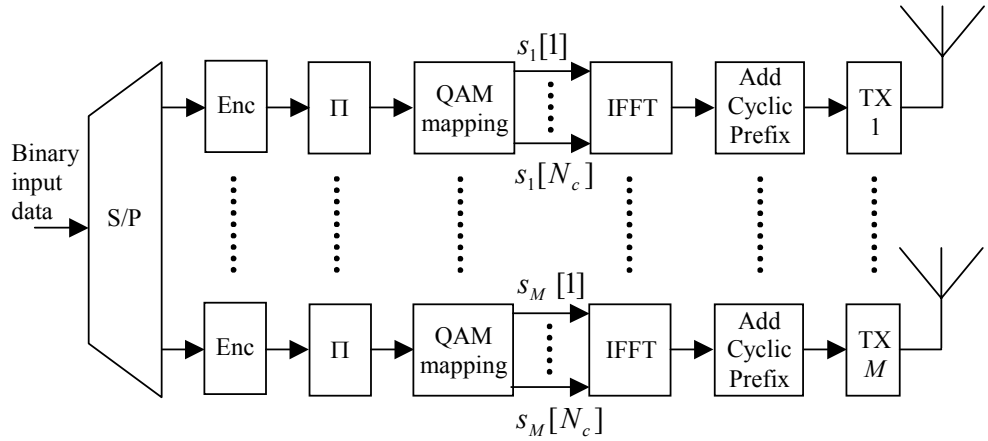

Figure 5-3: PAC MIMO OFDM transmitter scheme.

At the N_r receivers, the subcarrier information is separated by performing the N_c-point Fast Fourier Transformation (FFT). Then, in general, the symbols mapped onto subcarrier i are routed to the i-th MIMO detector to recover the M transmitted

data signals per subcarrier (see Figure 5-4). Finally, demapping, deinterleaving (Π^{-1}) and decoding are performed per receiver branch and the resulting data are combined to obtain the binary output data.

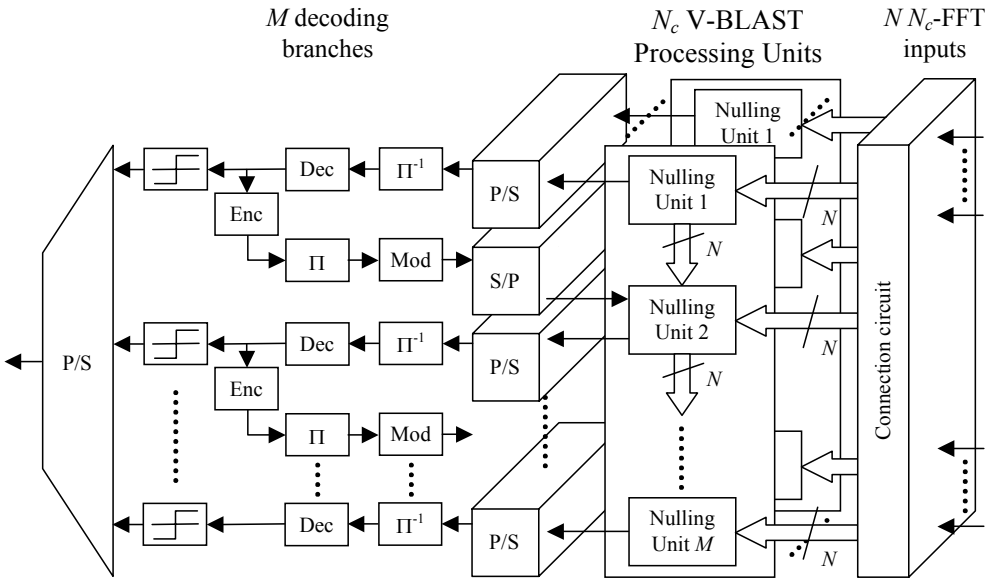

Figure 5-4: The PAC V-BLAST Detection and Decoding Block.

5.3 Performance evaluation: noise-limited scenarios

The goal of this section is to present the PER (64 bytes) versus SNR performance of the MIMO algorithms presented in Chapter 4. Although more results are presented in Chapter 6, results for some test case are presented here to provide a more practical understanding of the performance of the different MIMO algorithms. The channel used for the simulations is described in [B4-D2.2] and exhibits a RMS delay of 50ns. The algorithms deployed at the receiver were ZF, MMSE and MLD.

Figure 5-5 shows the PER (64 byte packet) versus SNR for a 2x2 system using coding rate 1/2 and QPSK modulation. MLD clearly achieves the best performance followed by MMSE and ZF. The spectral efficiency achieved by a 2x2 system with 1/2 rate convolutional code and QPSK modulation is 1.2 bps/Hz. This translates into a data rate of 24Mbps.

In Figure 5-6 coding rate 0.75 and 16QAM modulation are used at the transmitter. The spectral efficiency achieved by a 2x2 system with 3/4 rate convolutional code and 16QAM modulation is 3.6 bps/Hz. This translates into a data rate of 72 Mbps. All curves shift to the right due to the higher data rate that is now transmitted. MLD still shows the best performance. MMSE loses the advantage over ZF observed for lower constellations.

The performance degradation going from QPSK to 16QAM for MLD and ZF is around 11-12 dB at PER=10^{-2}, while for MMSE is almost 15dB.

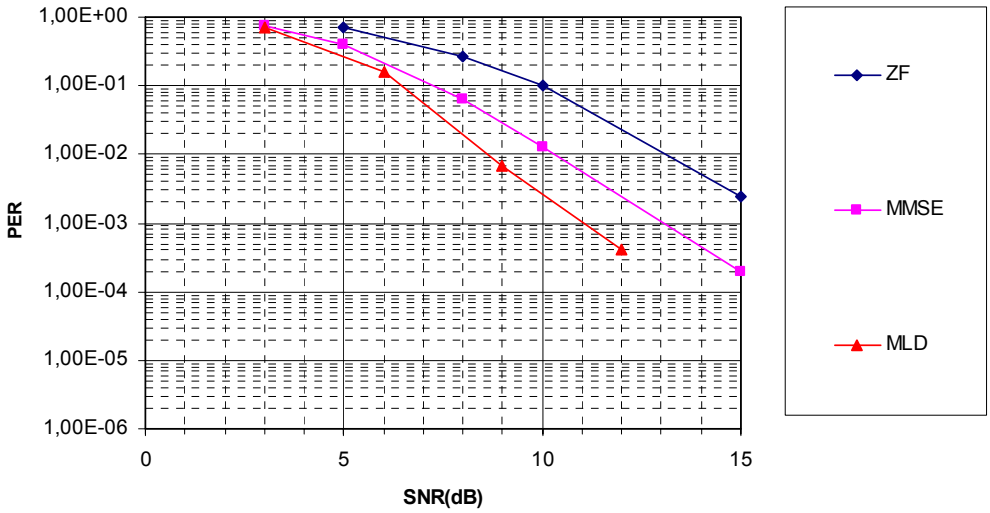

Figure 5-5: PER versus SNR performance of a 2x2 system for different receive algorithms. At the transmitter QPSK modulation and a convolutional coding rate of 1/2 are used. The RMS delay spread of the channel is 50ns.

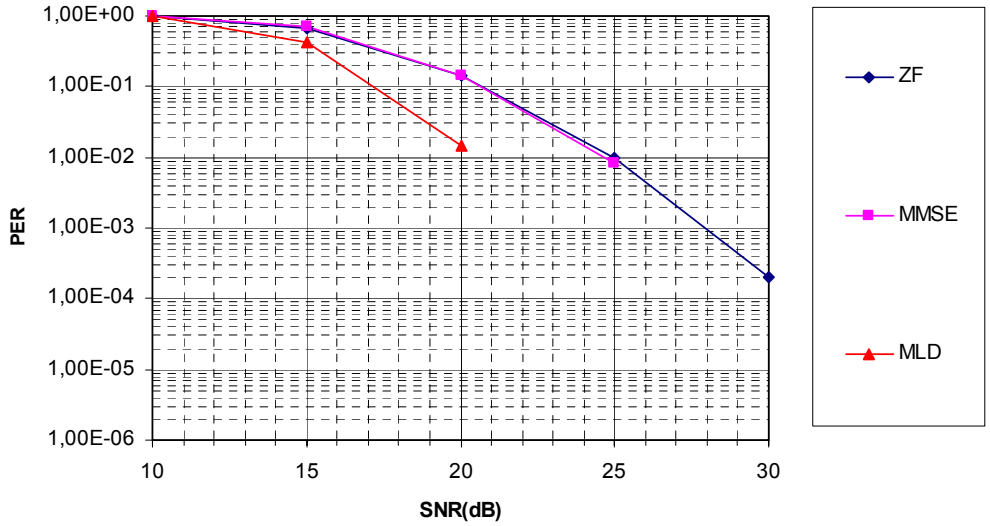

Figure 5-6: PER versus SNR performance of a 2x2 system for different receive algorithms. At the transmitter 16QAM modulation and a convolutional coding rate of 3/4 are used. The RMS delay spread of the channel is 50ns.

Figure 5-7 and Figure 5-8 use the same coding rate and modulations as Figure 5-5 and Figure 5-6, respectively, only then for a 4x4 system. The MLD curve is steeper than in the previous figures, which is due to the fact that the diversity order, which is proportional to the number of receive antennas, is now higher. As expected, the slope of the ZF curve does not change since the diversity order, which is given by N_t-N_r+*1* is still equal to 1 for the 4x4 case. Again for higher constellation MMSE degrades more than MLD and ZF.

The spectral efficiency achieved by a 4x4 system with coding rate equal 1/2 using QPSK is 2.4 bps/Hz, which translates in a data rate equal to 48Mbps. The spectral efficiency achieved by a 4x4 system with 3/4 rate convolutional code using 16 QAM is 7.2 bps/Hz. This translates into a data rate of 144 Mbps.

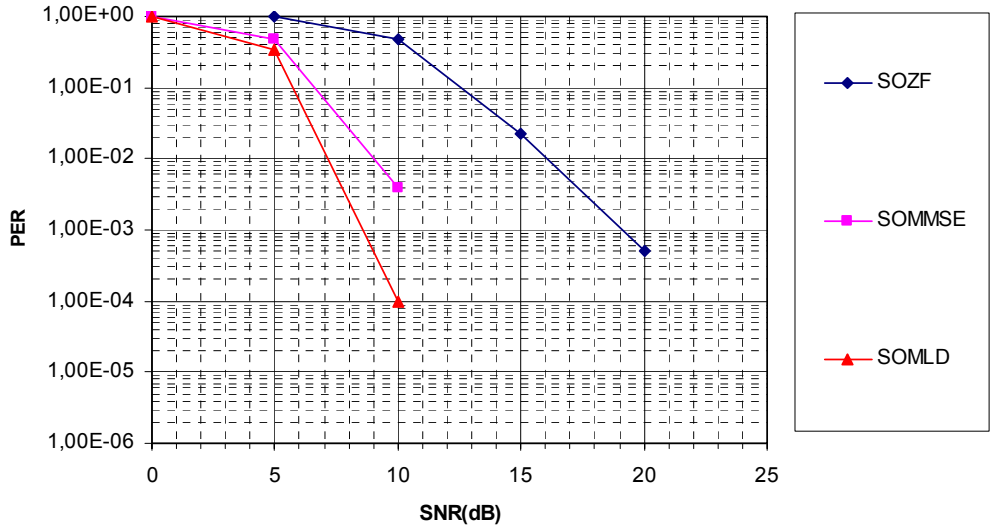

Figure 5-7: PER versus SNR performance of a 4x4 system for different receive algorithms. At the transmitter QPSK modulation and convolutional coding rate of 1/2 are used. The RMS delay spread of the channel is 50ns.

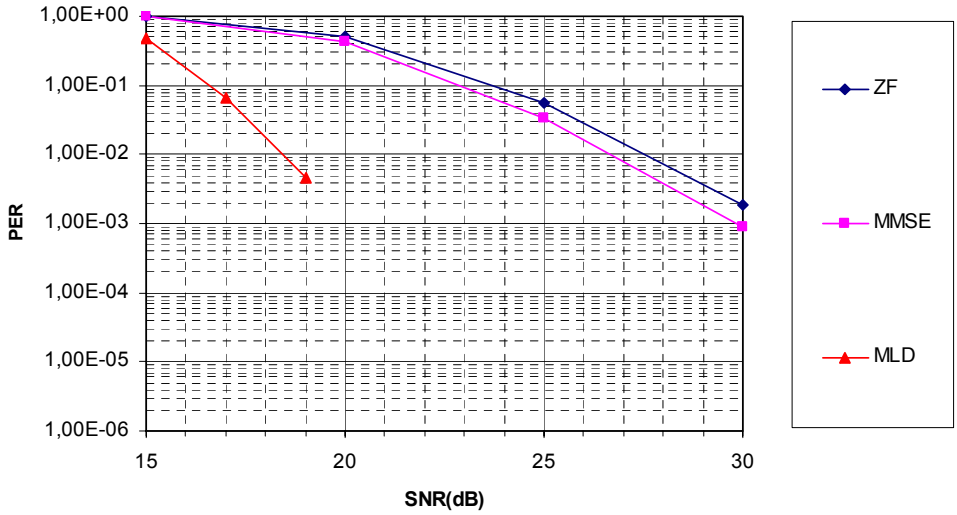

Figure 5-8: PER versus SNR performance of a 2x2 system for different receive algorithms. At the transmitter 16QAM modulation and convolutional coding rate of 3/4 are used. The RMS delay spread of the channel is 50ns.

The conclusion from these simulations results is that MLD is the best performing algorithm, especially for high number of antennas, followed by MMSE and ZF. More results are presented in Chapter 6, where the additional results give a broader view on performance of more MIMO algorithms for different channel delay spreads, constellations, codes and antenna configurations.

5.4 Performance evaluation: interference-limited scenarios

The goal of this section is to asses the performance of MIMO based WLAN system in co-channel interference limited environment. We regard the case where no attempt is made to cancel interference. First the co-channel interference model is described. Subsequently, the results from simulation with this model are presented.

5.4.1 Co-channel Interference model

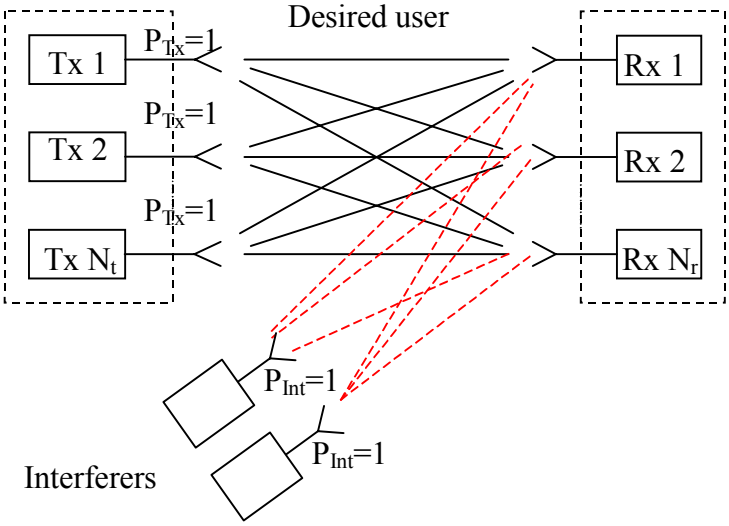

Figure 5-9: MIMO system model in presence of two sources of co-channel interference.

A source of interference has been implemented in MATLAB in order to test the robustness of a MIMO system in an interference-limited scenario. The interferers are OFDM systems transmitting in the same bandwidth of the desired user. The number of antennas used by the interferer can be selected to be single or multiple. Unless it is specified, the term interference will always be used for co-channel interference.

The interference signal is implemented as a random sequence of modulated symbols constantly overlapping the desired user signal and with power equal to one. The time version of the interference signal is convolved with a channel created in a similar way as the one of the desired user. To come to the right average signal-to–interference ratio (SIR), the signals from each interference source are multiplied by the square root of a factor beta defined as:

$$\beta = \frac{N_t}{N_{\text{int}} \cdot num_{\text{int}} \cdot SIR} \tag{4}$$

Where, N_t is the number of transmit antennas of the desired user, N_{int} is the number of transmit antennas of the interferer, num_{int} is the number of interferers and *SIR* is the signal to interference ratio. With $N_{\text{int}} \cdot num_{\text{int}}$ interference sources, the interference power is $N_{\text{int}} \cdot num_{\text{int}} \cdot \beta$. Whereas the power of the desired user is N_t. Thus we get the following ratio:

$$\frac{N_t}{N_{\text{int}} \cdot num_{\text{int}} \cdot \beta} = SIR \tag{5}$$

Notice that the interference signal power after using the beta factor is not anymore dependent on the number of transit antennas.
Finally, interference, desired signal and White Gaussian noise are added together.
In the simulation presented in next section, the interference source is constantly present during the transmission of the desired user (i.e. it has the same length *D* of the desired user packet and no temporal shift). Moreover the channel of the desired user is supposed ideally known and for all simulations and its RMS delay spread used is 50ns.
When co-channel interference is considered, the signal model is described by:

$$\mathbf{x} = \mathbf{Hs} + \sum_{i=1}^{num_{\text{int}}} \mathbf{H}_{\text{int},i}\mathbf{s}_{\text{int},i} + \mathbf{n} \tag{6}$$

where $\mathbf{H}_{\text{int,i}}$ is the channel experienced by the ith interference signal and $\mathbf{s}_{\text{int},i}$ is the ith interference signal.

5.4.1.1 Synchronous versus asynchronous model when the channel is ideally known

In the simulations that will follow, it is assumed that the interference source is constantly present during the transmission of the desired user. We will refer to this sort of interference as synchronous interference. When a uniformly distributed shift in the interval [-*D, D*] is created to produce a random temporal overlapping between the desired user and the interference, the average interference energy is half of the one experienced in the synchronous interference scenario. This result comes from the fact that the average overlapping time is *D*/2. Now let's assume that the channel is ideally known. It can be shown by means of simulations that the synchronous model and the asynchronous model produce the same BER versus SIR curves if the power of the asynchronous interference is doubled. It can be concluded that when the channel is considered perfectly known, the asynchronous case is a special case of the synchronous one. It is possible by a proper scaling to gather the BER performance for the asynchronous case from the synchronous one. For this reason in next sections, where channel is assumed perfectly known, the synchronous interference model has been used for the link level simulations.

5.4.1.2 Noise to model co-channel interference

When the number of co-channel interferers is high (>>1), the total interference signal can be more easily modelled as White Gaussian noise. The result of this is a better BER versus SIR performance, when coding is used. This is shown in Figure 5-10.

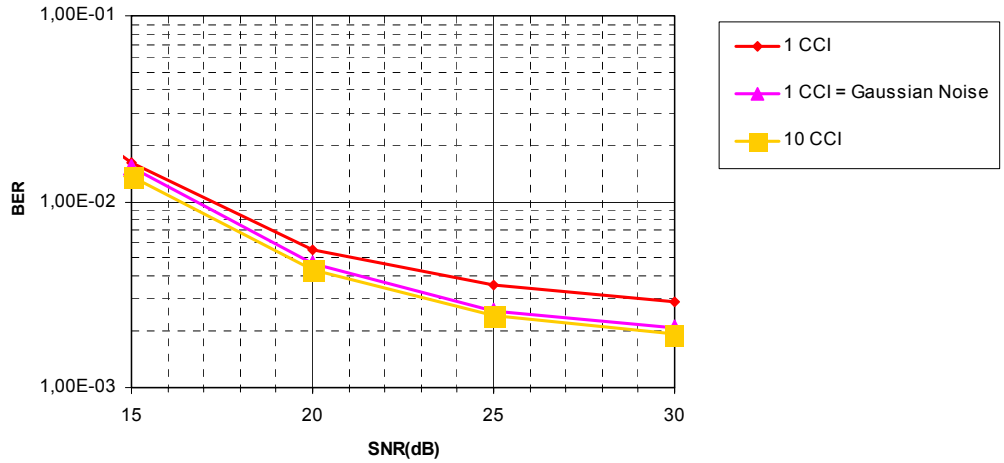

Figure 5-10: BER versus SNR performance for SIR=15dB, with 1 OFDM co-channel interference source, 10 OFDM sources, 1 noise modelled co-channel interference.

In general it is not expected that a high number of co-channel interference sources will be observed. However, it appears that an interference source exploiting multiple transmitters is less harmful that one exploiting a single antenna.

5.4.2 Impact of Co-Channel Interference on MIMO and SISO systems

In this section we analyse the performance of MIMO transceivers in an interference-limited scenario as described in 6.4.1. Our first goal is to compare the performance of a MIMO and SISO system in the same interference scenario.

Figure 5-11 shows the performance, in terms of BER versus SNR, of a 1x1 system versus a 2x2 system with different level of co-channel interference (SIR). QPSK modulation with no coding is used. There are two sources of interference, both having a single antenna. It is clear from Figure 5-11 that for high level of interference (SIR $\leq$ 10dB) the performance of both SISO and MIMO system is the same. When the SIR = 20dB, the spatial diversity exploited by the MIMO receiver produce a better BER performance. It is worthy to notice that the spectral efficiency achieved by MIMO is double of the one achieved by the SISO system. Thus we can conclude that a SISO and a MIMO system using the same data rate per antenna offer the same performance at low SIR values.

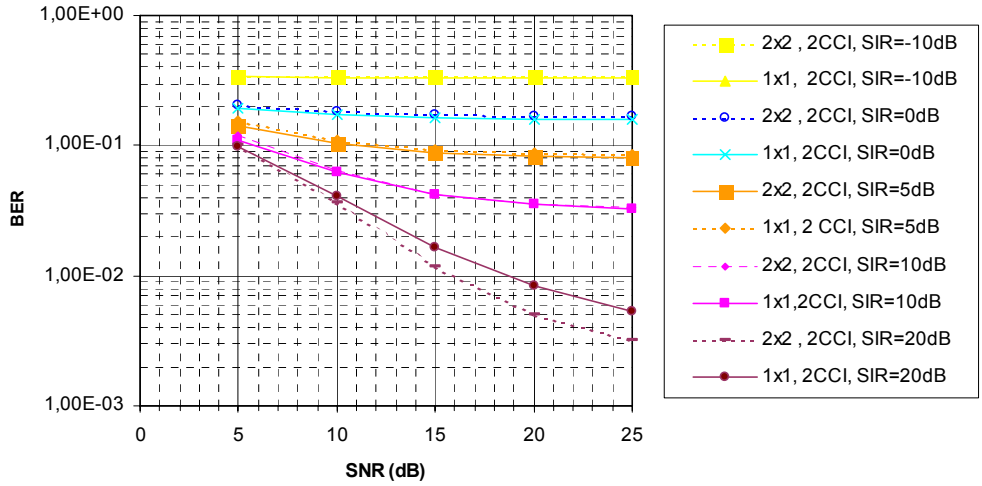

Figure 5-11: BER vs SNR for a 1x1 and a 2x2 system using QPSK no coding.

For the results shown in Figure 5-12 and Figure 5-13, coding and modulation are chosen in such a way that the spectral efficiency is the same in both systems. Figure 5-12 shows the comparison in BER versus SIR and SNR, of a 2x2 system using BPSK modulation and coding rate ½ and a 1x1 system using QPSK modulation and coding rate ½. In both cases the spectral efficiency is equal to 1,2 bps/Hz. We can conclude that for a given spectral efficiency, a MIMO system is more robust to interference than a SISO system. This is due to the fact that MIMO uses lower modulation schemes (per antenna) than SISO to achieve the same data rate. At system level more packets will be correctly delivered by a MIMO system increasing the total throughput. Figure 5-13 shows the same as 2x2 BPSK vs 1x1 QPSK, R=1/2. Both systems achieve the same spectral efficiency, equal to 2.4bps/Hz**.**

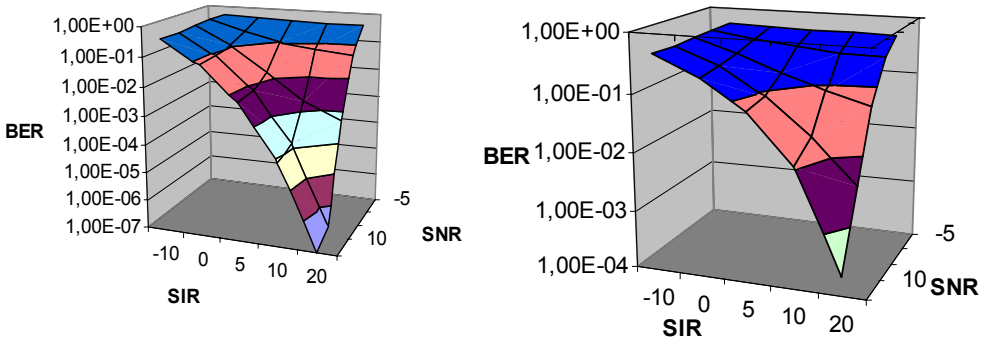

Figure 5-12: 2x2 BPSK vs 1x1 QPSK, R=0.5. Both systems achieve the same spectral efficiency, equal to 2.4bps/Hz.

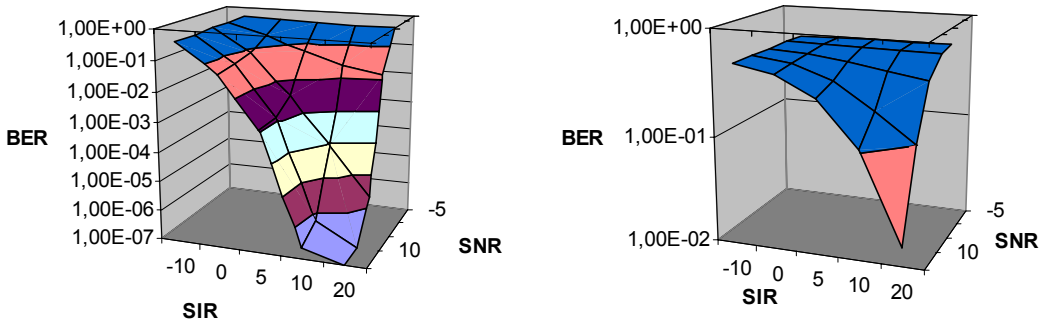

Figure 5-13: 4x4 BPSK vs 1x1 16QAM, R=1/2. Both systems achieve the same spectral efficiency, equal to 2.4bps/Hz.

5.4.2.1 Robustness of MIMO to co-channel interference

Figure 5-14 and Figure 5-15 show the BER performance versus SIR of a 2x2 system using PAC V-BLAST. BPSK modulation and a half rate code have been used. The difference between the two figures is the RMS delay spread: which is respectively 50ns and 250ns. For both simulations two interference sources has been considered: a single antenna transmitter (indicated in the legend of the figures below as SIMO) and a multiple antenna transmitter one (indicated in the legend of figures below as MIMO). The figures depicted below show the BER performance versus the SIR for the given SNR. The SNR value is chosen to get a BER around 10^{-4} or lower. As expected, all the curves tend to reach, for high SIR values (no interference), the BER value at the chosen SNR, which is identified in each figure by the asymptote. Note that in PAC V-BLAST the ideal knowledge of beta is assumed. So in order to minimize the Mean Square Error (over **D**), the processing at the receiver is equal to:

$$\mathbf{D} = \left(\alpha\mathbf{I} + \beta\mathbf{I} + \mathbf{H}^H\mathbf{H}\right)^{-1}\mathbf{H}^H \qquad (7)$$

where α equals N_t/SNR and β is as defined as in (4), where $\boldsymbol{H}$ is the N_rxN_t channel matrix.

For low delay spread, there is no difference in performance when the reception of a 2x2 system is corrupted by a single transmit antenna interference or by a multiple transmit antenna interference.

At a delay spread of 250 ns the performance in presence of a multiple antenna interferer is slightly better than in the case of a single antenna interferer. This is due to the fact that a higher number of interferers make the spectrum of the overall interferer signal flatter over frequency. For high delay spreads and when coding is used, this kind of spectrum has a lighter impact, on average, on each subcarrier of the received signal. This is more visible in Figure 5-17 for a 4x4 system.

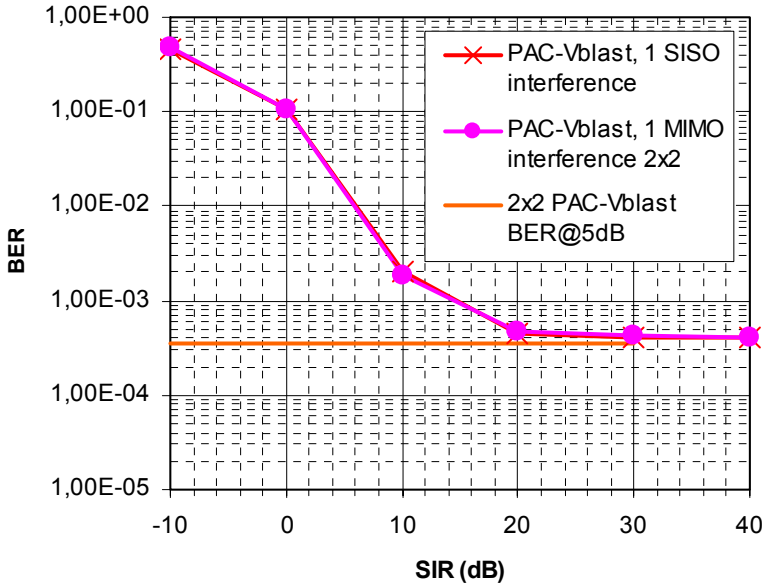

Figure 5-14: BER versus SIR for a 2x2 system. The RMS delay spread is 50 ns and the Eb/No is fixed at 5 dB. The source of interference is one terminal with either one or two transmit antennas.

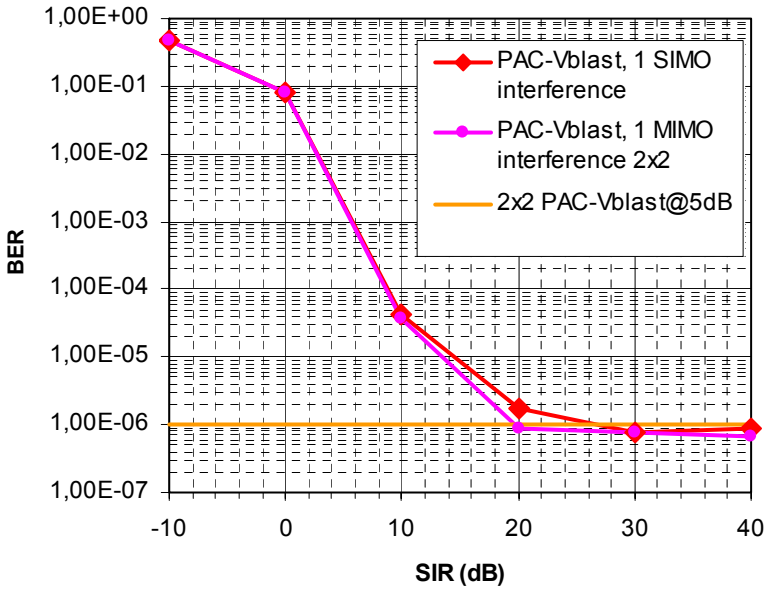

Figure 5-15: BER versus SIR for a 2x2 system. The RMS delay spread is 250 ns and the Eb/No is fixed at 5 dB. The source of interference is one terminal with either one or two transmit antennas.

Figure 5-16 and Figure 5-17 depict the same results as Figure 5-14 and Figure 5-15, only now for the 4x4 case. Here the source of interference is either a single transmit antenna system or a four transmit antenna system. For low delay spread there is no difference between the performances in presence of different sources of interference.

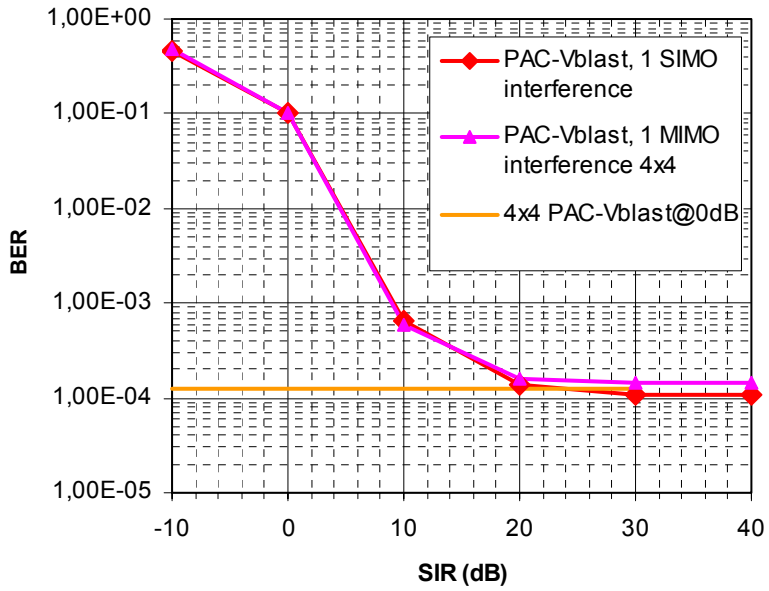

Figure 5-16: BER versus SIR for a 4x4 system. The RMS delay spread is 50 ns and the Eb/No is fixed at 0 dB. The source of interference is one terminal with either one or four transmit antennas..

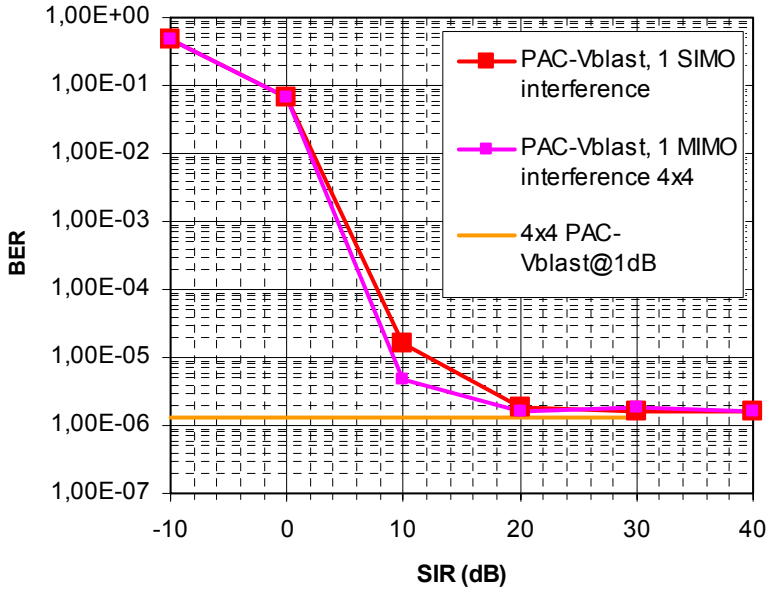

Figure 5-17: BER versus SIR for a 4x4 system. The RMS delay spread is 250 ns and the Eb/No is fixed at 1 dB. The source of interference is one terminal with either one or two transmit antennas.

For high delay spread, as previously seen, the system is more robust when a multiple transmit antenna interferer is present. This is due to the flatter spectrum of the interference signal.

From the figures above, we can conclude that at a SIR of 20 dB, the degradation on performance due to the interference is negligible; at a SIR of about 10 dB, the BER performance looses 1 decade and for values of SIR lower than 10 dB the BER performance of PAC V- BLAST rapidly decrease (circa 1 decade per 2 dB for 250 ns delay spreads and 1decade for 4 dB for 50 ns delay spread). It is important to

notice that these results were obtained for the worse case scenario in which the interference is constantly present.

5.5 Conclusions

The results of link level simulations reported in Section 5.3, support the conclusion that MLD is clearly the best performing MIMO technique for different constellations and antenna configurations. However, the complexity of MLD grows exponentially with the number of transmit antenna.

Another conclusion can be drawn from Section 5.4, i.e., MIMO and SISO present the same robustness to co-channel interference if compared for the same data rate per antenna. When MIMO is compared to SISO for the same total spectral efficiency than MIMO is more robust than SISO.

6 Link-level simulation results of multiple antenna extensions of 802.11a

6.1 Introduction

This chapter compares different MIMO techniques for various antenna configurations in terms of BER/PER vs SNR performance for noise limited scenarios. The goal is to give a broad view of high throughput MIMO solutions and to choose, from a link-level prospective, the most efficient one as the "Broadband Radio@hand" algorithm. The selected MIMO techniques will be chosen as the base for Broadband Radio@hand WLAN system level studies.

Section 6.2 presents two different MIMO architectures. The first proposed MIMO orthogonal frequency division multiplexing (OFDM) architecture is based on spatial division multiplexing (SDM), while the second is based on space-time coding (STC).

In Section 6.3, MIMO systems using receive antenna subset selection are introduced. A major impediment in deploying multiple antennas is the cost of the hardware associated with each antenna (radio frequency power amplifiers, AD/DA converters, etc). Antenna subset selection where transmission/reception is performed through a selection of the total available antennas is a powerful solution that reduces the need for multiple radio frequency (RF) chains yet retains many diversity benefits. Early work on antenna selection focuses on SIMO and multi-input single-output (MISO) systems [Win01]. A well-known result in SIMO systems is that the diversity order achievable with selection is the same as that achievable with maximum ratio combining (MRC). Recently, there has been increasing interest in applying antenna subset selection techniques to MIMO links (see e.g. [Gor00], [Mol01], [Gor02]). A comprehensive information-theoretic study of the receive antenna subset selection for MIMO systems may be found in [Gor03-2], [Gor03-1].

In Chapter 5 the performance evaluation of SDM algorithms was briefly discussed, to give an indication of the performance under some specific test cases. Now a more complete overview of the algorithms presented in Chapter 5 is presented in Section 6.4 .The complete list of test cases used for the simulations can be found in Chapter 7 of this deliverable. Section 6.4 is divided in two parts. In the first part (Section 6.4.1), the performance of SDM algorithms is analyzed. In the second part (Section 6.4.2), SDM with receive antenna selection is compared with the STC architecture.

Section 6.5 offers a summary of the complexity of SDM techniques, subsequently the Broadband Radio@hand algorithm is chosen in Section 6.6 based on the conclusion about performance and complexity of the analyzed techniques. Finally

Section 6.7 shows the performance of MIMO SDM techniques using measured channels. The performances of these techniques are compared to the one based on the B4 indoor channel model presented in [B4-D2.2].

6.2 Transceiver Architectures

6.2.1 SISO OFDM

The baseline 802.11a/g transceiver architecture is shown in Figure 6-1. The upper part of the figure corresponds to the transmitter and the lower part to the receiver. For more explanation about OFDM, cyclic prefix etc, we refer to C. At the transmitter, data bits are encoded using the (133_8, 171_8) convolutional encoder with coding rate 1/2, 2/3, or 3/4 depending on the puncturing pattern. Then frequency interleaving is applied to benefit from any possible frequency diversity. Next, the sequence of interleaved bits is mapped into a sequence of symbols following the standard quadrature amplitude modulation (QAM) schemes. Finally, the symbol sequence undergoes multicarrier modulation, prior to transmission via the antenna. At the receiver, the original data stream is recovered using one received signal. In case that selection diversity is used, this signal is selected out of K_r receive antennas (not shown in the picture). Then, the captured signal is filtered and sampled in order to obtain a symbol-rate discrete-time signal, which is fed to the FFT block. The samples obtained after the FFT correspond to the transmitted symbols multiplied by the corresponding subcarrier gain plus noise. Denote by $x(\upsilon)$ the output of the FFT block that corresponds to the subcarrier υ. One can check that

$$\boldsymbol{x}(\nu_k) = \sqrt{E_s}\,\boldsymbol{h}(\nu_k)\,\boldsymbol{s}(\nu_k) + \boldsymbol{n}(\nu_k), \quad 1 \le k \le N, \tag{1}$$

where $s(\upsilon)$ is the symbol transmitted at the subcarrier υ, $n(\upsilon)$ is the corresponding observation noise, $h(\upsilon)$ is the corresponding channel gain, E_s is the signal energy per channel use and $\{\upsilon_1, \ldots, \upsilon_N\}$ is the set of subcarriers, with $N = 48$ in 802.11a/g. We assume complex circular additive white Gaussian noise (AWGN) with variance $N_o/2$ per real dimension.

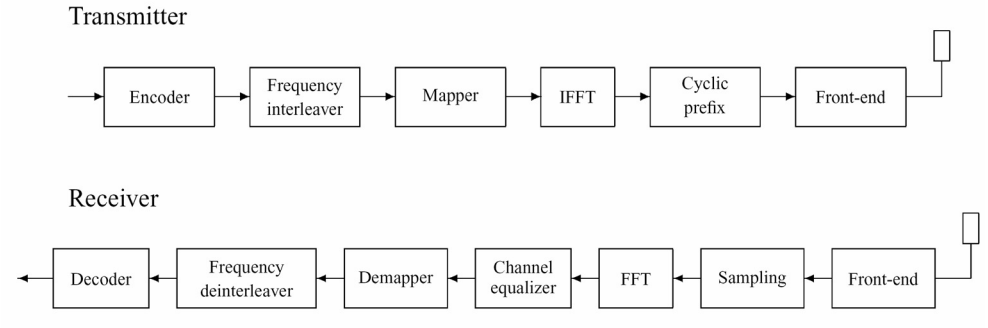

Figure 6-1: IEEE 802.11a/g compliant transceiver.

The frequency selective channel $h(\upsilon)$ is estimated at the receiver using a preamble. Since the channel estimation problem is beyond the scope of this section, we will assume perfect channel state information at the receiver. Then, at the receiver, the

estimated data symbol $\hat{s}(v)$ can be extracted by compensating for the subcarrier gain:

$$\hat{s}(\nu) = \frac{1}{\sqrt{E_s}\,\boldsymbol{h}(\nu)}\,\boldsymbol{x}(\nu). \qquad (2)$$

The channel equalization block carries out this operation. The extracted data symbols are subsequently fed to a soft-decision de-mapper with bitwise maximum likelihood metric computation based on the channel state information. The subsequent deinterleaving and soft-input Viterbi decoding provide decisions on the user bits.

6.2.2 SDM OFDM

In Figure 6-2, the SDM transceiver architecture is shown. Such a transceiver performs spatial multiplexing over N_t transmit antennas in order to increase the data rate by a factor of N_t compared to the standard 802.11a/g. At the receiver, the original data stream is reconstructed from N_r received signals. When antenna subset selection is used, these N_r signals are selected out of K_r receive antennas. Thus, there are $\binom{N_r}{K_r}$ N_r-antenna sets to choose from. More details on antenna selection may be found later in a coming section. At the transmitter, data bits are encoded using the standard coding and puncturing. After that, the coded bits are distributed in a round Robin fashion between the N_t transmit streams.

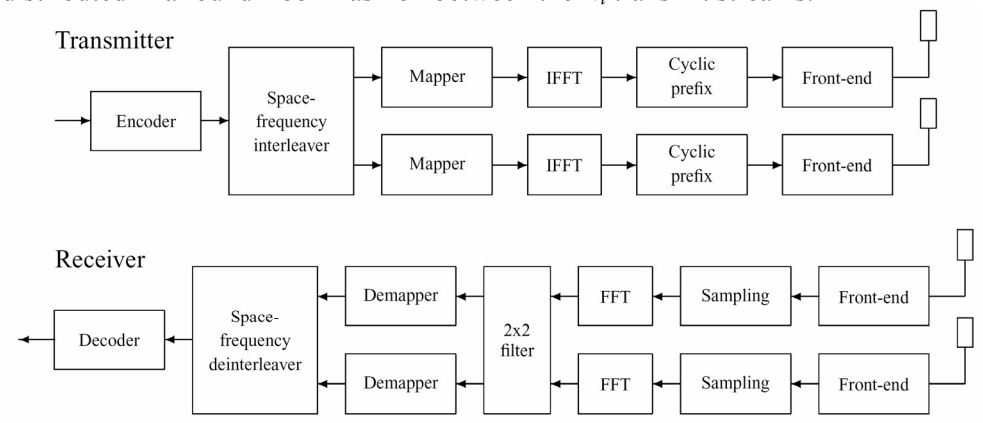

Figure 6-2: Spatial Multiplexing transceiver with two transmit and two receive antennas.

Then, the standard frequency interleaving scheme is applied to every stream. In Figure 6-2, these two operations are carried out by the space-frequency interleaver. Space-frequency interleaving of the coded bits ensures full transmit diversity, since the code benefits from both spatial and frequency diversity. Next, the sequences of interleaved bits are mapped into N_t sequences of symbols following the standard QAM and multicarrier modulation, prior to transmission via N_t transmit antennas. At the receiver, the captured signals are filtered and sampled in order to obtain N_r symbol-rate discrete-time signals. These signals are fed subsequently to N_r FFT blocks. The samples obtained after the FFT are noisy mixtures of the symbols

transmitted at the corresponding subcarriers. Denote $\boldsymbol{x}(\upsilon) = [x_1(\upsilon),\ldots,x_{Nr}(\upsilon)]^T$ a N_r x 1 vector sampled at the outputs of the FFT blocks that corresponds to the subcarrier υ. One can check that

$$\boldsymbol{x}(\nu_k) = \sqrt{E_s}\,\boldsymbol{H}(\nu_k)\,\boldsymbol{s}(\nu_k) + \boldsymbol{n}(\nu_k), \quad 1 \le k \le N, \tag{3}$$

where $\boldsymbol{s}(\upsilon) = [s_1(\upsilon),\ldots,s_{Nt}(\upsilon)]^T$ is the vector of data symbols transmitted by the N_t antennas at the subcarrier υ, $\boldsymbol{n}(\upsilon) = [n_1(\upsilon),\ldots,n_{Nr}(\upsilon)]^T$ is the corresponding observation noise, $\boldsymbol{H}(\upsilon)$ is the N_r x N_t channel matrix corresponding to the subcarrier υ, E_s is the signal energy per channel use and $\{\upsilon_1,\ldots, \upsilon_N\}$ is the set of used subcarriers. We assume complex circular AWGN with variance $N_o/2$ per real dimension. As in the previous system, it is assumed that the frequency selective MIMO channel $\boldsymbol{H}(\upsilon)$ is perfectly known. Then, the estimated data symbols $\hat{\boldsymbol{s}}(\upsilon) = [\hat{s}_1(\upsilon),\ldots, \hat{s}_{Nt}(\upsilon)]^T$ can be extracted by applying a linear filter $\boldsymbol{F}(\upsilon)$ at every subcarrier:

$$\hat{\boldsymbol{s}}(\nu) = \frac{\boldsymbol{F}(\nu)}{\sqrt{E_s}}\,\boldsymbol{x}(\nu). \tag{4}$$

The available filters $\boldsymbol{F}(\upsilon)$ used at the receiver to decode the received symbols can be found in Chapter 4. The extracted data symbols are subsequently fed to soft-decision demappers, deinterleaved, and decoded using a soft-input Viterbi decoder.

6.2.3 STC OFDM

In Figure 6-3, the MIMO diversity transceiver architecture is shown. This architecture does not increase the 802.11a/g data rates. Instead, it increases coverage by taking full advantage of the available spatial diversity. At the receiver, the original data stream is reconstructed from the received signals by performing MRC. The structure of the transmitted signal allows the receiver to recover the original stream of data without inter-symbol interference, and yet obtaining full diversity gain. Such a transceiver performs per-subcarrier coding over N_t transmit antennas and N_t or more OFDM symbol periods, depending on the STC scheme. That means that several OFDM symbols periods have to be stored before space-time coding or decoding can start. More details on the construction of STC schemes may be found in [Tar99-1] and [Ala98].

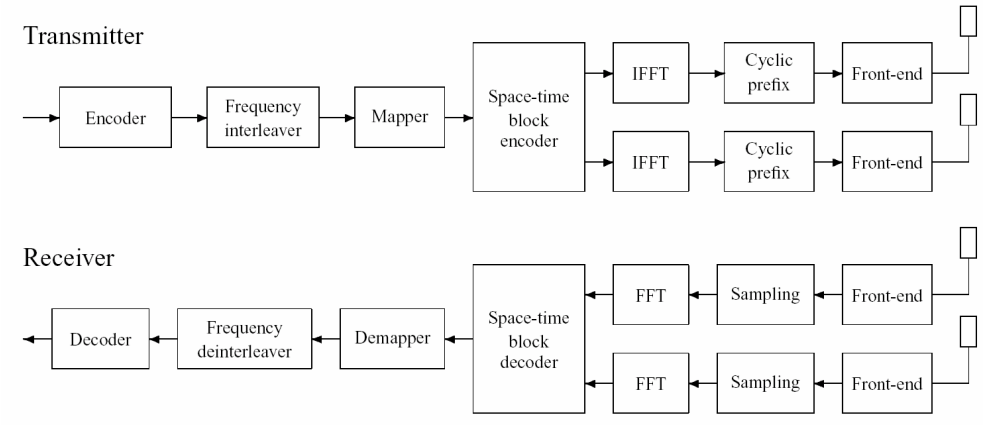

Figure 6-3: Spatial diversity transceiver with two transmit and two receive antennas.

At the transmitter, data bits are encoded, interleaved and modulated according to the standard. After that, symbols are buffered and encoded using a STC scheme across N_t antennas. After the space-time encoder, the N_t antenna symbol streams are modulated in parallel following standard OFDM modulation. At the receiver, the captured signals are filtered and sampled in order to obtain N_r symbol-rate discrete-time signals. These signals are fed subsequently to N_r FFT blocks. The samples obtained after the FFT are noisy mixtures of the space-time code symbols transmitted at the corresponding subcarriers. Samples are stored for several OFDM transmission periods, depending on the STC scheme, before the actual space-time decoding can start. For N_t =2, the STC scheme described in [Ala98] can be used. In this case, a pair of QAM symbols is mapped into the same sub-carrier of two consecutive OFDM symbols. After space-time decoding, one can check that one detected symbol of the pair is

$$\hat{\boldsymbol{s}}(\nu_k,1)=\boldsymbol{s}(\nu_k,1)+\frac{\sum_{j=1}^{Nr}h_{j1}^{*}(\nu_k)n(\nu_k,1)-h_{j2}^{*}(\nu_k)n^{*}(\nu_k,2)}{\sqrt{E}_s\sum_{j=1,i=1}^{Nr,2}\left|h_{ji}(\nu_k)\right|^2} \tag{5}$$

and the other

$$\hat{\boldsymbol{s}}(\nu_k,2)=\boldsymbol{s}(\nu_k,2)+\frac{\sum_{j=1}^{Nr}h_{j2}^{*}(\nu_k)n(\nu_k,1)-h_{j1}^{*}(\nu_k)n^{*}(\nu_k,2)}{\sqrt{E}_s\sum_{j=1,i=1}^{Nr,2}\left|h_{ji}(\nu_k)\right|^2} \tag{6}$$

where $n^*(\upsilon, q)$ is the noise sample at subcarrier υ at the OFDM symbol q, and $h_{ji}(\upsilon)$ is the channel gain between transmit antenna i and receive antenna j at subcarrier υ. The detected data symbols are subsequently de-mapped, deinterleaved and decoded similarly to previous architectures.

6.3 Receive antenna selection

As already mentioned, antenna subset selection offers a low cost opportunity to increase reliability of a MIMO link in fading environments. Adaptive antenna selection is particularly important for spatial multiplexing transceivers with linear

(MMSE or ZF) de-multiplexing of signals at the receiver. Indeed, linear interference cancellation makes use of the spatial degrees of freedom thereby reducing the effective amount of receive diversity seen at the output of the filter. Adaptive antenna selection compensates for this loss. The selection criterion proposed in [Gor02] maximizes the Shannon capacity of an N_r x N_t flat fading MIMO channel which results from selecting N_r out of K_r antennas at the receiver. The diversity order achieved with this approach equals the diversity order that can be achieved with a K_r x N_t MIMO channel. Furthermore, a suboptimal extension of this approach for the frequency selective environments has been developed in [Gor02]. In the present paper, we recall the antenna selection algorithm. Denote $I = \{I_1, \ldots, I_{Nr}\}$ a collection of distinct indexes corresponding to a possible set of N_r receive antennas: $I_p \neq I_q$ and $I_p \in \{1, \ldots, K_r\}$, $1 \leq p \neq q \leq N_r$. Let $\boldsymbol{y_I}(k) = [y_{I1}(k), \ldots, y_{INr}(k)]^T$ be a N_r x 1 sample of signals sampled at the output of the selected antennas in the time domain. A (scaled) covariance matrix of the signals captured with the set I can be estimated:

$$\hat{\boldsymbol{R}}_I = \sum_{k=1}^{T} \boldsymbol{y}_I(k)\boldsymbol{y}_I(k)^H \tag{7}$$

where the number of samples T should be at least as big as the expected rank of the true covariance matrix $\boldsymbol{R_I} = E\{ \boldsymbol{y_I}\, \boldsymbol{y_I}^{\boldsymbol{H}} \}$. Choosing $T \geq 2N_r$ would keep performance losses negligible. It is worthwhile repeating that the entries of $\boldsymbol{y_I}(k)$ for all possible $\binom{N_r}{K_r}$ sets I may be acquired by sounding all K_r antennas by the available N_r receive chains. Finally, the set $\tilde{I}$ of N_r antennas to be used is identified according to

$$\hat{\mathcal{I}} = \arg\max_{\mathcal{I}} \det(\hat{\boldsymbol{R}}_{\mathcal{I}}), \tag{8}$$

wherein the maximization is over all possible sets I. Note that the complexity of

$$\hat{\boldsymbol{R}}_I = \sum_{k=1}^{T} \boldsymbol{y}_I(k)\boldsymbol{y}_I(k)^H \tag{9}$$

scales exponentially with K_r and/or N_r. To highlight the relationship between the selection rule and the maximum capacity criterion, we recall that the Shannon capacity $C(\boldsymbol{H}_I)$ of a flat fading channel $\boldsymbol{H_I}$ associated with the set I is given by

$$C(\boldsymbol{H}_I) = \log_2 \det(\boldsymbol{I}_{Nr} + (E_s / N_0)\boldsymbol{H}_I \boldsymbol{H}_I^H) \tag{10}$$

whereas the associated covariance matrix $\boldsymbol{R_I}$ is given by

$$\boldsymbol{R}_I = E_s \boldsymbol{H}_I \boldsymbol{H}_I^H + N_0 I_{Nr} \tag{11}$$

6.4 Link level performance results

Link-level simulations are carried out to study the performance of different OFDM systems. We look into the packet error rate for different signal to noise ratios (SNR) and transmission data rates. The SNR measure that we use does not take into account power losses due to pilot insertion or cyclic prefix insertion, which are intrinsic losses of OFDM. The user information sequence (or packet) length is set to either 64 or 1000 bytes, and then this sequence is zero-padded till its length is a multiple of the amount of user bits in one OFDM symbol.

For every transmit-receive antenna pair, an independent identically distributed (i.i.d.) channel realization is drawn. Every channel realization is in fact a discrete-time sequence consisting of a number of independently distributed taps. The channel responses follow an exponential decaying power delay profile, which decaying speed is function of the RMS delay spread. The study has been carried out for different RMS delay spread values: 10ns, 30ns, 50ns, 100ns and 250ns. The channels used for the simulations are described in [B4-D2.2]. For every packet, a new set of channel realizations is used, which distribution is independent from the previous realization.

6.4.1 Performance of SDM algorithms

The goal of this section is to present the packet error rate (PER) (for packet lengths 64 and 1000 bytes) versus SNR performance of the SDM MIMO algorithms, ZF, MMSE, V-BLAST and MLD. For more details on the algorithms the reader can refer to Chapter 5.

In general, MLD is the best performing algorithm for all antenna configurations and data rates. This is due to its higher diversity order, which causes the curves to fall off faster to low BER/PER compared to the other algorithms, see Figure 6-4 to Figure 6-6 where BER vs. SNR examples are given for 50ns delay spread.

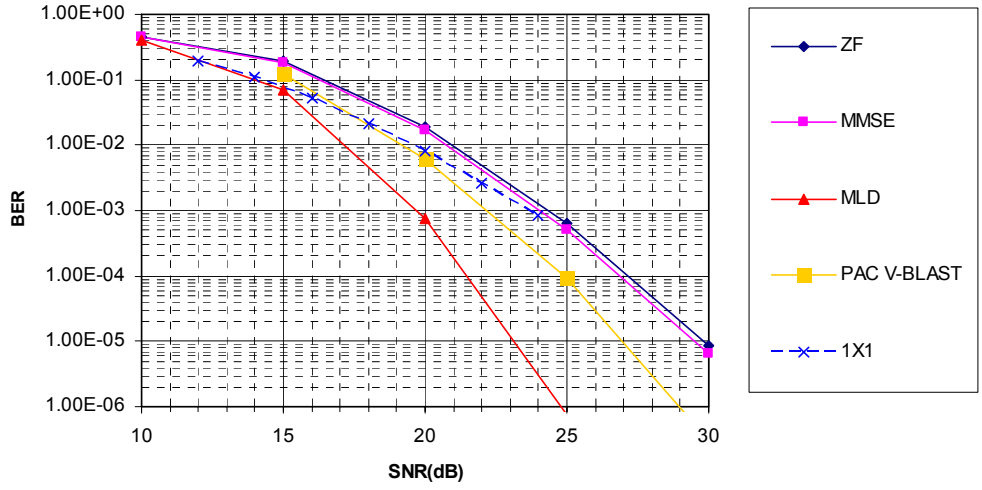

Figure 6-4: 2x2, 16QAM, R=3/4, 72 Mbps, 50ns.

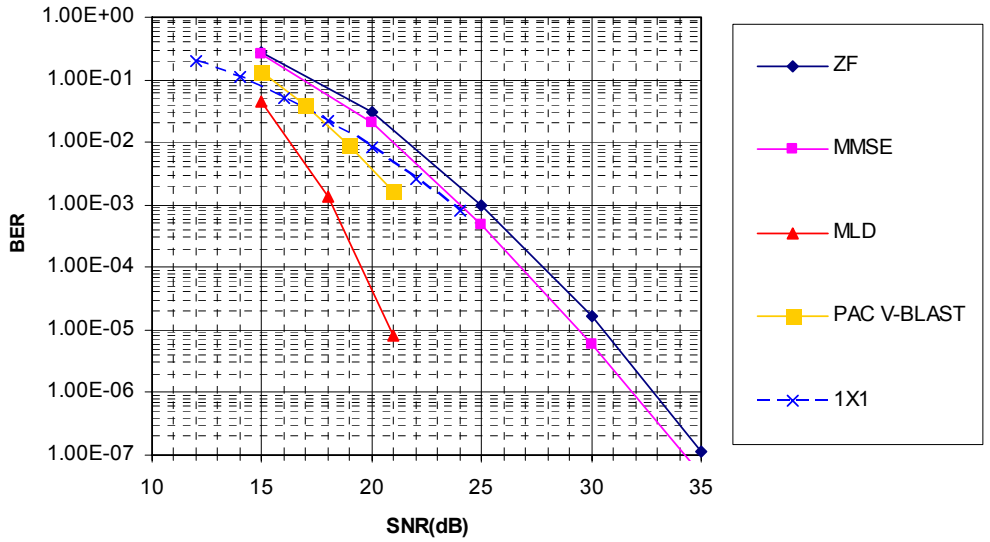

Figure 6-5: 3x3, 16QAM, R=3/4, 108 Mbps, 50ns.

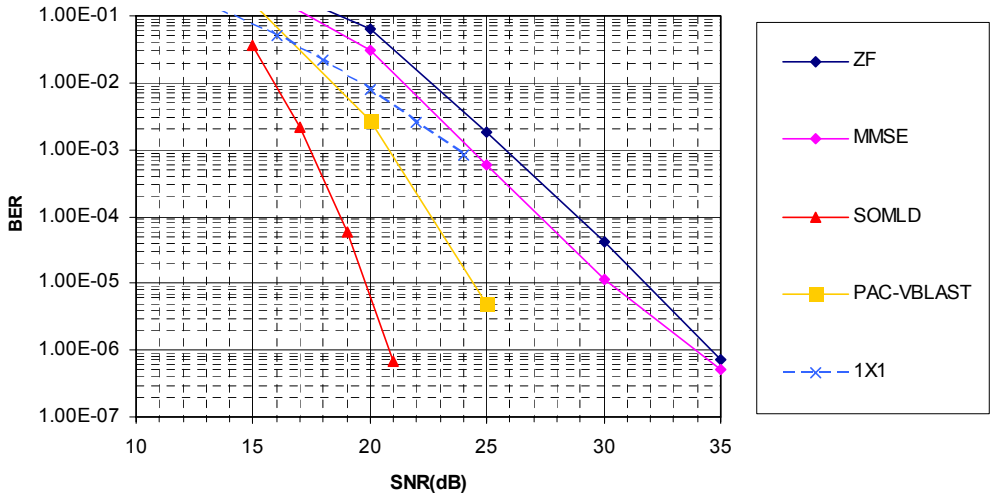

Figure 6-6: 4x4, 16QAM, R=3/4, 108 Mbps, 50ns.

The joint coding architecture deployed with MLD gives a slight advantage over the per antenna coding (PAC) architecture when space diversity is larger than frequency diversity, i.e. at lower delay spreads, see Figure 6-7-Figure 6-8.

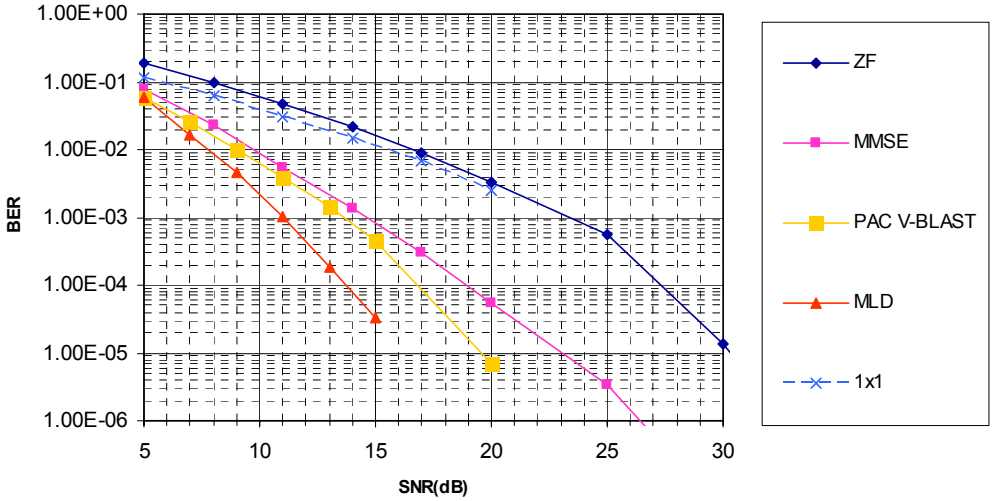

Figure 6-7: 2x2, QPSK, R=1/2, 24 Mbps, 10ns.

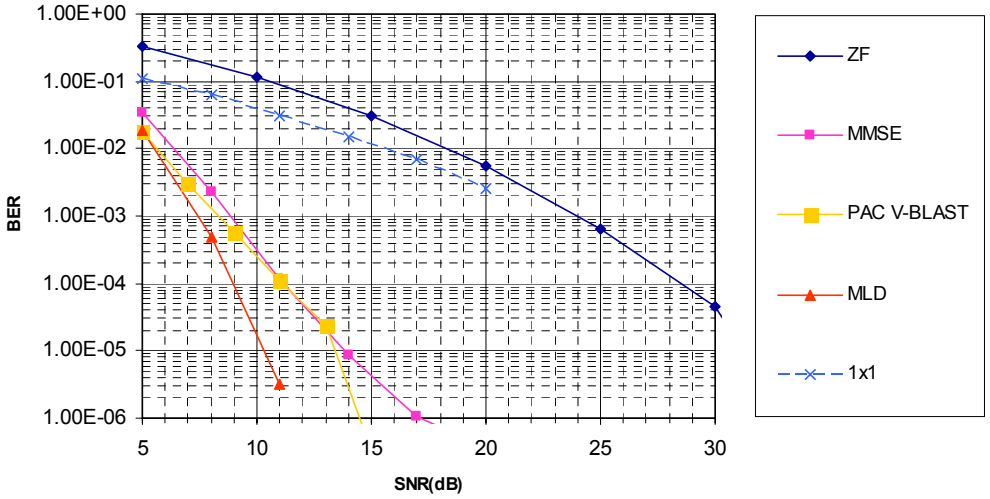

Figure 6-8: 4x4, QPSK, R=1/2, 48 Mbps, 10ns.

For higher delay spread values (50 ns and higher) and lower constellation sizes PAC V-BLAST performs better than MLD. This is due to the fact that the PAC architecture can exploit better the frequency diversity offered by the channel thanks to the fact that the code words are now spread over frequency (per antenna) rather than over space. This advantage is only visible for a lower constellation size (QPSK) because then the system is still working in a low SNR region where the higher space diversity of MLD is not yet visible, see Figure 6-9 and compare to Figure 6-5.

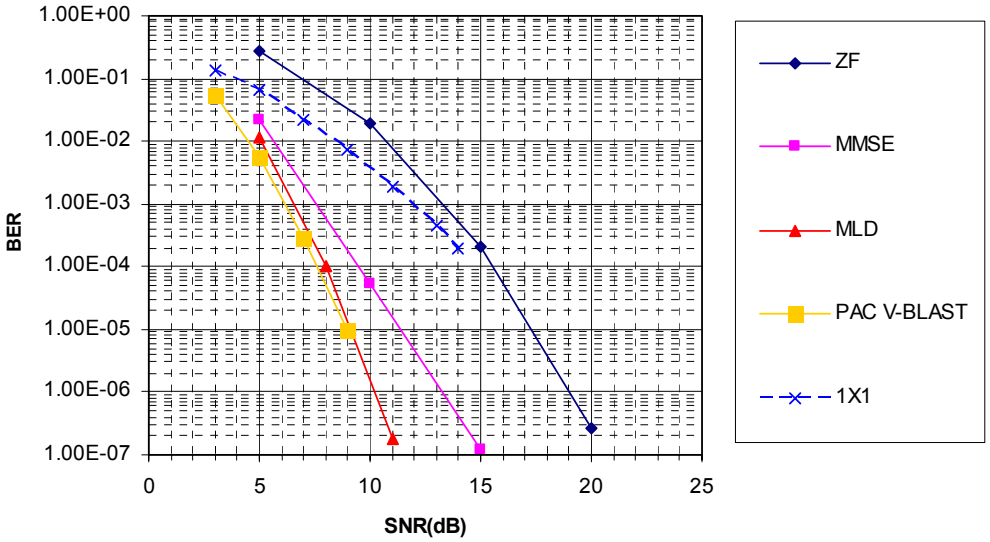

Figure 6-9: 3x3, QPSK, R=1/2, 36 Mbps, 50 ns.

PAC V-BLAST is the second best algorithm. Its performance is very good for low constellation sizes (low SNR region) and delay spreads higher than 10 ns. For higher modulation schemes than QPSK, its PER versus SNR performance is still good but few dBs away (depending on the packet size) from MLD. Its performance remains good also for high antenna configurations and high constellations. It is remarkable that, for a RMS delay spread of 10ns, a 4x4 system deploying V-BLAST with 64 QAM modulation (R=3/4) requires 34 dB of SNR at a PER= 10^{-2}, which is 10 dB less than MMSE/ZF (see Figure 6-10) and 3 dB less than a 1x1 system using the same per antenna rate. For an RMS delay spreads of 30 ns the required SNR drops to 30dB and for 50 ns to 29 dB. From the comparison between BER vs. SNR and PER vs. SNR, it seems that the errors occur mostly in bursts with the effect of corrupting a lower number of packets. This result is expected since the wrong decoding of the first layer is catastrophically propagating on all subsequent layers, see Figure 6-11, reporting BER versus SNR, and compare to Figure 6-12, displaying PER versus SNR for the same test cases.

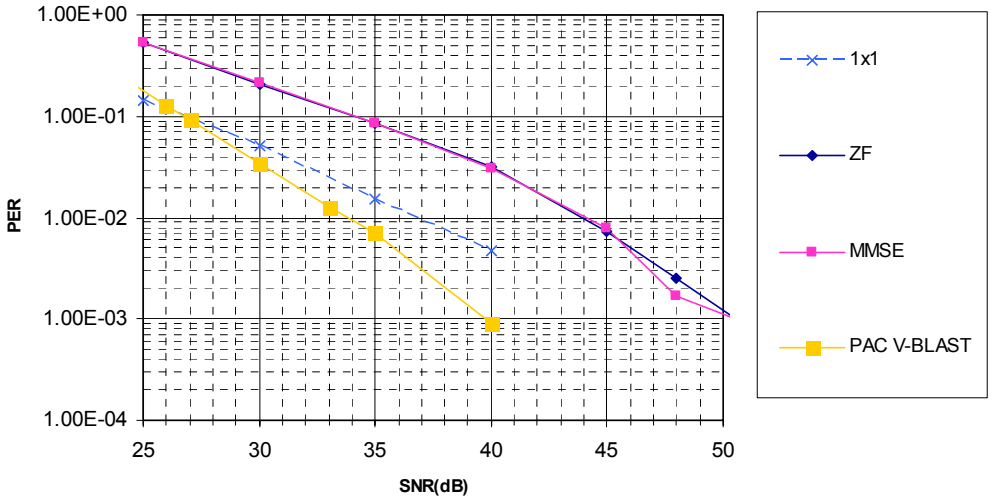

Figure 6-10: 4x4, 64QAM, R=3/4, 216 Mbps, 10 ns.

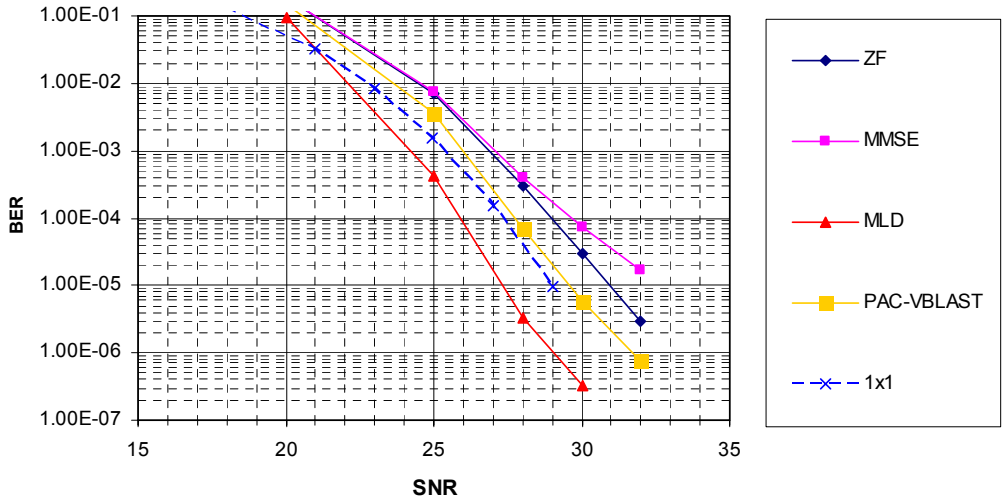

Figure 6-11: 2x2, 64QAM, R=3/4, 108 Mbps, 100 ns.

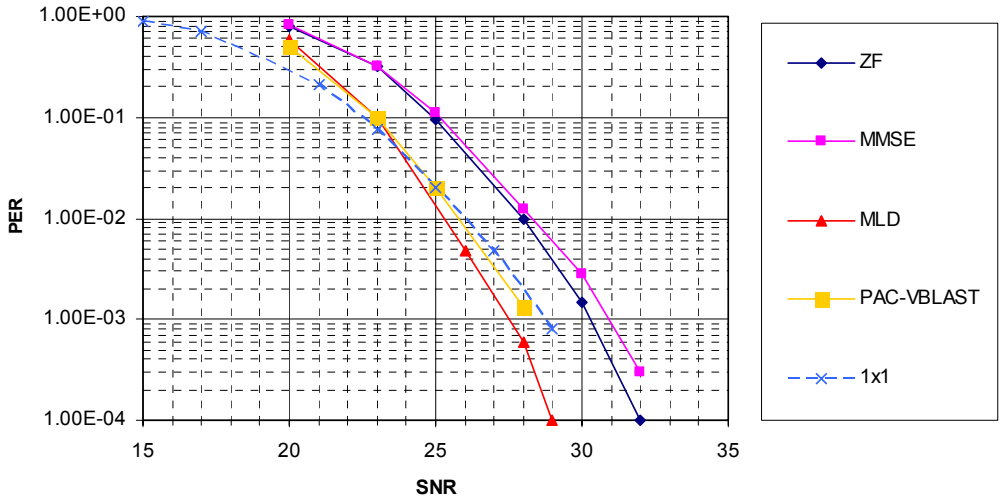

Figure 6-12: 2x2, 64QAM, R=3/4, 108 Mbps, 100 ns, 64 bytes.

Finally, MMSE and ZF are the worst performing algorithms. As expected, in the low SNR region (i.e. when QPSK is used) the advantage of MMSE over ZF is remarkable for any RMS delay spread, see for example Figure 6-4 to Figure 6-9. For higher constellation sizes, the two algorithms are expected to achieve the same performance. However in the simulation results there is an unexpected shift in many plots, see Figure 6-12. This gap is probably the lack of accuracy or to the approximation used to calculate the soft values. More effort should therefore be spent to find more accurate soft values.

It is noteworthy that for the antenna configurations 2x3 and 2x4, the performance curves of all of the above algorithms are very close, all falling in an interval of 1or 2 dB at the PER of interest, see for example Figure 6-13 and Figure 6-14.

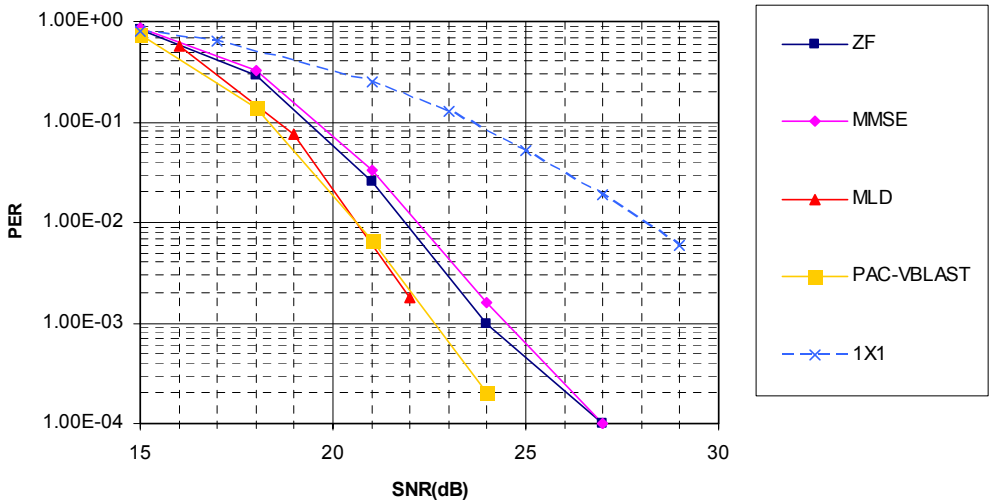

Figure 6-13: 2x3, 64QAM, R=3/4, 108 Mbps, 50 ns, 64 bytes.

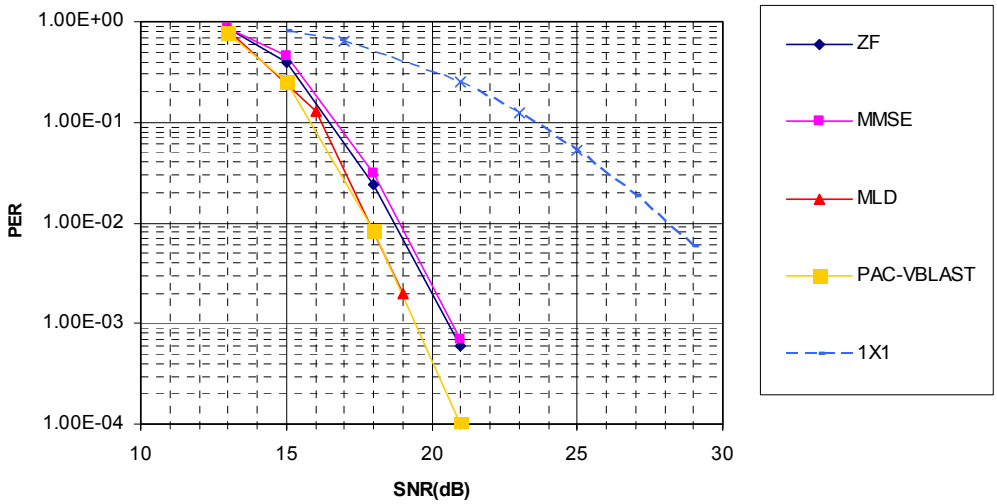

Figure 6-14: 2x4, 64QAM, R=3/4, 108 Mbps, 50 ns, 64 bytes.

Finally, for 250 ns delay spread inter-symbol interference (ISI) starts to play a role in the performance of all algorithms. This is visible mostly for high constellation sizes which, operating at high SNR values, show a remarkable performance floor due the effect of ISI, which is dominant over the noise (see Figure 6-15).

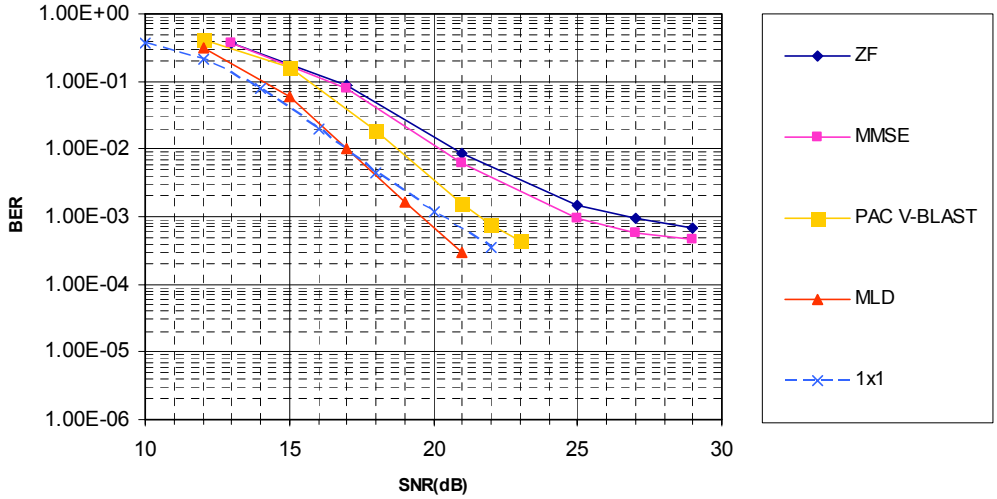

Figure 6-15: 2x2, 16QAM, R=3/4, 72 Mbps, 250 ns.

6.4.2 Performance of SDM with receive antenna selection

In this section, the performance advantage of receive antenna selection is analyzed for both SIMO and MIMO systems. Moreover, it is shown how selection diversity can increase the robustness of SDM systems.

Simulations have been carried out for two RMS delay spread values: 0 ns (flat fading), and 30 ns. None of these delay spread values causes inter-carrier interference (ICI) thanks to the cyclic prefix of 0.8µs defined in the standard. The packet length used is equal to 1000 bytes.

The transmission rates under study are 6, 12, 24, 48, and 54 Mbps for SISO, SIMO and MIMO STC architectures and 12, 24, 48, 96, and 108 Mbps for MIMO spatial multiplexing (SM) architectures. The latter rates are achieved by making use of the modulations and coding rates of 802.11a/g with N_t transmit antennas. In all PER vs. SNR figures displayed in this paper, each transmission-rate curve uses a consistent marker. Five-pointed star is used for 6 Mbps, square for 12 Mbps, triangle for 24 Mbps, circle for 48 Mbps, point for 54 Mbps, asterisk for 96 Mbps and diamond for 108 Mbps. Table 6-1 summarizes the coding rates and modulation schemes used for each transmission rate.

SISO / MIMO SM rate	Modulation	Coding Rate	Bytes/packet
6 Mbps/ 12 Mbps	BPSK	1/2	1002
12 Mbps/ 24 Mbps	QPSK	1/2	1008
24 Mbps/ 48 Mbps	16QAM	1/2	1008
48 Mbps/ 96 Mbps	64QAM	2/3	1008
54 Mbps/ 108 Mbps	64QAM	3/4	1026

Table 6-1: Data rates and the associated transmission parameters.

Each PER is measured with a number of independent channel trials ensuring at least 200 lost packets. This means that for measuring a PER of 1%, the transmission of approximately 20000 packets was simulated.

In Figure 6-16 we plot the PER versus SNR for an 802.11a/g system in a flat fading environment. In Figure 6-17 the performance of the same transceiver with receive antenna selection over K_r= 4 receive antennas is shown. As it follows from Figure 6-16 and Figure 6-17, receive antenna selection yields a gain of about 15.5 dB at PER of 1%. The slope of the curves in Figure 6-17 is 4 times steeper than the slope of the curves in Figure 6-16. This is in accordance with antenna diversity theory as shown in [Jak74]. In Figure 6-18 and Figure 6-19 the performance of the two systems is displayed again, but now with 30 ns RMS delay spread channels. From the figures, it follows that receive antenna selection yields a gain of about 8.75 dB at a PER of 1%. The overall gain obtained through antenna selection has been reduced because the system already presents some sort of diversity to capitalize on, namely frequency diversity. It can be observed that the system without antenna selection substantially benefits as the RMS delay spread changes from 0 ns to 30 ns (up to 5.4 dB gain at PER 1%). Conversely, the performance of the system using antenna selection deteriorates when going from 0 ns to 30 ns RMS delay spread. In this case, the change in slope due to frequency diversity is not visible in the SNR region of interest (around 20 dB). The results on the performance gain due to antenna selection for the 802.11a system are summarized in Table 6-2.

Rate (Mbps)	RMS delay spread	Gain 1x1 (out of 4) vs. 1x1
6	0 ns	15.5 dB
6	30 ns	8.75 dB
54	0 ns	16.5 dB
54	30 ns	8.75 dB

Table 6-2: Gain of receive selection: $N_r = N_t = 1$, PER 1%.

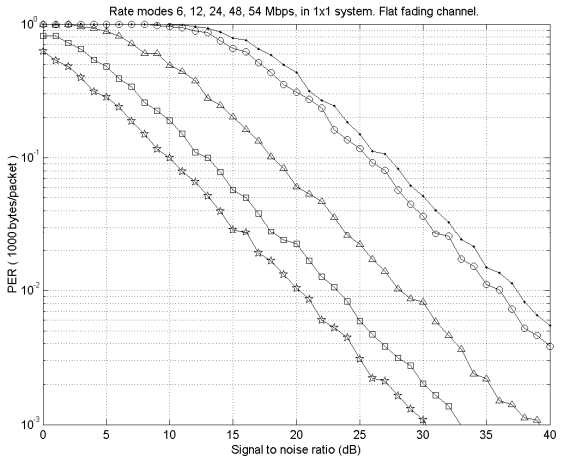

Figure 6-16: PER vs. SNR of an 802.11a/g compliant system for different data rates. RMS delay spread of the channel is 0 ns.

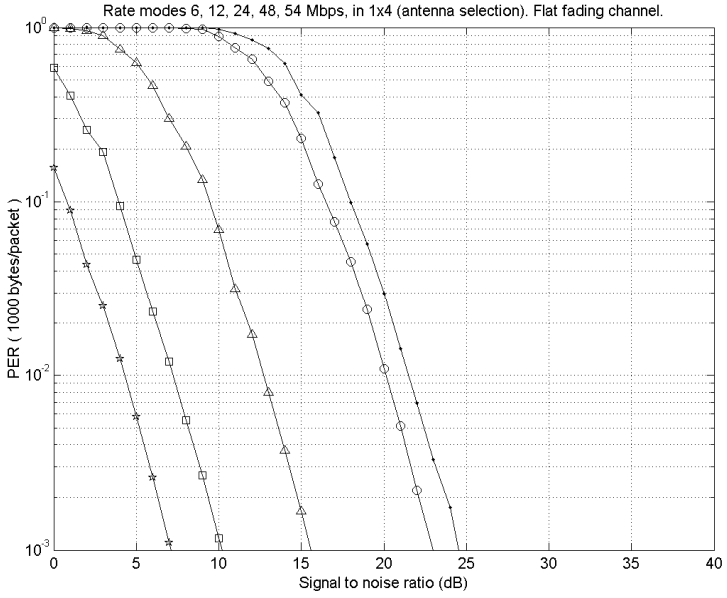

Figure 6-17: PER vs. SNR of 802.11a/g compliant system with antenna selection out of 4. RMS delay spread of the channel is 0 ns.

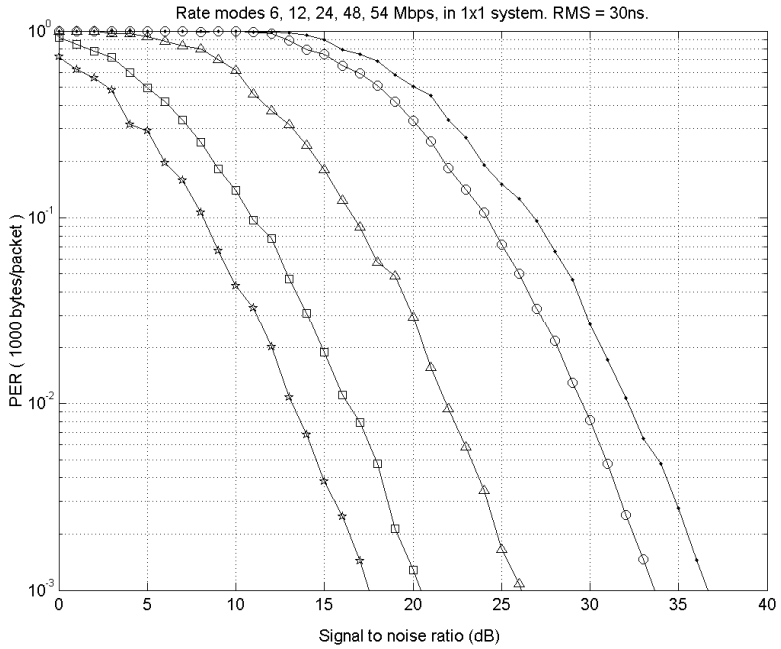

Figure 6-18: PER vs. SNR of an 802.11a/g compliant system for different data rates. RMS delay spread of the channel is 30 ns.

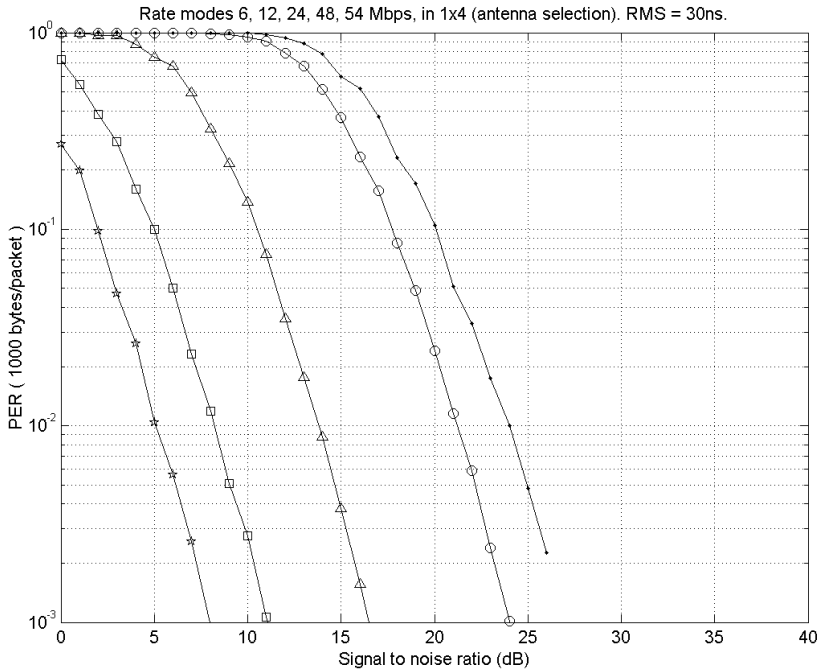

Figure 6-19: PER vs. SNR of 802.11a/g compliant system with antenna selection out of 4. RMS delay spread of the channel is 30 ns.

In Figure 6-20 we plot the PER versus the SNR for a spatial multiplexing transceiver with N_t =2 transmit, N_r =2 receive antennas and MMSE filtering. In this first case, the RMS delay spread was set to 0 ns. If we compare the performance of this system with the performance of the SISO system shown in Figure 6-16, we see that the first one outperforms the second one by roughly 10 dB for the 12 Mbps mode and 5 dB for the 48 Mbps mode. If we compare the MIMO spatial multiplexing system with the SIMO system inFigure 6-17 we see that the second system outperforms the first one by 8 dB for the 12 Mbps mode and 10 dB for the 48 Mbps mode. The performance of the spatial multiplexing transceiver with receive antenna subset selection is shown in Figure 6-22. Here, a subset of N_r =2 out of K_r =4 receive antennas is adaptively chosen at the receiver as explained in Section 6.3. Since no preamble is simulated, we substitute the empirical covariance matrices by the true values $\boldsymbol{R}_I$. As it follows from Figure 6-20 and Figure 6-21, receive antenna subset selection yields a gain of about 14.5 dB at a PER of 1% for the 108 Mbps transmission mode. For the same PER, antenna selection yields 8 dB gain for the 12 Mbps mode. The slope of the curves in Figure 6-21 is three times steeper than the slope of the curves in Figure 6-20. This confirms the equivalence in diversity order between the full system (using all four receive signals) and the system with antenna selection.

In Figure 6-22 and Figure 6-23 the performance of two spatial multiplexing systems is displayed again, but now with 30 ns RMS delay spread channels. From Figure 6-22 and Figure 6-23 it follows that receive antenna selection yields a gain of about 5 dB at a PER of 1% for the 108 Mbps transmission mode and 3 dB gain for the 12 Mbps mode. As before, the overall gain obtained through antenna selection has been reduced because the system presents frequency diversity. The system without antenna selection gains up to 5 dB as the RMS delay spread changes from 0 ns to 30 ns. The performance of the system using antenna selection deteriorates when going from 0 ns to 30 ns RMS delay spread. If we compare Figure 6-22 with Figure 6-18 we see that the MIMO system keeps outperforming the SISO system when the RMS delay spread is 30 ns, while the performance of the MIMO spatial multiplexing system gets comparable to the one of the SIMO system shown in Figure 6-19. The main observations on the performance gain due to antenna subset selection are summarized in Table 7.3. The last two columns show the gain of MMSE when N_t=2 and the number of the receive antenna is respectively N_r=4 and N_r=3. As already mentioned in Section 6.3, selection diversity allows reducing the number of radio frequency (RF) chains at the receiver yet retaining a certain diversity gain. Here, the aim is to show the trade-off between complexity and gain, comparing the performanace of receive selection diversity with the one of a receive diversity for a MMSE 2x4 and 2x3 system. From Table 6-3, it appears that for a flat fading channel, the selection of 2 out of 4 receive antennas is slightly superior to MMSE 2x3. For a scenario in which the RMS delay spread equals 30 ns, the MMSE outperforms selection diversity bya maximum of 4 dB. Thus antenna selection can provide a good trade-off between performance and complexity.

Rate (Mbps)	RMS delay spread	Gain 2x2 (out of 4) vs. 2x2	Gain 2x3 vs. 2x2	Gain 2x4 vs. 2x2
12	0 ns	8 dB	8 dB	11 dB
12	30 ns	3 dB	5 dB	7,5 dB
24	0 ns	11,5 dB	11 dB	15 dB
24	30 ns	4 dB	6,5 dB	9,5 dB
108	0 ns	14,5 dB	13 dB	17,5 dB
108	30 ns	5 dB	9 dB	13 dB

Table 6-3: Gain of receive subset selection: $N_r = N_t = 2$, PER =1%.

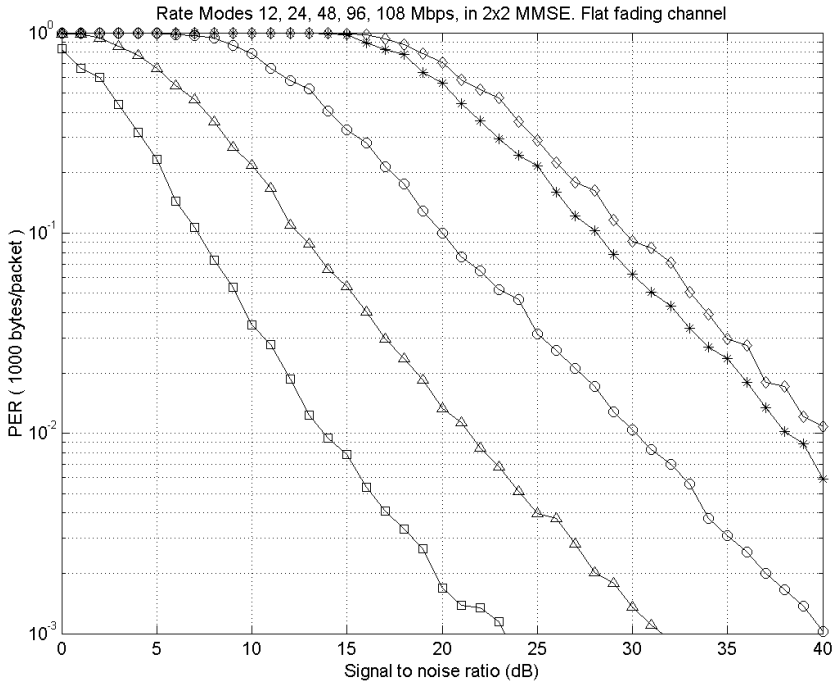

Figure 6-20: PER vs. SNR of a 2x2 MMSE system for different data rates. RMS delay spread of the channel is 0 ns.

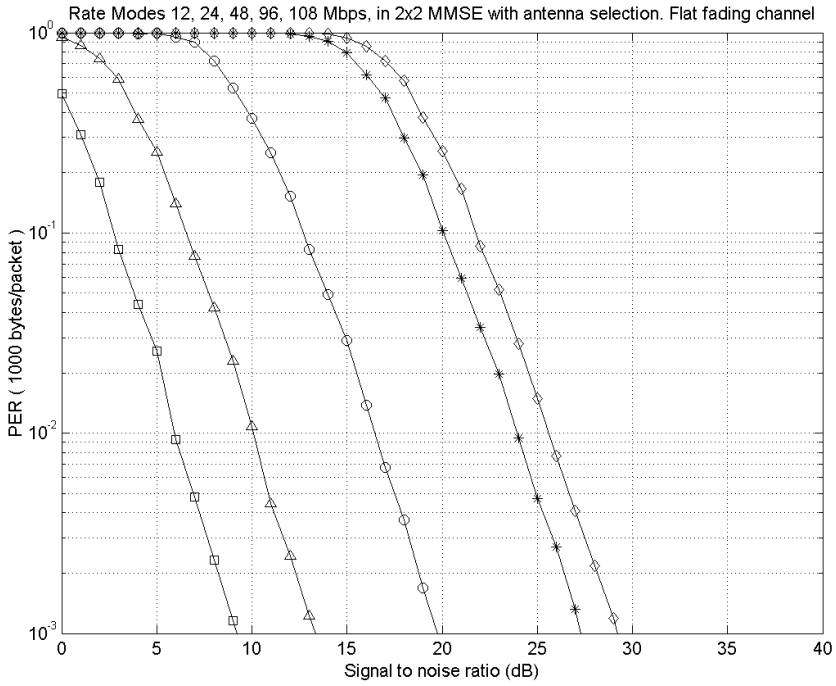

Figure 6-21: PER vs. SNR of a 2x2 MMSE system with antenna selection out of 4. RMS delay spread of the channel is 0 ns.

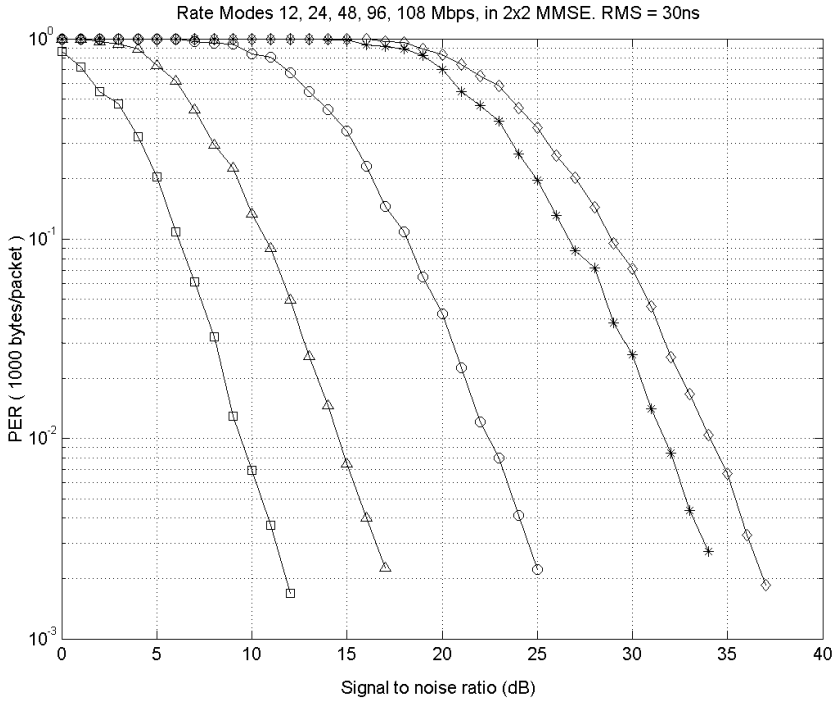

Figure 6-22: PER vs. SNR of a 2x2 MMSE system for different data rates. RMS delay spread of the channel is 30 ns.

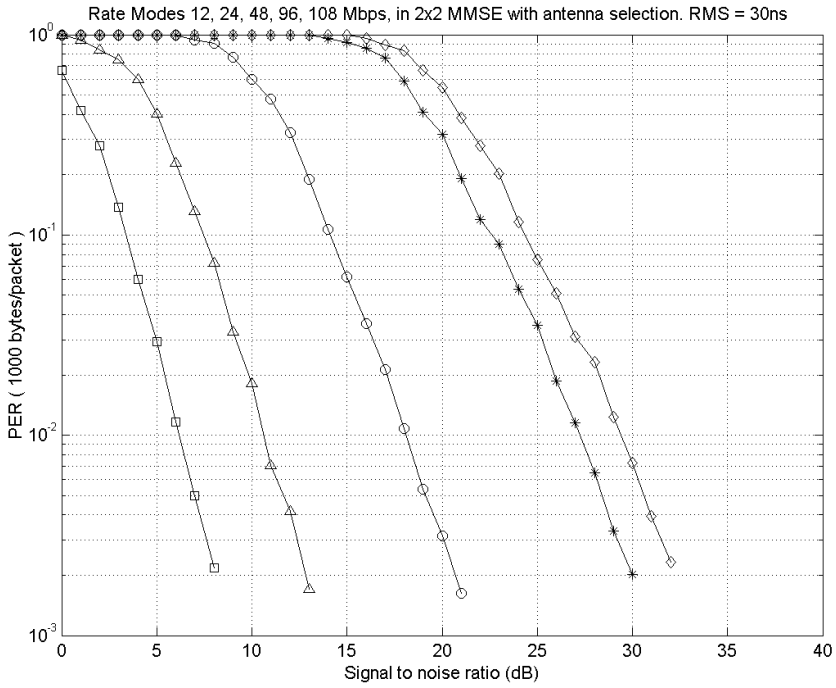

Figure 6-23: PER vs. SNR of a 2x2 MMSE system with antenna selection out of 4. RMS delay spread of the channel is 30 ns.

In all MIMO spatial multiplexing results shown up to here, MMSE filters were used to recover the transmitted symbols. The MMSE filter minimizes the signal to noise and interference ratio at its output. For poor input signal to noise ratios, the MMSE behaves like a match filter, and for high signal to noise ratios behaves like a channel inverter or ZF filter. In principle, the calculation of the MMSE filter coefficients requires more operations than the calculation of the ZF filter coefficients. Therefore, it is interesting to compare the two filtering techniques and see to what extend MMSE is desirable. In Figure 6-24 we show the results of a spatial multiplexing system using ZF. The RMS delay spread of the channel is 0 ns. Comparing Figure 6-24 to Figure 6-20 for the highest rates, 48, 96, or 108 Mbps, we see no significant difference between the two detection strategies. This is to be expected since MMSE is equivalent to ZF in the high SNR region. However, for the 24 Mbps transmission mode, a loss of 3,75 dB at a PER of 1% when using ZF is observed. For the 12 Mbps transmission mode the loss increases to 8.5 dB.

To conclude, in Figure 6-25 we plot PER versus SNR for a system based on the Alamouti architecture shown in Figure 7.4 under a flat fading channel. Figure 7.27 shows the performance of the same system when the channel presents an RMS delay spread of 30 ns. As expected, the curves in Figure 6-25 perfectly match those shown in Figure 6-17. This is because both systems present the same diversity order, 4, and the 3 dB loss in average SNR gain of the $K_r = 4$ selection system with respect to a $K_r = 4$ MRC system compensates for the 3 dB loss in the $N_t = 2$, $N_r = 2$ STC scheme due to the sharing of the power between the two transmit antennas. On the other hand, comparing Figure 6-19 and Figure 6-26 we see that the STC MIMO system benefits by around 2.25 dB from an increased RMS delay spread, while the SIMO system is hampered by around 2.5 dB in the worse case.

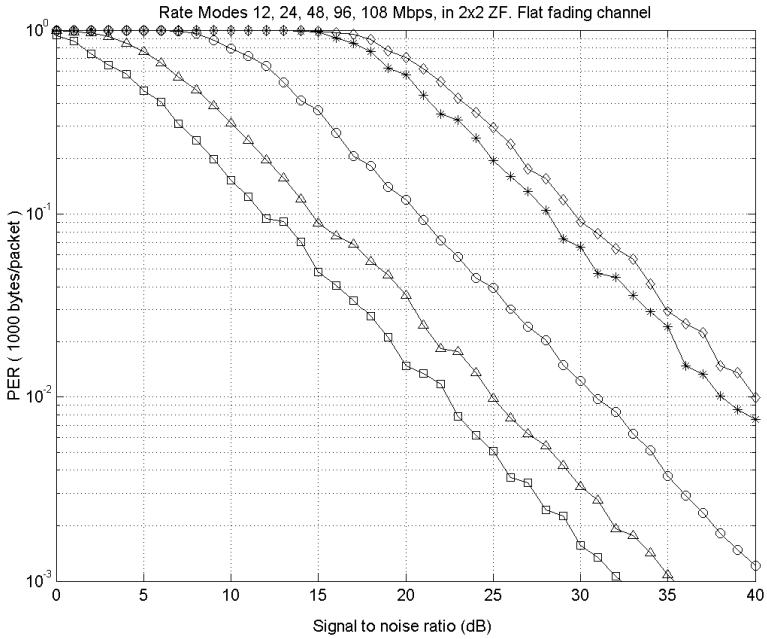

Figure 6-24: PER vs. SNR of a 2x2 ZF system for different data rates. RMS delay spread of the channel is 0 ns.

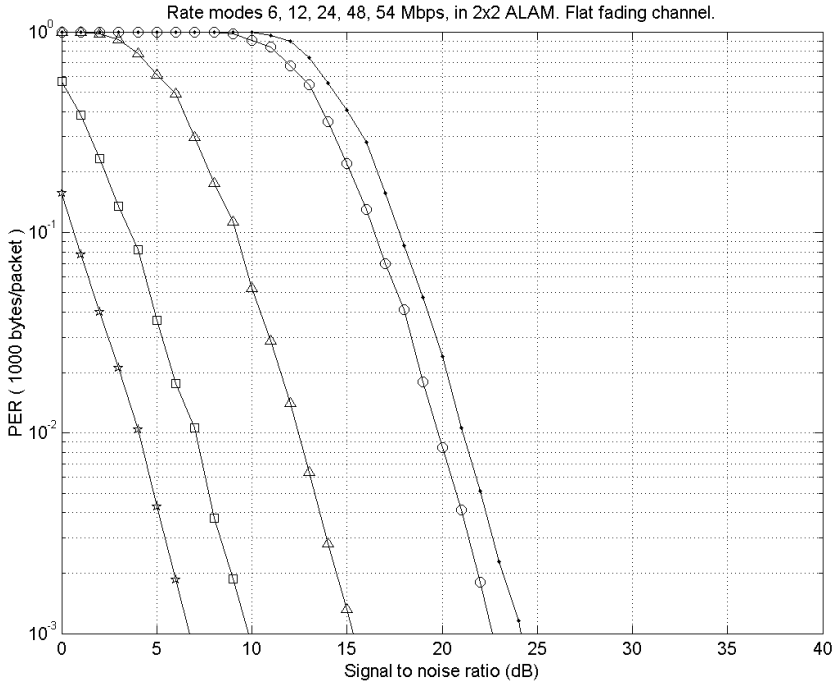

Figure 6-25: PER vs. SNR of a 2x2 spatial diversity system for several data rates. RMS delay spread of the channel is 0 ns.

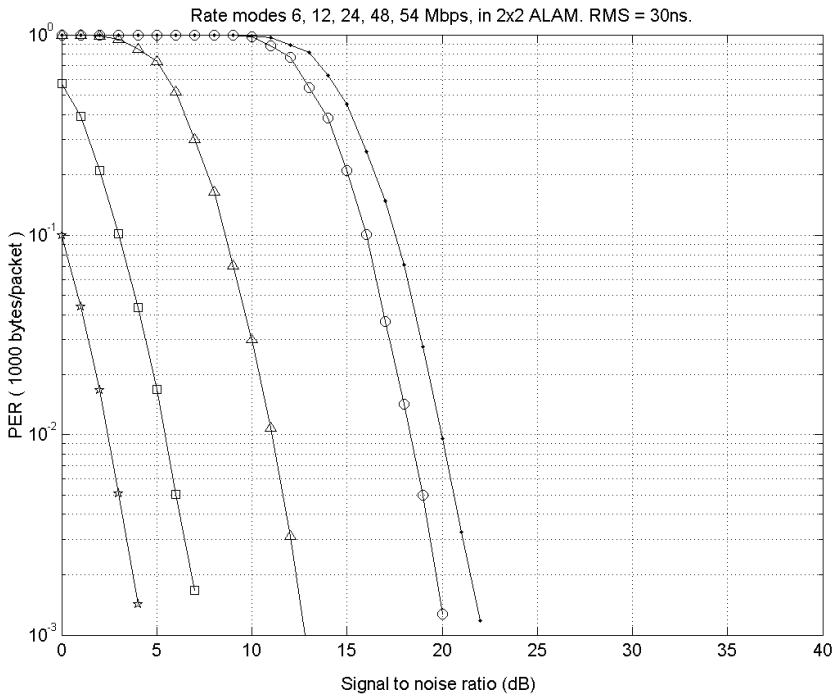

Figure 6-26: PER vs. SNR of a 2x2 spatial diversity system for different data rates. RMS delay spread of the channel is 30 ns.

6.5 Complexity

In this section we summarize the complexity of each of the MIMO algorithms in terms of number of operations at the receiver. The final result of the complexity analysis will be given in real additions (R_ADDs) and real multiplications(R_MULs). For more details on the complexity analysis refer to the work done by Van Zelst within the B4 framework [Zel04].

The complexity of each technique has been divided in two parts: the complexity of the preamble phase and the complexity of the payload phase. In the preamble phase the matrices used to carry out the processing of the received vector are calculated (e.g. $\boldsymbol{H}^{+}$ for ZF, D for MMSE and $\boldsymbol{Hs}_i$ for MLD, refer to [B4-D3.2,Chapter 3] for more details). In this phase the channel matrix H must be estimated. We will not take into account the complexity of channel estimation since it is a common term that adds up to the complexity of any of the considered MIMO algorithms. The preamble phase takes place at the beginning of each packet.

In the payload phase the transmit symbol vector s is estimated. Differently from the preamble phase, the complexity of the payload phase is encountered for each received symbol-vector $\boldsymbol{x}$ within a packet.

For MLD, we show the complexity for three variants of the algorithms. The first two only differ from memory management. In MLD with maximum amount of memory, the $K=M^{Nt}$ possible received vectors (where M is the constellation size) are calculated and stored in the preamble phase. In MLD with minimum amount of memory just the products of the columns of $\boldsymbol{H}$ times the constellation points are stored in the preamble phase. Note that, in this case, for every vector in the

payload, all possible combinations of $\boldsymbol{Hs}_i$ (where $\boldsymbol{s}_i$ is the transmit symbol vector), have to be determined.

The third MLD variant approximates the L2 norm by the L1 norm for the calculation of Equation (22) in Chapter 3 of [B4-D3.2]. The L2 norm is the Euclidean distance between two vectors, hence $||a-b||^2$. The L1 norm is given by $|Re(a-b)|+|Im(a-b)|$. Using the L1 norm instead of the L2 norm substantially reduces the complexity.

The complexity is listed in Table 6-4 and Table 6-5, see [Zel04].

Algorithm	Preamble processing complexity (per subcarrier)	Payload processing for every received vector x (per subcarrier)
ZF	$4N_t^3 + N_t^2(8N_r - 2) - 2N_tN_r$ R_ADDs	$2N_t N_r + 2N_t(N_r-1)$ R_ADDs
	$4N_t^3 + 8N_t^2 N_r$ R_MULs	$4N_tN_r$ R_MULs
MMSE	$4N_t^3 + N_t^2(8N_r-2) - 2N_tN_r + N_t$ R_ADDs	$2N_tN_r + 2N_t(N_r-1)$ R_ADDs
	$4N_t^3 + 8N_t^2N_r$ R_MULs	$4N_tN_r$ R_MULs
VBLAST	$\frac{1}{3}N_t(3N_t^3 + 4N_t^2(1+2N_r) + +3N_t(1+3N_r) + N_r - 1)$ R_ADDs	$2N_t(4N_r-1)$ R_ADDs
	$N_t^2(N_t+1)^2 + +8N_r\frac{N_t(N_t+1)(2N_t+1)}{6}$ R_MULs	$8N_tN_r$ R_MULs
MLD (max memory)	$2M^2N_r\frac{M^{N_t-1}-1}{M-1} + 2MN_rN_t$ R_ADDs	$4KN_r-1$ R_ADDs
	$4MN_rN_t$ R_MULs	$2KN_r$ R_MULs
MLD (min memory)	$2MN_rN_t$ R_ADDs	$2N_rM\frac{K-1}{M-1} + 2KN_r - 1$ R_ADDs
	$4MN_rN_t$ R_MULs	$2KN_r$ R_MULs
MLD (norm approx)	$2MN_rN_t$ R_ADDs	$2N_rM\frac{K-1}{M-1} + 2KN_r - 1$ R_ADDs
	$4MN_rN_t$ R_MULs	-

Table 6-4: Complexity, as number of operations, of the considered MIMO receive algorithms.

Algorithm	Op	Pre.	Payl.	Pre.	Payl.	Pre.	Payl.	Pre.	Payl.	Pre.	Payl.
		2x2		3x3		4x4		2x3		2x4	
ZF	+	80	12	288	30	704	56	108	20	136	28
	x	96	16	324	36	768	64	128	24	160	32
MMSE	+	82	12	291	30	708	56	110	20	138	28
	x	96	16	324	36	768	64	128	24	160	32
VBLAST	+	98	28	425	66	1236	120	132	44	166	60
	x	116	32	480	72	1360	128	156	48	196	64
MLD (max memory)	+	16897	32767	1,5M	~3,1M	~136M	~268M	~1,5M	49151	~136M	65535
	x	1024	16384	2304	~1,5M	4096	~134M	1536	24576	2048	32768
MLD (min memory)	+	512	33023	1152	~3,1M	2048	~270M	768	49535	1024	66047
	x	1024	16384	2304	~1,5M	4096	~134M	1536	24576	2048	32768
MLD (norm approx)	+	512	33023	1152	~3,1M	2048	~270M	768	49535	1024	66047
	x	1024		2304	-	4096	-	1536	-	2048	-

Table 6-5: Calculation of the complexity for different antenna configurations and modulation equal to 64 QAM.

where M stands for million. Assuming that real multiplication is as complex as 10 real additions the complexity of all 3x3 above MIMO algorithms can be compared.

The conclusions are:
The training part of MLD is roughly 7 times more complex than the training phase of the rest.
The data phase complexity of MLD (using 64 QAM) using L1 norm is roughly 8000 and 4000 times more complex than ZF and MMSE with feedback, respectively.

6.6 Latency

High latency could be expected for MIMO algorithms employing decision feedback i.e. PAC V-BLAST. As already discussed in Section 3.2 of [B4-D3.2], PAC V-BLAST uses the output from the Viterbi decoder as the feedback value. The disadvantage is the high latency inherent to the Viterbi decoder. The inherent latency related to the trace-back length of the OFDM Viterbi decoder is 96 coded bits. That means that a reliable feedback could be available only 96 coded-bits after the bits related to a QAM symbol are sent from the MIMO processor to the Viterbi input.

6.7 Verificication of performance Broadband Radio@hand algorithm with measured channels

Finally, the performance of the above studied SDM algorithms using the channel model given in [B4-D2.2] is compared with the performance when using the channels measured at Philips Natuurkundig Laboratorium, in Eindhoven [Dol02].

The aim is to validate the PER-SNR curves from simulations. This is done by replacing the exponential decaying channel model by a call to the database of the measured channel **H** for each channel realization. Results are presented here for detection based on V-BLAST and MLD.

In general, it can be remarked from the figures (Figure 6-27-Figure 6-32) below that the diversity order of the experimental curves is between to the one offered by a 30 ns and a 50 ns RMS delay spread channel. In particular we observe the following:

- 2x2 and 2x3 MLD with the measured channel presents a diversity order similar to the one offered by a 30 ns simulated channel. While the performance for 3x3 is more similar to the one obtained by simulating a 50 ns simulated channel. It is however noted that, since the diversity of the curves for 30 and 50 ns are very similar in the plotted range, it is difficult to judge only on the slope of the curves.
- V-BLAST with the measured channels show a diversity order very similar to the one obtained simulating a 30 ns RMS delay channel. V-BLAST shows a slightly worse performance than the one with the measured channel when higher modulation order is used, see e.g. Figure 6-30.

Overall it can be concluded that the indoor channel model used for MIMO WLAN link-level simulations shows the same characteristics as the measured channels and can be used to asses system performance in indoor environments.

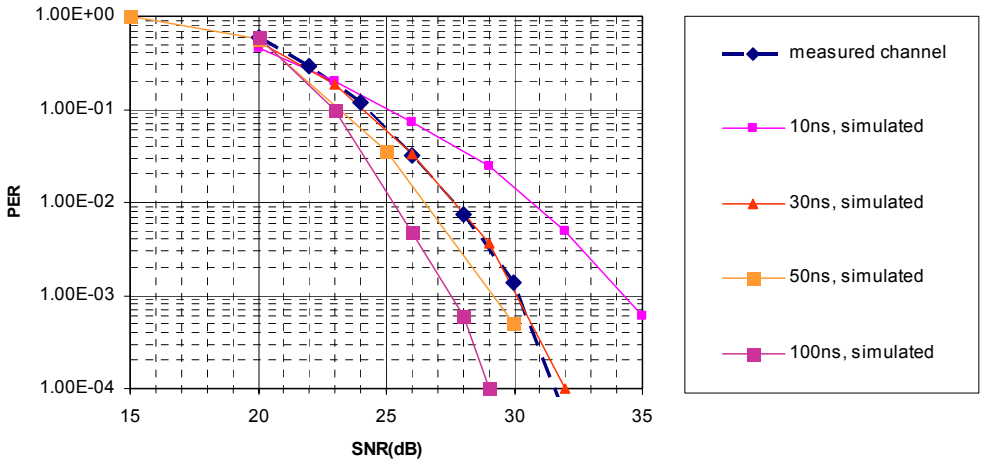

Figure 6-27: 2x2, MLD, 64 QAM, R=3/4, 64 bytes.

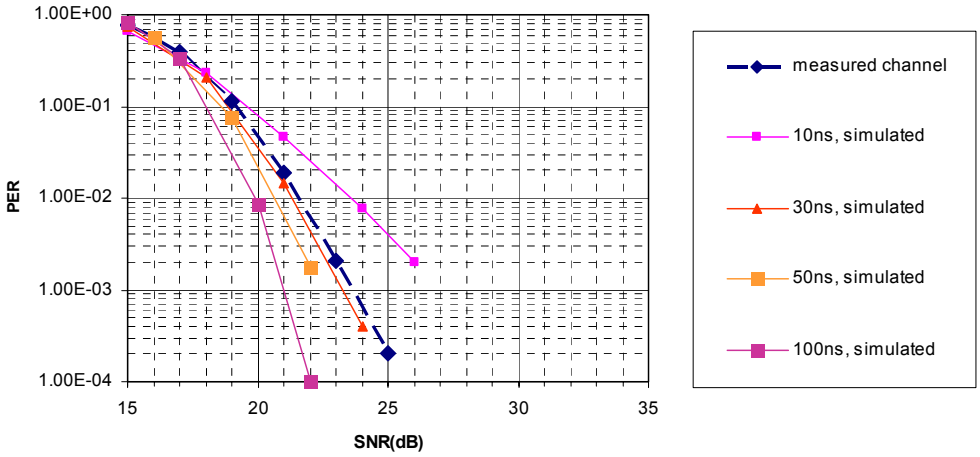

Figure 6-28: 2x3, MLD, 64 QAM, R=3/4, 64 bytes.

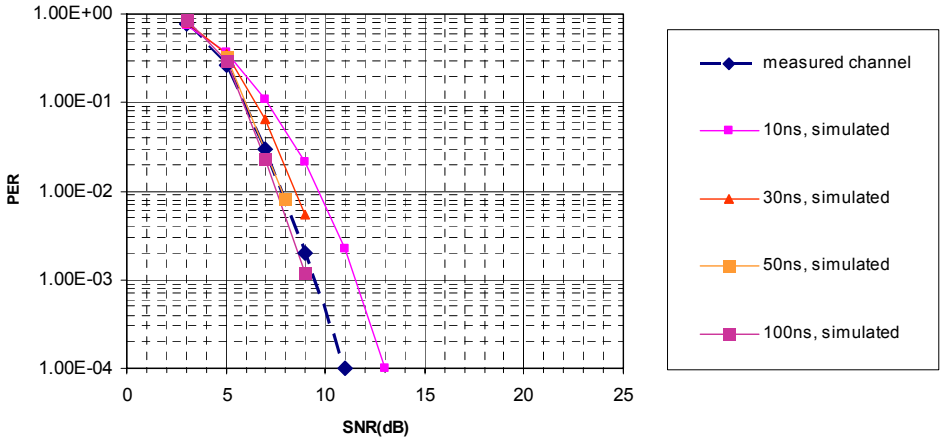

Figure 6-29: 3x3, MLD, QPSK, R=1/2, 64 bytes.

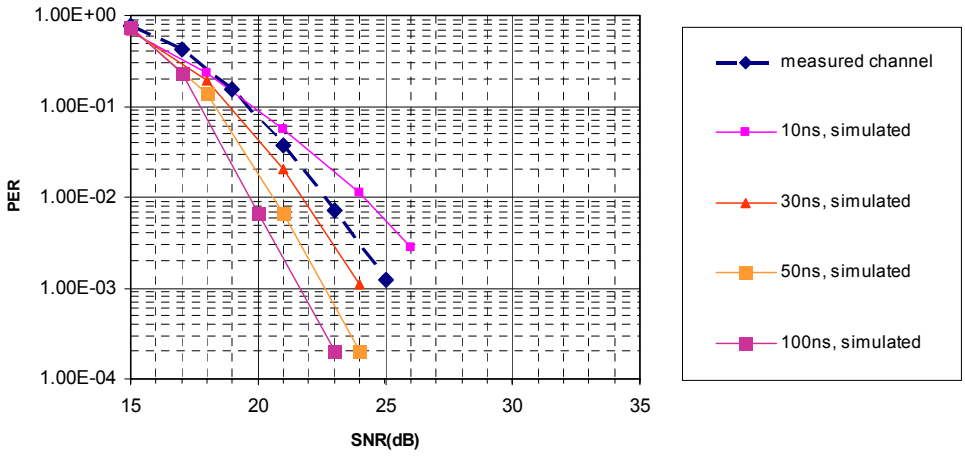

Figure 6-30: 2x3, V-BLAST, 64QAM, R=3/4, 64 bytes.

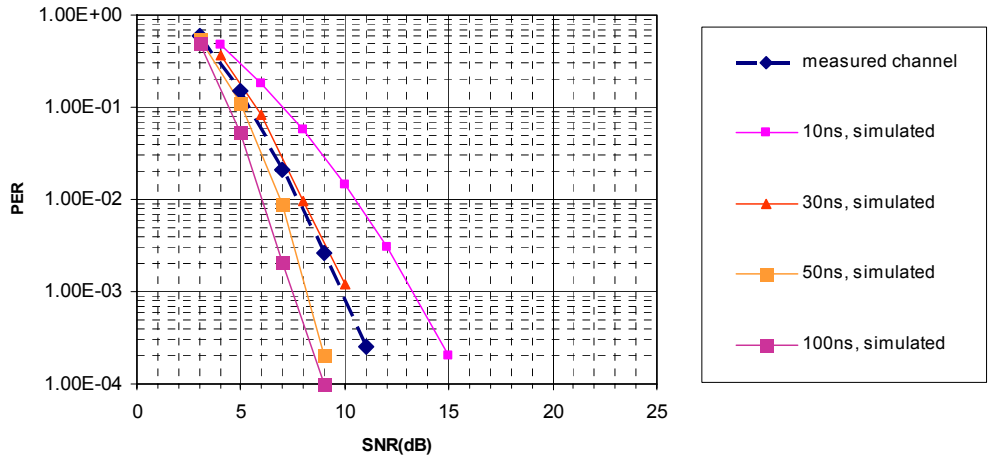

Figure 6-31: 3x3, V-BLAST, QPSK, R=1/2, 64 bytes.

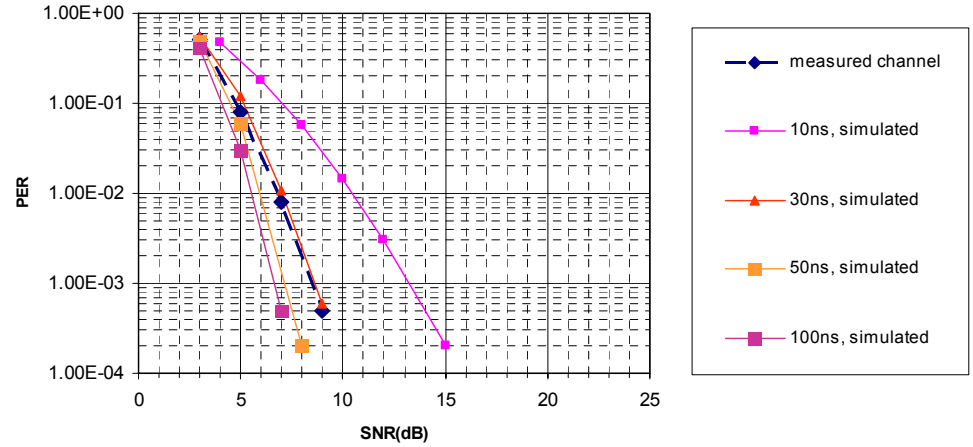

Figure 6-32: 4x4, V-BLAST, QPSK, R=1/2, 64 bytes.

6.8 Conclusions and choice of Broadband Radio@hand algorithm

The simulations results presented in this chapter show that the best performing algorithm (in terms of BER/PER versus SNR) is Maximum Likelihood Detection (MLD), which is also the most complex one in terms of operations. V-BLAST is the second best algorithms in terms of performance and complexity. Its performance is comparable to the one of MLD for asymmetric antenna configurations and slightly worse than the one of MLD for symmetric ones. However its latency could be an obstacle in a real implementation. ZF is the least complex algorithm but also the one that in general performs worst. MMSE is slightly more complex than ZF and outperforms the latter for low and moderate SNR levels. This makes MMSE more attractive than ZF.

Using receive diversity together with MIMO (i.e. $N_r > N_t$) the quality of the link is remarkably improved and the performance gap between MLD and the others SDM

techniques is reduced. This result adds value to algorithms as ZF and MMSE, whose advantage for a symmetrical antenna configuration is the lower complexity and scalability rather than a competitive performance. To further reduce complexity and still make use of the diversity offered by the channel, receive antenna selection has been shown as an efficient solution especially for low delay spread scenarios.

When SDM architectures, like MMSE detection, are compared to diversity architectures based on space-time coding (STC), simulation results show that the coverage of MIMO diversity schemes is substantially bigger than the coverage of MIMO SDM schemes based on MMSE or ZF. However, the coverage gap reduces when comparing the performance of SDM architectures aided with antenna subset selection.

As the complexity of MLD grows like M^{N_t} (where M is the constellation size and N_t is the number of transmit antennas) and as research did not find yet any way of effectively reducing such complexity, it seems unfeasible to use MLD for high order MIMO systems. In contrast, scaling up MIMO MMSE and ZF algorithms seems to be rather straightforward and feasible.

Given the above considerations, the best compromise in terms of complexity and performance is certainly given by V-BLAST if latency is ignored. However, when latency is considered, then MMSE results in a better choice. In the latter case, the most efficient solution to increase robustness is to use MMSE with receive diversity ($N_r > N_t$) deploying all the N_t available antennas or just a subset of it using the selection criterion explained in Section 6.3.

Finally, in Section 6.6 we have shown the validity of the channel model used by the Broadband Radio@hand project for WLAN simulations by comparing the PER vs. SNR performance curves for the measured channel with the simulated one.
The measured channels present a diversity order, whose value lies between the one offered by a simulated channel with a RMS delay spread of 30 ns and 50 ns.

7 Flow link-level (WP3) to system-level (WP5)

7.1 Test cases for WLAN link-level simulations

During the course of the project the following test-cases were simulated and their results were input to WP5. The system description is given in Chapters 5 and 6 and the underlying channel models can be found in [B4-D2.2].

CHANNEL [D2.2]	*RMS Delay Spread (ns)*	10, 30, 50, 100
MIMO SYSTEM	*Algorithms*	ZF MMSE VBLAST MLD Alamouti MRC
	Antenna configurations	2x2 3x3 4x4 2x3 2x4 1x3 1x2 1x4
	Data Rate (Mbps)	12 (QPSK +1/2 CC) 36 (16QAM +3/4 CC) 54 (64QAM +3/4 CC)
	Packet Length	68 bytes (short) 1000 bytes (long)
1 CC-INTERFERENCE	*Number of transmit Antenna*	*2*
	Modulation	QPSK
	Temporal nature	synchronous

Table 7.1: Overview of the test cases investigated within WP3 of the Broadband Radio@hand project.

The results of all link-level simulations are contained in Deliverable 3.3 [B4-D3.3] of this project.

7.2 PHY-layer description 802.11a in MLDESIGNER

System planning of a Broadband Radio@hand system is carried out by traffic simulations. System level simulations are typically carried out on a per-packed or a per-frame basis. For this purpose, the partners used the system package "Mldesigner" to carry out system-level simulations in a multi-cell scenario. The traffic distribution varies in time and space and depends on the type of traffic:

video, audio or data. Output results are, e.g., throughput, latency and number of satisfied/unsatisfied users. More details can be found in the deliverables of WP5.

The behaviour of link-level algorithms, presented in the previous chapters, have to be linked to the system-level simulator. A link-level algorithm is typically evaluated on a per-bit basis. However, a system-level simulator will use a coarse time-step to prevent memory overload problems or unpractical simulation runs. This means that care has to be taken to incorporate the link-level simulation in the system simulator. One way to achieve this goal is to make use of pre-computed look-up tables, which are provided by the link-level simulations carried out in WP3. The validity of the system simulation depends on how properly the system is modelled. If an important aspect is missing, the performance results could be misleading.

As an introduction, a brief overview of the PHY implementation in the system-level simulator "Mldesign" will be given. At top level, a station is subdivided in a MAC-layer and a PHY-layer section (Figure 7-1). The path-loss and the wireless channel properties are stored in memory blocks.

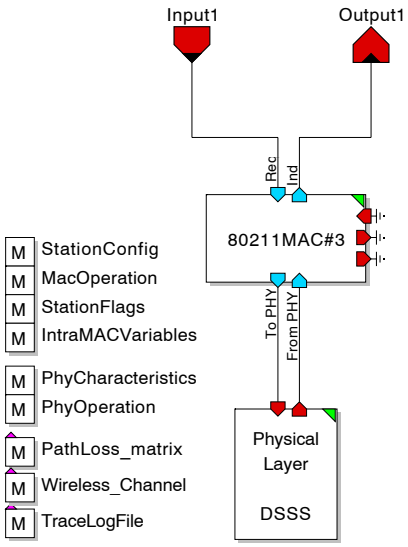

Figure 7-1: 802.11a station.

The physical layer DSSS block is given in detail in Figure 7-2. From this figure it is clear that the wireless channel is read and written by the finite-state-machine block FSM 802 PHY.

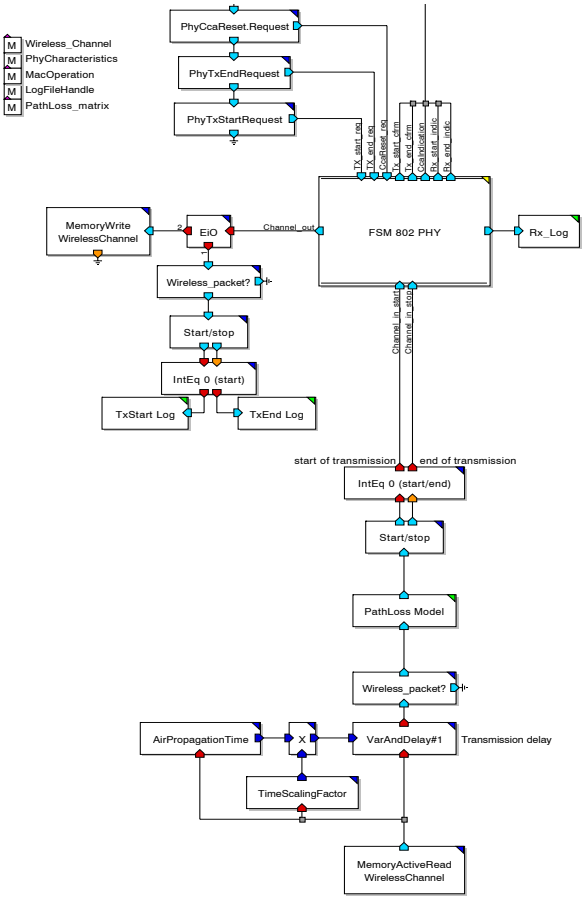

Figure 7-2: PHY layer of 802.11a DSSS.

The FSM 802 PHY block is further worked out presented in Figure 7-3.

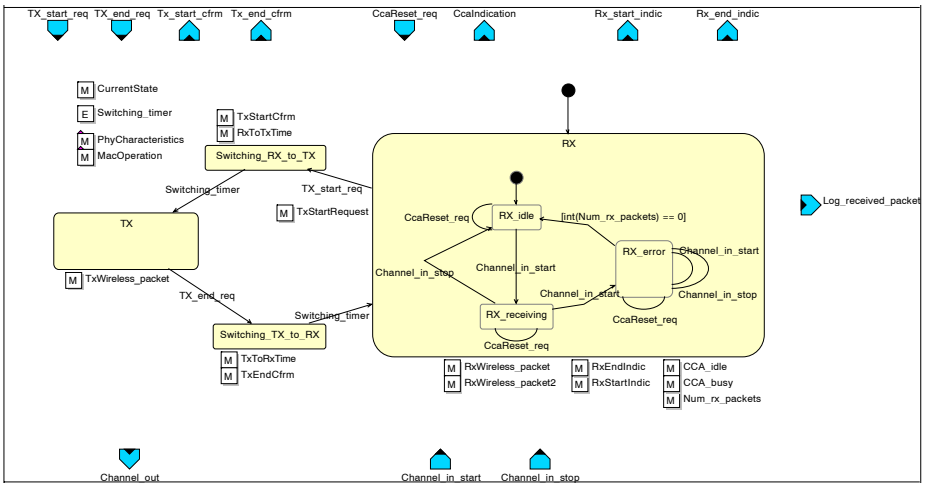

Figure 7-3: Finite-state-machine description of PHY layer of 802.11a DSSS.

Please note that the description above is only an example. More details can be found in the WP5 deliverables.

8 System-level simulation results of multiple antenna extensions of 802.11a

8.1 Introduction

In the previous chapters, BER/PER tables were generated for various SNIR conditions using a PHY layer model. In this chapter, an estimation of the throughput in a system with an access point (AP) and multiple mobile terminals (MT) is made. For this purpose, a network system model is developed based on an analytical approach. The BER/PER tables are linked to the network model.

This model includes the effect of link adaptation (LA) and transmit power control (TPC). The throughput is calculated in a single radio cell only, where the SNR is purely limited by the background noise. The procedure for extending the method for a multiple radio cell layout with interference is briefly explained in this chapter.

8.2 Interference, link adaptation and power control mechanisms

The analysis in this chapter will be restricted to a single radio cell. Since each user in this cell asks permission before actually using the air medium, the assumption will be made that there is no interference in our single radio cell layout.

In this case, the performance is purely limited by the signal strength and the background noise. The assumption will be made that the AP informs the MTs about its own transmit power and indicates at which power level it expects to receive. The MT will adjust its transmit power until the expected receive power at the AP is reached (power control). However, one has to consider that the power of the mobile terminal is usually limited to a certain maximum value. This means that the received power at the AP will start to drop at a certain distance between AP and MT. This will lead to a decreased SNR. It can happen that a lower data rate has to be chosen to keep the BER/PER at an acceptable level. Therefore, link adaptation (LA) and transmit power control (TPC) are not independent.

In a cellular network, intercell interference will occur since frequencies are reused at a certain distance. Given the rules for LA and TPC, an AP can increase the data throughput in its cell by increasing the transmit power, enabling the use of higher data rates. This, however, raises the inter-cell interference of other cells.

An important link-level quality parameter is the percentage of the coverage area where the achievable SNR is above a minimum value. This minimum value is usually defined by a maximum allowed bit or packet error rate, which still guarantees a minimum level of the perceived quality.

A possible network-level quality measure is the throughput a user experiences. With a selective repeat automatic repeat request (SR-ARQ), the throughput I is given as a function of the packet error rate (PER), which is a function of the SNR and the maximum achievable data rate R**:**

$$I = R\,(1 - PER(SNR)) \tag{1}$$

In the remainder of this chapter this maximum achievable data rate is calculated from the PER results of Chapter 7. Moreover, an approximation of the expected achievable uplink throughput is given as a function of the radius of a single radio cell. This analysis is done for uniform distributed mobile terminals and as a basis a simplified path loss model with one breakpoint is used, as described in [Rad03].

8.3 Scenario with a delay-spread of 100ns

The quality of a radio link, which depends on the radio environment, changes over time and in accordance with traffic in surrounding radio cells. To cope with variations, usually a link-adaptation scheme is applied: the adaption of the physical layer mode- the code rate and the modulation scheme – is based on measurements of the link quality. The access point selects the final PHY mode for both the uplink and downlink. The individual throughput curve for various code rates, modulation schemes and MIMO systems are computed in this section for one of the chosen scenarios of [B4-D2.2], namely a delay-spread of 100 ns.

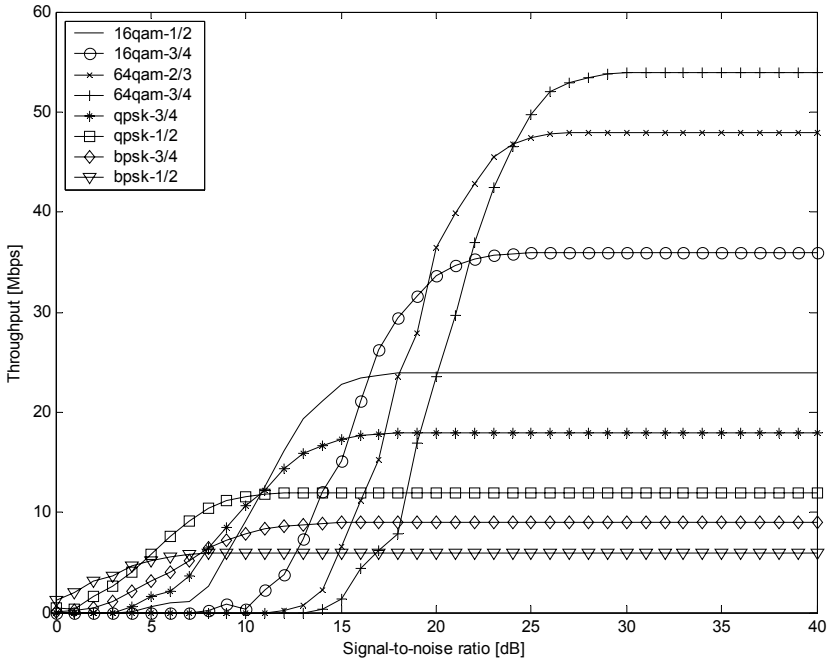

Figure 8-1: Maximum throughput versus SNR for a 100 ns channel with a 1 x 1 system.

Figure 8-1 represents the throughput I for various modulation schemes. A link adaptation scheme would select the envelope of these curves to maximize the throughput for each SNR value.

A way to increase the maximum throughput is to make use of the MIMO schemes, as described in Chapter 4. Consider a 2x2 system, for which the total rate is doubled compared to the 1x1 system rate. As an example, the 64QAM and 16QAM rates of a 2x2 MIMO system are presented in Figure 8-2 and Figure 8-3.

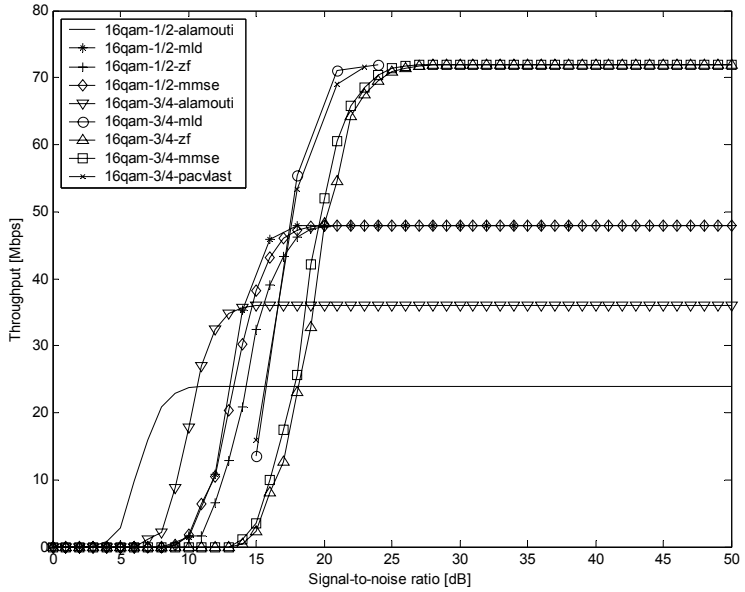

Figure 8-2: Maximum throughput versus SNR for a 100 ns channel with a 2x2 system with 16-QAM.

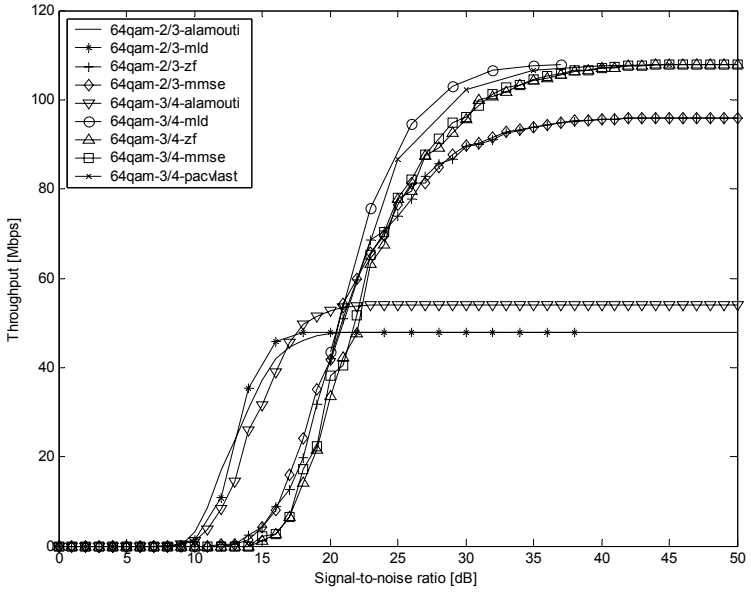

Figure 8-3: Maximum throughput versus SNR for a 100 ns channel with a 2x2 system with 64-QAM.

Note that more than 25 dB of SNR is necessary to achieve a two-fold increase in throughput compared to the 1x1 system. As described in Chapter 6, a reduction in required SNR is feasible by using an extra receiver branch (2x3 system).

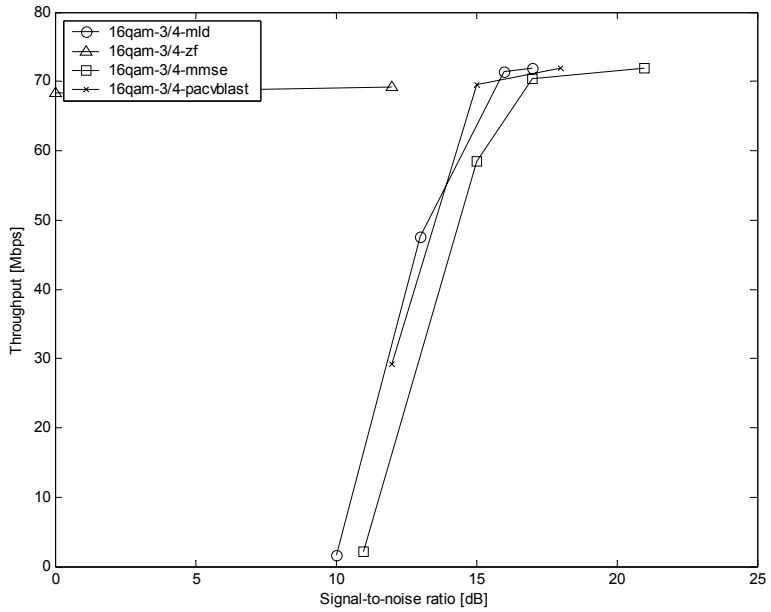

Figure 8-4: Maximum throughput versus SNR for a 100 ns channel with a 2x3 system with 16-QAM.

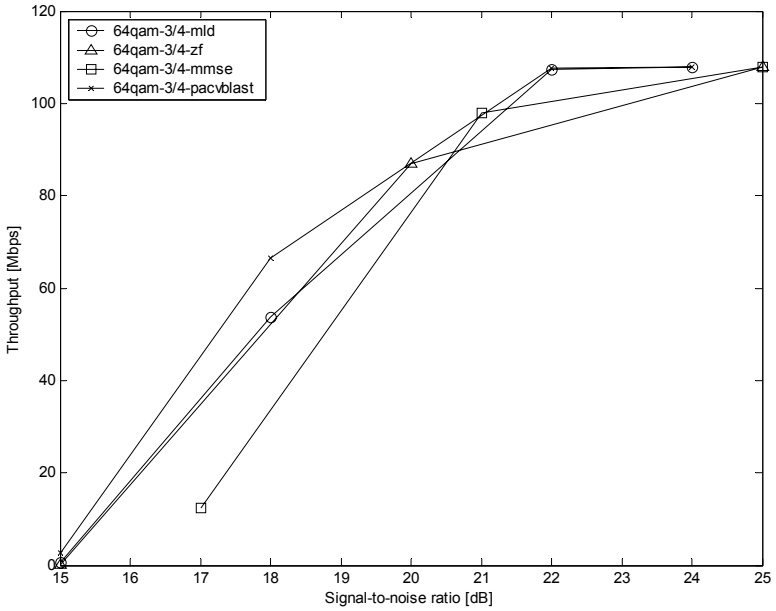

Figure 8-5: Maximum throughput versus SNR for a 100 ns channel with a 2x3 system with 64-QAM.

A reduction in the required SNR can be observed when increasing the number of receive branches. Compare Figure 8-3 with Figure 8-4 and Figure 8-5.

A three-fold or four-fold increase in throughput compared to a 1x1 system is shown in Figure 8-6 and Figure 8-7 for 3x3 and 4x4 MIMO systems.

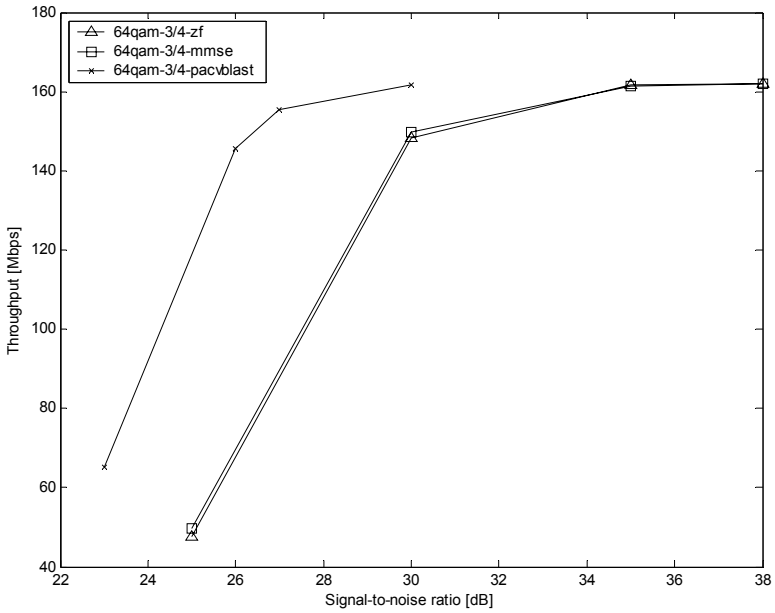

Figure 8-6: Maximum throughput versus SNR for a 100 ns channel with a 3x3 system with 64-QAM.

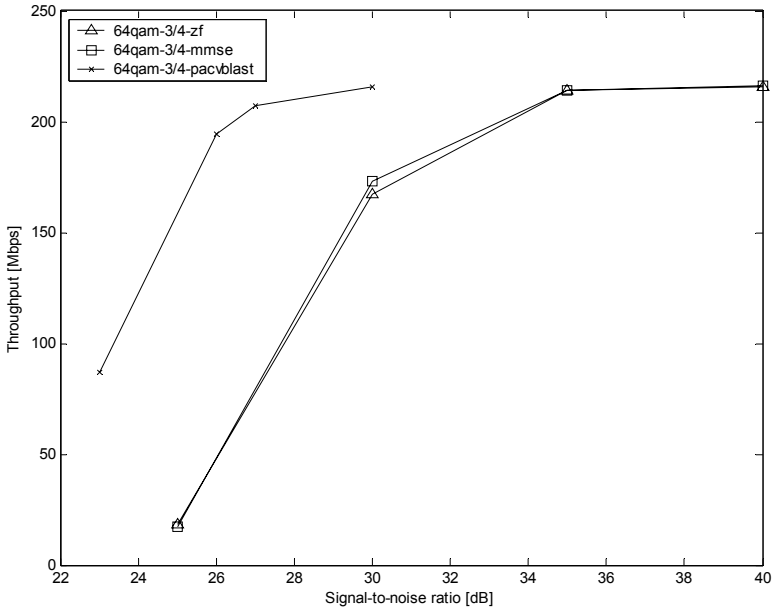

Figure 8-7: Maximum throughput versus SNR for a 100 ns channel with a 4x4 system with 64-QAM.

The minimum required SNR to achieve these high throughputs is little higher than the threshold SNR of a 1x1 system for the highest modulation mode.

8.4 Scenario with a delay-spread of 10ns

As another example, the scenario of deliverable [B4-D2.2] with the low delay-spread of 10 ns is chosen. The throughputs are given in Figure 8-8 – Figure 8-13.

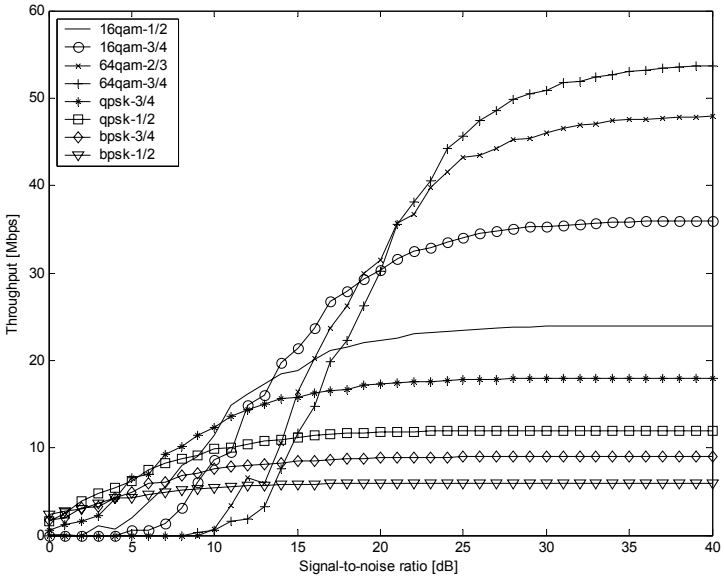

Figure 8-8: Maximum throughput vs. SNR for a 10 ns channel: a 1x1 system.

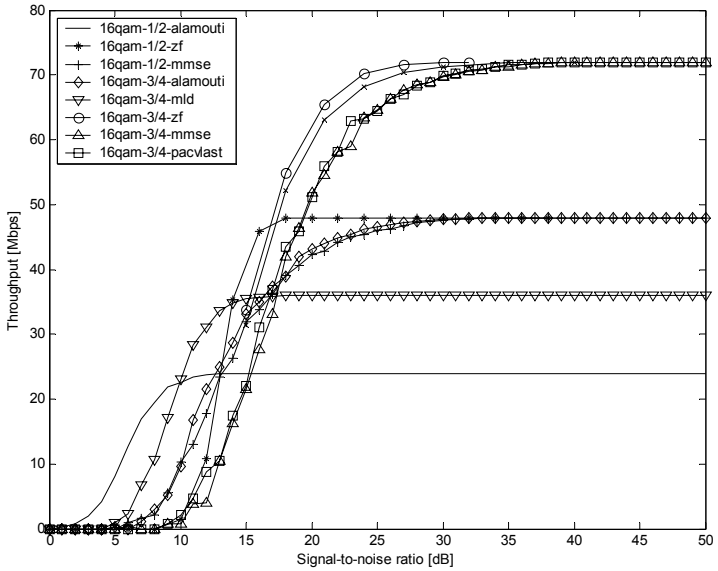

Figure 8-9: Maximum throughput versus SNR for a 10 ns channel with a 2x2 system with 16-QAM.

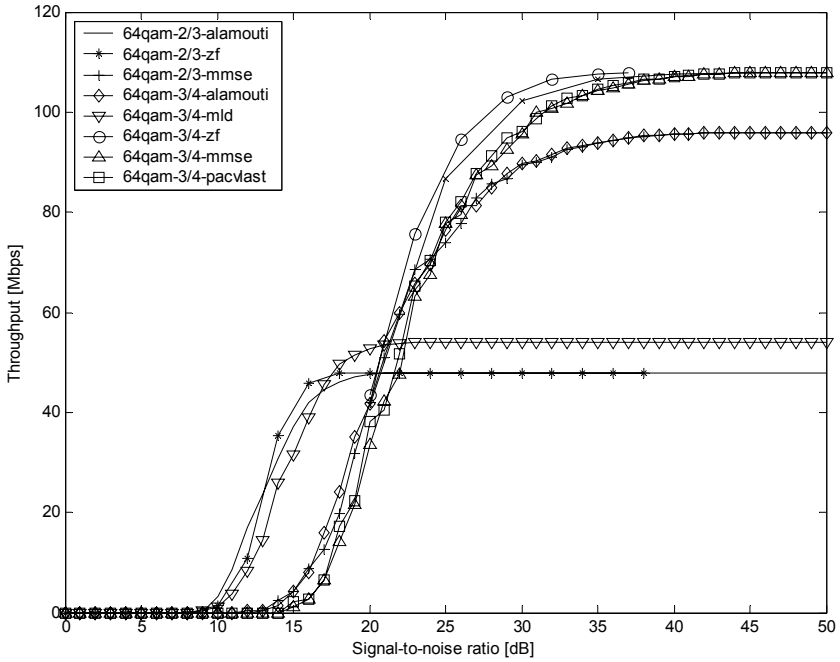

Figure 8-10: Maximum throughput versus SNR for a 10 ns channel with a 2x2 system with 64-QAM.

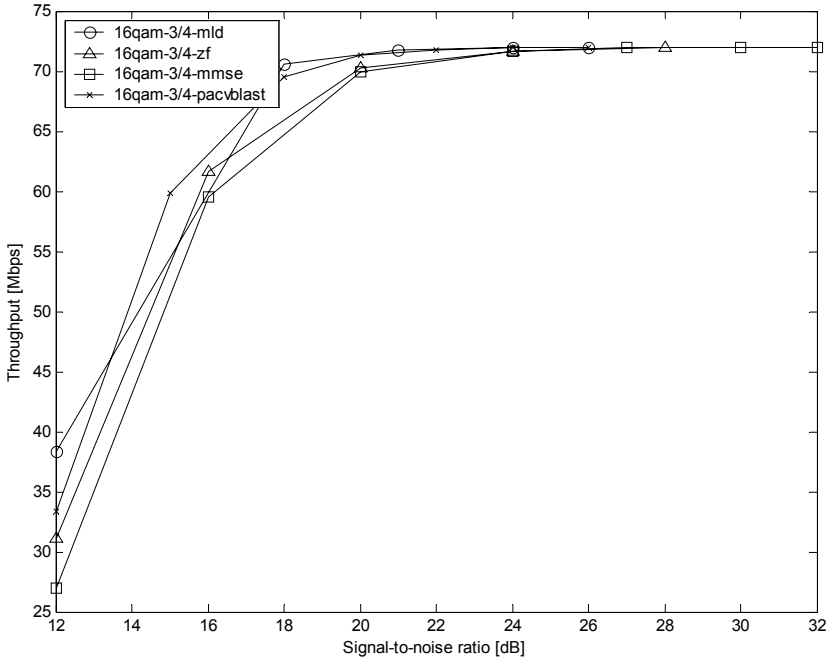

Figure 8-11: Maximum throughput versus SNR for a 10 ns channel with a 2x3 system with 16-QAM.

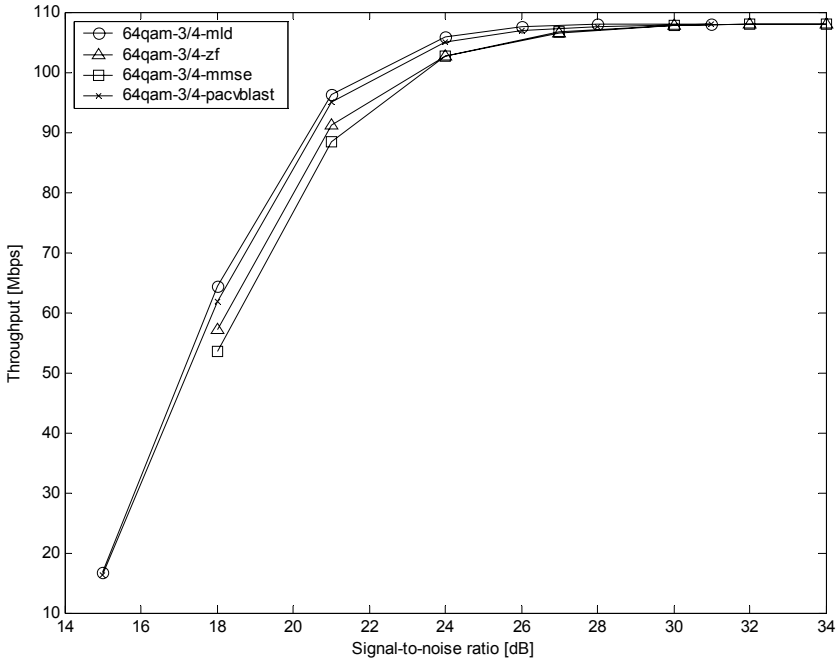

Figure 8-12: Maximum throughput versus SNR for a 10 ns channel with a 2x3 system with 64-QAM.

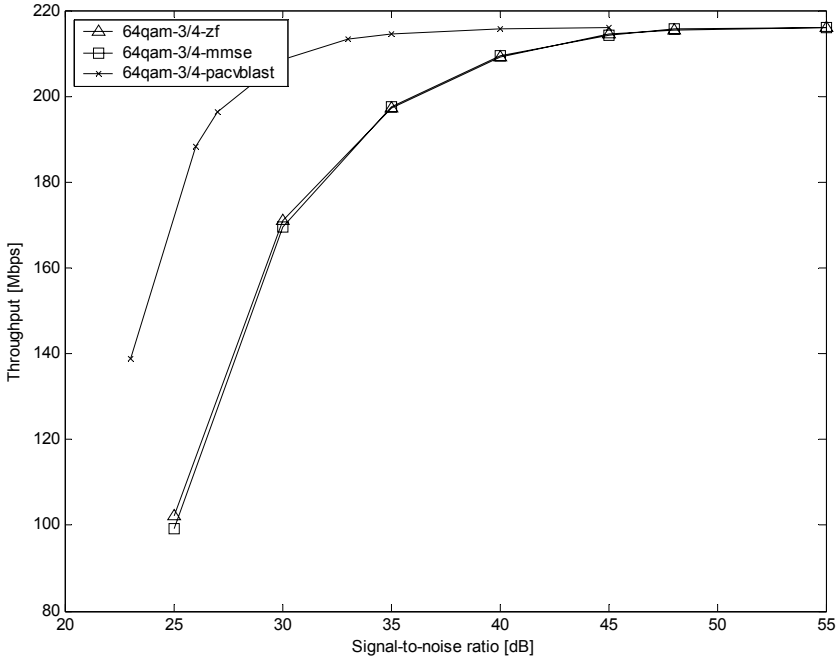

Figure 8-13: Maximum throughput versus SNR for a 10 ns channel with a 4x4 system with 64-QAM.

8.5 Achievable throughput in a single radio cell

The model is based on the assumption that up to 5 m distance from the transmitter, a line of sight path exists, whereas obstacles can be expected for larger distances which result in a higher path loss coefficient [Rad03]. This is a model particular well suited for office environments. It is assumed for all investigations that the background noise N_0 has a level of –95 dBm (thermal noise + amplifier noise). Furthermore, it is assumed that for a single radio cell system that the signal-to-noise (SNR) is purely limited by the background noise.

The transmit power control is assumed to work in such a way that the access point (AP) announces its downlink (DL) transmit power $P_{t,AP}$ and the expected uplink (UL) reception power $P_{e,AP}$ in every MAC frame.

The mobile terminals (MT) can calculate the path loss L from their reception power $P_{r,MT}$ and the known $P_{t,AP}$ and derive the required MT transmit power $P_{t,MT}$:

$$P_{t,MT} = P_{e,AP} + L \quad [dB] \tag{2}$$

where $P_{t,MT}$ is limited to $P_{t,MT,max}$. We will set $P_{t,MT,max}$ equal to 23 dBm.

As mentioned before, we consider a breakpoint between two regions at a distance of 5 m. The extra path loss is assumed to be 35 dB per decade in the region > 5 m, and 20 dB per decade in the region < 5 m. In the two regions, a fixed path loss is assumed of 36 and 46 dB, respectively. Furthermore, a minimum distance of 2 meters is taken between MT and AP. With these assumptions, we arrive at the following path loss model L. The required transmit power $P_{t,MT}$ of the mobile terminal is:

$$P_{t,MT} = \begin{cases} P_{e,AP} + 46 + 20\log_{10} d; & 2m \le d \le 5m \\ P_{e,AP} + 36 + 35\log_{10} d; & 5m < d \le 10^{(P_{t,MT,max} - 36 - P_{te,AP})/35} m \\ P_{t,MT,max}; & \text{otherwise} \end{cases} \tag{3}$$

Note that the minimum distance is set to 2 meters. When $P_{t,,MT}$ and the path loss L is known, the expected received power of the access point $P_{e,AP}$ can be calculated.

Assume that $P_{e,AP}$ is –60 dBm as an example of an uplink (MT -> AP) transmission. The transmit power of the mobile terminal is then given by Figure 8-14**.**

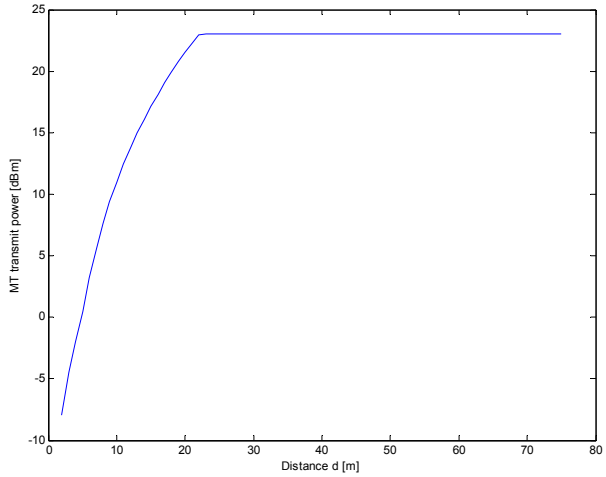

Figure 8-14: The required transmit power of a mobile terminal $P_{t,MT}$ to achieve an expected reception power at the access point $P_{e,AP}$ of –60 dBm.

Note that the terminal has to transmit more power when the distance increases. At a certain distance the power is at its maximum value of 23 dBm. The received power of the access point is given in Figure 8-15:

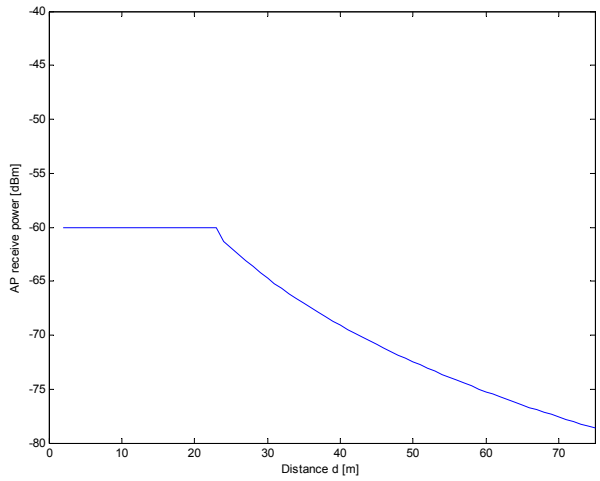

Figure 8-15: The received power of an access point $P_{r,AP}$.

Note that the received power at the access point is –60 dBm until the distance where the mobile terminal is bounded by its maximum transmit power of 23 dBm. For larger distances, the received power decreases according to the described path loss model.

The next step is to derive the pdf of the SNR at the AP for a single radio cell. Assume that the MTs are equally distributed in a circle with radius R around the AP. The pdf of the SIR is derived from the pdf of the distance d of the MTs from the AP and the earlier described path loss model.

$$f_{\gamma_{AP}}(\gamma_{AP}) = f^{(1)}{}_{\gamma_{AP}}(\gamma_{AP}) + f^{(2)}{}_{\gamma_{AP}}(\gamma_{AP}) \quad (4)$$

with

$$f^{(1)}{}_{\gamma_{AP}}(\gamma_{AP}) = \min\left\{1, \frac{1}{R^2-4}.\left[10^{2(P_{t,MT,max}-36-\gamma_{AP}-N_0)/35} - 4\right]\right\}.\delta(P_{e,AP} - N_0) \quad (5)$$

and

$$f^{(2)}{}_{\gamma_{AP}}(\gamma_{AP}) = \frac{2\ln 10}{35(R^2-4)}\left[10^{2(P_{t,MT,max}-36-\gamma_{AP}-N_0)/35} - 4\right]; \quad P_{r,AP}(R) - N_0 \le \gamma_{AP} < P_{e,AP} - N_0$$
$$0; \quad otherwise \quad (6)$$

With the pdfs of the SNR for the uplink and the downlink, we can now calculate the achievable throughput. For this purpose, we have to determine the time during which the radio resource is used. This time share is determined by the scheduling algorithm in the MAC layer of the system, which meets the decision on who uses the radio resource when and for how long. Let $R\{Phy\}$ be the maximum possible data rate of the current PHY mode and max*(PM)* the PHY mode with the highest throughput for a given SNR, i.e., a selection function for all the envelope curves in the previous section.
In order to make the results comparable, the same scheduling scheme is assumed for the mathematical model. A normalization of the pdf of the SNR is needed. For this purpose, the time norm of $f_\gamma(\gamma)$ is defined as:

$$\tau_{norm} = \int_0^\infty f_\gamma(\gamma).\sqrt{\frac{54Mbps}{R\{\max(PM)\}}}d\gamma \quad (7)$$

If $I_{PM}(\gamma)$ represents the throughput for given γ and the selection of the PHY mode PM according to the theoretical throughput curves, the expected value is calculated as:

$$E(I_{\max}) = \frac{1}{\tau_{norm}}\int_0^\infty f_\gamma(\gamma).I_{\max}(PM).\sqrt{\frac{54Mbps}{R\{\max(PM)\}}}d\gamma \quad (8)$$

All the parameters of this function are calculated in a MATLAB routine where the throughput curves I_{max} are created from the PER results of Chapter 6. For a MIMO scheme, the value of 54Mbps will be updated to the highest rate of the MIMO system. The results are shown in the next section.

Although no results will be presented here for the two radio cell case, guidelines will now be given how to extend the model. For two radio cells, both cells will have different radii. When the interference power is defined as P_i , the SNR can be calculated by subtracting the received power by the noise and the interference power. Interference will be generated from MT to MT, AP to MT, MT to AP and

AP to AP. For example, the throughput in the downlink of cell 1 is determined by the interference that is generated by the AP and the MTs in cell 2. When the interference pdfs at the MTs and at the AP in cell 1 are known, the throughput can written as a sum of the normalized MT throughput and the normalised AP throughput.

8.6 Uplink throughput with link adaptation and power control

The tables containing the results of the simulation presented in Chapter 6 contain 8 different modulation schemes for the 1x1 system. The maximum throughputs are shown in Figure 8-16.

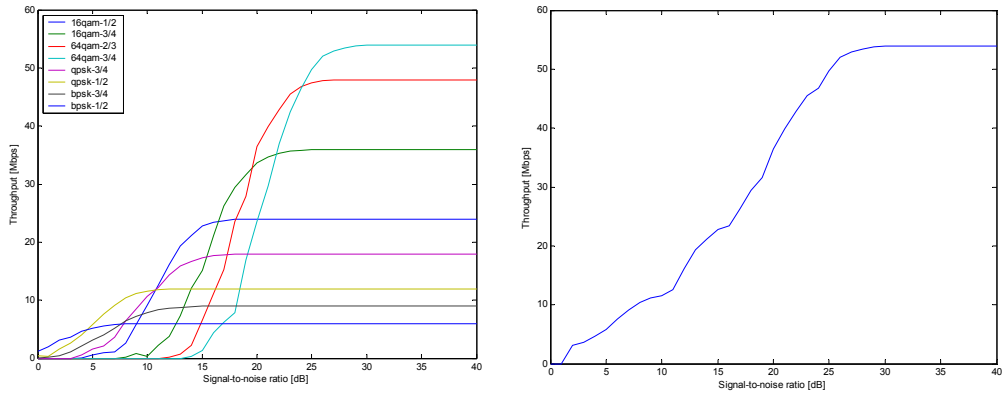

Figure 8-16: Maximum throughput vs. chosen modulation (left figure) and envelope using link adaptation (right figure).

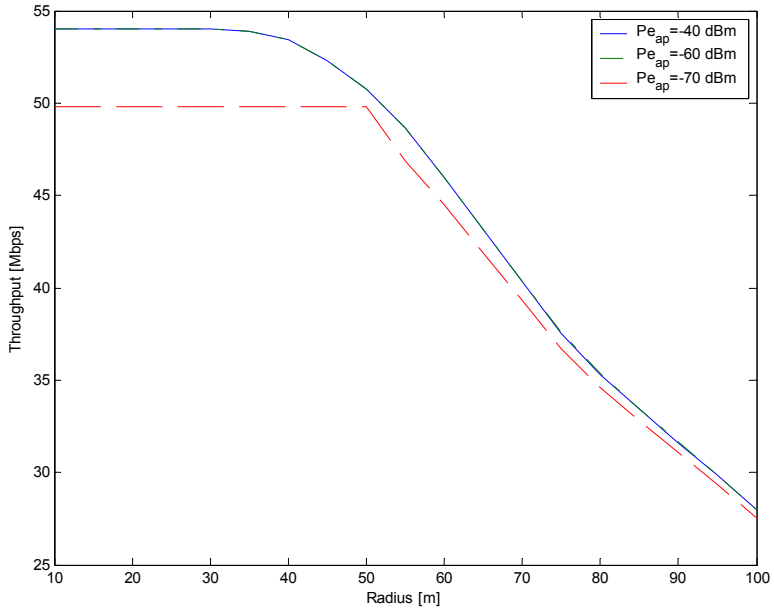

Figure 8-17: Throughput vs. cell radius in the uplink for various Pe_{ap} of a 1x1 system.

The achievable throughput for a 1x1 system is given in Figure 8-17.

The throughput is constant until the distance is crossed where the transmitted power of the MT is at its maximum. When the expected power of the AP decreases, more bit-errors will occur and the throughput will decrease.

A 2x2 MIMO system will now be studied to calculate the achievable throughput. Let's consider a system with only 4 modes: ¾ 64QAM, ¾ 16QAM, ¾ QPSK and ½ QPSK. The rates are shown in Figure 8-18.

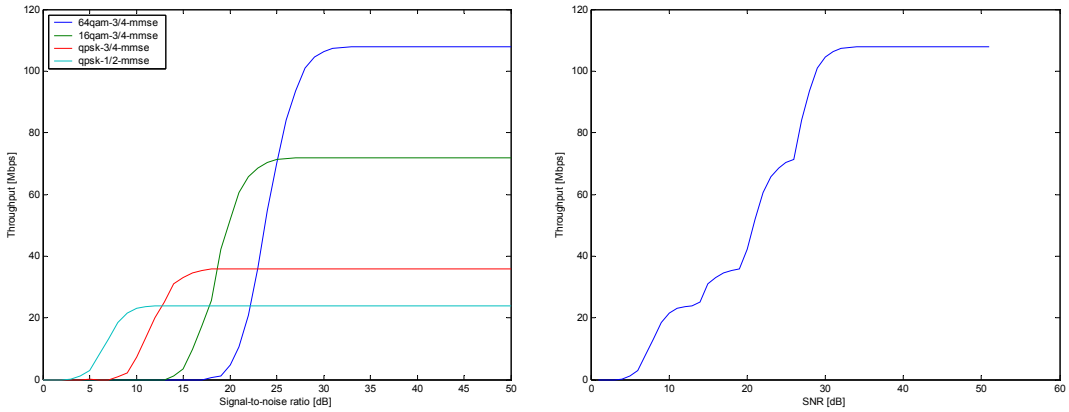

Figure 8-18: Maximum throughput vs. SNR of the chosen modes of a MMSE 2x2 system (left figure) and the envelope using a link-adaptation algorithm (right figure).

The achievable throughput for a 2x2 MMSE-MIMO system is given in Figure 8-19

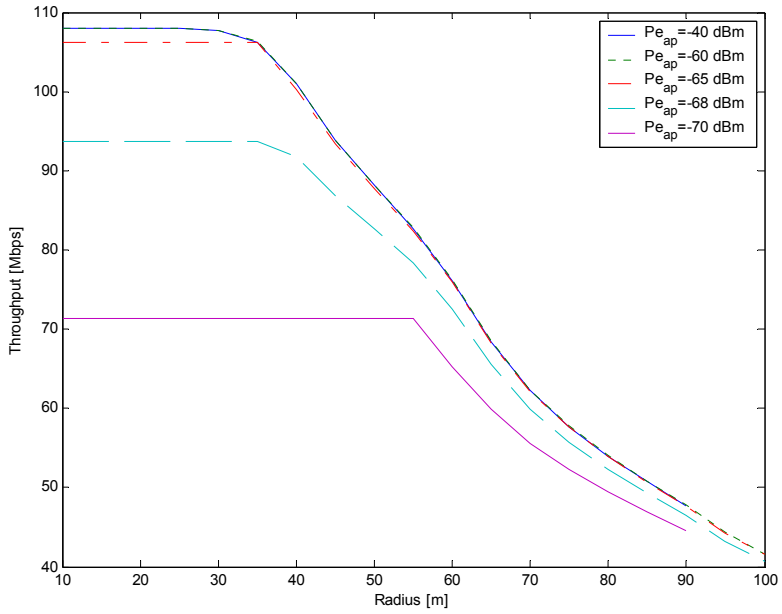

Figure 8-19: Throughput vs. cell radius in the uplink for various Pe_{ap} of a 2x2 MMSE MIMO system.

The comparison between the SISO system of Figure 8-17 with the MIMO system of Figure 8-19 is shown in Figure 8-20.

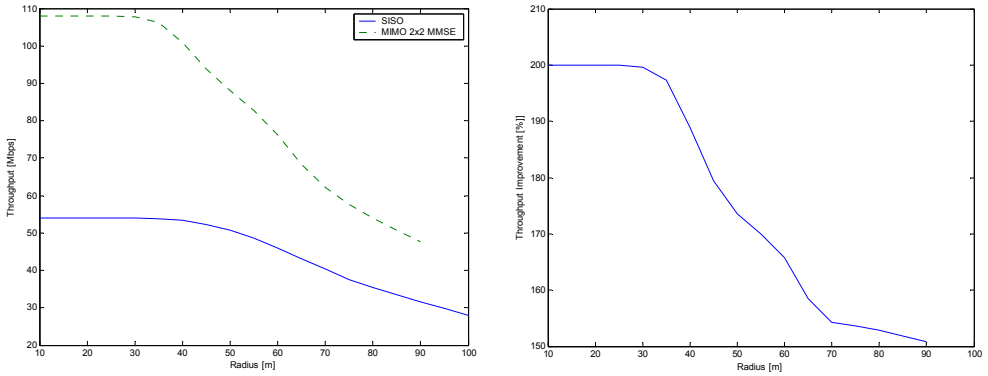

Figure 8-20: Throughput comparison between SISO and 2x2 MMSE MIMO (left is throughput, right is percentage improvement) vs. cell radius in the uplink for a Pe_{ap} of –40 dBm.

Although the negative slope of the throughput vs. distance is higher of MIMO systems than SISO systems, the throughput gain of using MIMO is substantial.

8.7 Conclusions

This chapter uses a theoretical framework [Rad03] that allows us to approximate the throughput of wireless networks with analytical equations.

The procedure is as follows:

- From the PHY tables (PER/BER-SNR) of Chapter 7, the maximum throughput curves for all PHY modes is computed and a selection for the envelope curve is made to maintain the maximum throughput by switching the PHY mode. In the PHY tables, the effect of fast fading is included. This procedure leads to PHY maximum throughput tables.
- From the simple path loss model with one breakpoint, a probability density function (PDF) of the signal-to-noise ratio (SNR) is determined when the mobile stations are uniform distributed in the single radio cell (radius R).
- The PDF of the SNR is combined with the PHY maximum throughput tables, wherefrom the expected value of the achievable downlink and uplink throughputs can be calculated

As expected, the achievable throughputs decrease for increasing cell radius. The throughput of MIMO systems is substantial higher than SISO systems even for a relative large distance between AP and MT.

The model considers only part of the network loss mechanisms. It analyses the bit and/or packet errors for adaptive power control systems. The model does not take into account the overhead of the control traffic, MAC protocol and the convergence layer. To obtain the real throughput, the achievable throughput has to be multiplied with a so-called overhead factor. This overhead factor is approximately 0.8 for a single bi-directional connection and can be as high as 0.56 for 10 bi-directional connections [Rad03].

9 Conclusions

This deliverable describes the public results of Workpackage 3 of the broadband radio@hand project for the period April 1st, 2001 – July 1st, 2005.

Smart antenna and MIMO concepts, models, test-beds and measurements are described. The description of the link-level simulator is explained in detail. Various MIMO algorithms are presented, i.e., zero-forcing (ZF), minimum mean-squared error (MMSE), decision feedback (DF), maximum likelihood (MLD) and space-time block codes. Subsequently, the OFDM specific parameters for WLAN systems are presented. To be able to evaluate the robustness of MIMO algorithms, a co-channel interference model is introduced.

The BER/PER curves for the identified Broadband Radio@hand scenarios have been found with link-level simulations. From these results it is concluded that the preferred MIMO scheme is MMSE with receive diversity (more receive antennas than transmit antennas). For symmetric transmit/receive MIMO systems, V-BLAST is preferred when latency is not an issue. The validity of the channel models used in the scenarios is checked with measurements; most measured delay-spread values lie between the simulated channels of 30 ns and 50 ns.

A workflow for combining the link-level simulations with system-level simulations is described. This provides a guideline how to incorporate the results achieved in WP3 within the system simulations of WP5.

An estimation of the throughput in a single radio cell network with an access point and mobile terminals has been made. The model includes the effect of link adaptation and transmit power control. A simple path-loss model combined with the BER/PER scenario simulations is used to compute the achievable throughput vs. cell radius. It can be concluded that the throughput of a 2x2 MIMO-MMSE system is between 150 and 200% of a 1x1 system for various cell radii.

References

[Ala98] S.M. Alamouti, “A simple transmit diversity technique for wireless communications”, *IEEE Journal on Selected Areas in Communications*, vol. 16, October 1998, no. 8, pp. 1451-1458.

[B4-D2.2] E. Martijn, M. Jevrosimovic, M. Herben, S. Savov, and G. Dolmans,"Broadband Radio@hand deliverable 2.2: Development of propagation models for UMTS and WLAN, preliminary results", 5 June 2003.

[B4-D3.2] G. Dolmans, M. Jevrosimovic , P. Mattheijssen , I. Modonesi , T.C.W. Schenk, B. Vandewiele, A. van Zelst, “Broadband Radio@hand deliverable 3.2: Broadband Radio@hand PHY layer”, 30 April 2003.

[B4-D3.3] M. Collados, G. Dolmans, C.F. Li, P. Mattheijssen, I. Modonesi, T.C.W. Schenk, Xiao-Jiao Tao and B. Vandewiele, “B4 Broadband Radio@hand deliverable D3.3: Broadband Radio@hand link-level algorithms, system-level study and imperfections study”, June 2004.

[Dol97] W.M.C. Dolmans, “Effect of indoor fading on the performance of an adaptive antenna system”, PhD thesis, Eindhoven University of Technology, 1997

[Dol02] W.M.C. Dolmans, M. Collados, "Broadband measurement analysis of indoor space-time channels", *Proc. of URSI General Assembly 2002*, Maastricht, Aug. 17-24, 2002

[Fos98] Foschini G.J. and M.J. Gans, “On Limits of Wireless Communications in a Fading Environment When Using Multiple Antennas”, *Wireless Personal Communications*, Volume 6, March 1998, no. 3, pp. 311-335.

[Gor00] D. Gore, R. Nabar and A. Paulraj, "Selecting an optimal set of transmit antennas for a low rank matrix channel", in *Proc. ICASSP*, May 2000.

[Gor02] A. Gorokhov, "Antenna selection algorithms for MEA transmission systems", in *Proc. ICASSP*, Orlando, FL, May 2002, pp. 1926-1934.

[Gor03-1] A. Gorokhov, D. Gore and A. Paulraj, "Receive antenna selection for MIMO flat fading channels: theory and algorithms", *IEEE Tr. on Info. Theory*, Oct. 2003.

[Gor03-2] A. Gorokhov, D. Gore and A. Paulraj, "Receive antenna selection for MIMO spatial multiplexing: theory and algorithms", *IEEE Tr. on Sig. Proc.*, Nov. 2003.

[Hag89] Hagenauer J. and P. Hoeher, “A Viterbi Algorithm with Soft-Decision Outputs and its Applications”, *Proc. IEEE Globecom 1989*, Dallas, Texas, Nov. 1989, pp. 47.1.1-47.1.7.

[Jak74] W. Jakes, "Microwave mobile communications", New York: Wiley, 1974

[Li00] X. Li, H. Huang, G.J. Foschini and R.A. Valenzuela, "Effects of iterative detection and decoding on the performance of BLAST", *IEEE Global Telecommunications Conference (GLOBECOM) 2000*, Vol. 2, pp. 1061-1066.

[Li01] Ye Li, J.H. Winters and N.R. Sollenberger, “Signal detection for MIMO-OFDM wireless communications”, *IEEE International Conference on Communications (ICC) 2001*, Vol. 10, pp. 3077-3081.

[Lie01] T.H. Liew, B.J. Choi and L. Hanzo, “Comparative study of concatenated turbo coded and space-time block coded as well as space-time trellis coded OFDM”, *IEEE VTS 53rd Vehicular Technology Conference (VTC) 2001 Spring*, Vol. 2, 2001, pp. 781-785.

[Mol01] A. Molisch and M. Win and J. Winters, "Capacity of MIMO systems with antenna selection", in *Proc. Int. Conf. Communications*, Helsinki, Finland, June 2001, vol. 2, pp. 570-574.

[Nee00] R. van Nee and R. Prasad, "OFDM for Mobile Multimedia Communications", Boston, Artech House, 2000.

[Nee00-1] R. van Nee, A. van Zelst and G.A. Awater, “Maximum Likelihood Decoding in a Space Division Multiplex System”, *IEEE Vehicular Technology Conf. 2000-Spring*, May 2000.

[Rad03] M. Radimirsch and K. Jobmann, “System Model for Wireless Data Networks”, In *COST 273* TD(03)004, Barcelona, Spain, Jan. 15-17, 2003

[Rap89] Rappaport T.S. and C.D. McGillem, "Characterization of UHF multipath Radio Channels in Factory Buildings", *IEEE Transactions on Antennas and Propagation*, vol. 37, August 1989, no. 8, pp. 1058-1069.

[Rap96] Rappaport T.S., “Wireless Communications, Principles and Practice”, New Jersey, Prentice-Hall, 1996.

[Str88] Strang G.,“Linear Algebra and its Applications”, Third Edition, San Diego, Harcourt Brace Jovanovich, Publishers, 1988.

[Tar99] V. Tarokh, H. Jafarkhani and A.R. Calderbank, “Space-time block coding for wireless communications: performance results.” *IEEE*

Journal on Selected Areas in Communications, Vol.17, No. 3, March 1999.

[Tar99-1] V. Tarokh, N. Seshadri, R. Calderbank, "Space-time codes for high data rate wireless communication: performance criterion and code construction", *IEEE Tr. on Info. Theory*, vol. 44, no. 2, pp. 744-765, May 1999.

[Uys01] M. Uysal, N. Al-Dhahir and C.N. Georghiades, "A space-time block-coded OFDM scheme for unknown frequency-selective fading channels", *IEEE Communications Letters*, Vol. 5, No. 10, Oct. 2001, pp. 393-395.

[Van02] B. Vandewiele and P. Mattheijssen, *"An experimental broadband 4x4 MIMO test-bed"*, *Proc. of URSI General Assembly 2002*, Maastricht, Aug. 17-24, 2002**.**

[Win94] Winters J.H. and J. Salz, R.D. Gitlin, "The impact of antenna diversity on the capacity of wireless communication systems", *IEEE Trans. on Commun*., vol. 42, Feb./Mar./Apr. 1994, no. 2, pp. 1740-1751.

[Win01] M. Win and J. Winters, "Virtual branch analysis of symbol error probability for hybrid selection/maximal-ratio combining in Rayleigh fading", *IEEE Tr. on Comm.*, vol. 49, no. 11, pp. 1926-1934, Nov. 2001.

[Wol98] Wolniansky P.W. and G.J. Foschini, G.D. Golden, R.A. Valenzuela, "V-Blast: An Architecture for Realizing Very High Data Rates Over the Rich-Scattering Wireless Channel", *1998 URSI International Symposium on Signals, Systems, and Electronics, ISSSE 98*, Pisa, 29 Sept. - 2 Oct. 1998, pp. 295-300.

[Zel03] A. van Zelst, "Per-Antenna-Coded schemes for MIMO OFDM", *IEEE International Conference on Communications (ICC) 2003*, Anchorage, Alaska, May 2003, Vol. 4, pp. 2832–2836.

[Zel04] A. Van Zelst, "MIMO OFDM for Wireless Local Area Networks", PhD Thesis, Eindhoven University of Technology, April 2004.

[ZelSc04] A. van Zelst and T.C.W. Schenk, "Implementation of a MIMO OFDM-Based Wireless LAN System", *IEEE Trans. on Signal Proc.*, vol.52, no. 2, pp.483-494, Feb. 2004.